

Identifying and characterising potential pathfinder elements to IOCG style mineralisation on Central Yorke Peninsula

Thesis submitted in accordance with the requirements of the University of
Adelaide for an Honours Degree in Geology.

Kym Michael Custance
November 2015



TITLE

Identifying and characterising potential pathfinder elements to IOCG style mineralisation on Central-Northern Yorke Peninsula

RUNNING TITLE

Identifying IOCG pathfinder elements: Yorke Peninsula

ABSTRACT

The central Yorke Peninsula in the southern Gawler Craton, South Australia forms the Southern extent of the Olympic Copper-Gold Province. The area is known for its iron oxide-copper-gold (IOCG) style mineralisation, yet the pathfinder elements associated with mineralisation and the processes and/or lithological controls effecting the distribution of potential pathfinder elements within mineral phases are poorly understood. Analyses of whole rock geochemical data from basement lithologies identified Au, As, Ag, Bi, Ce, Cu, La, Mo, S and W as pathfinder elements towards potential (IOCG) mineralisation in the area. Mineral phases that preserved these trace element signatures were investigated with SEM back scatter analysis and Laser-Ablation Inductively-Coupled Mass Spectroscopy (LA-ICP-MS) analysis. SEM analyses determined LREE's are host within bastnäsite, which has a documented occurrence across Yorke Peninsula. Sulphide phases were identified to host elements Ag, As, Au, Bi, Cu, Mo and S. Within pyrite, pathfinder elements are preferentially hosted within inclusion rich areas. Chalcopyrite was determined to host concentrations of Au. A prospectivity index was created for central Yorke Peninsula by combining identified pathfinder elements to create an IOCG index for representative samples. The index highlights an area proximal to the township of Alford as a potential hotspot for mineralisation/exploration within central Yorke Peninsula.

KEYWORDS

Iron oxide-copper-gold (IOCG), Whole rock geochemistry, Geochemical vectors, Mineral hosts, Pathfinder elements, Central Yorke Peninsula

TABLE OF CONTENTS

Title.....	i
Running title	i
Abstract.....	i
Keywords.....	i
List of Figures and Tables	3
Introduction	6
Geological Setting/Background.....	10
Methods	12
Logging and sampling.....	12
Geochemistry	12
Petrological analysis and elemental mapping.....	13
Mineral chemistry	13
Observations and Results	16
Logging and sampling.....	16
Granites	16
Metasediments	17
Felsic volcanics	17
Mafic volcanics	18
Gniess	18
Metasomatite.....	18
Whole Rock Geochemistry.....	21
Major element chemistry.....	21
Trace element chemistry.....	24
Petrology	26
Sample 1949789 -.....	26
Sample 1949023 –.....	26
Sample 1960847 –.....	27
Element Mapping.....	29
Sample 1949789.....	29
Sample 1949023.....	29
Sample 1960847.....	30

Mineral chemistry	34
Pyrite	34
Chalcopyrite	35
Disscussion	40
Whole rock geochemistry	40
Major elements	40
Trace elements	41
Pathfinder elements to potential IOCG mineralisation	43
Element deployment.....	48
IOCG prospectivity index.....	55
Implications for exploration.....	58
Future work.....	58
Conclusions	59
Acknowledgements	60
References	60
Appendix A: Raw geochemical data and Element suite analysed and analytical techniques	64
Appendix B: SEM images Order: (Map 1 - 1949789) – (Map 2,3,4 1949023) – (map 5,6 – 1960847).....	85
.....	85
Appendix C: Raw LA-CP-MS Data from sulphides analysed	91
Appendix D: Pathfinder element Criteria	93

LIST OF FIGURES AND TABLES

Figure 1 - Geological map showing the Olympic Domain within the Galwer Craton and location of major IOCG mineralisation in the area. The location of the Yorke Peninsula area is also shown in boxed area. Modified after Conor et al. (2010)..... Figure 2 - Interpreted solid geology map of Northern Yorke Peninsula highlighting the Moonta-Wallaroo and Hillside mineralised areas and associated alteration within and around these deposits. Locality of samples chosen for analysis highlighted by coloured circles. Location shown on figure 1. Modified after Conor at al. (2010)..... Figure 3 - Major element geochemical analysis of Wallaroo basement rocks within Central Northern Yorke Peninsula displaying elements that best distinguished lithological groups from one another. a) Wt. % plot SiO ₂ v's MgO. b) Wt. % plot SiO ₂ v's Al ₂ O ₃ . c) Wt. plot SiO ₂ v's TiO ₂ Figure 4 - Probability plots for trace elements within Wallaroo basement rocks on the Central Northern Yorke Peninsula showing concentration of elements in individual lithologies. Black line shows element detection limit. . a) Ba ppm. b) Hf ppm. c) Zr ppm. d) Ta ppm. e) Ce ppm. f) U ppm. g) Th ppm. h) La ppm. i) Cr ppm. j) Co ppm. k) V ppm. l) Ni ppm. m) Sb ppm. n) W ppm. o) Te ppm. p) Cs ppm. Figure 5 - Petrological images from selected samples; 1949789 (a,b,c,d), 1949023 (e,f,g,h), 1960847 (i,j,k,l,m). a) CPL image of siderite vein within a quartz/k-feldspar matrix. b) Reflected light image of same area in (a)) displaying small pyrite and galena growth within siderite veining. c) Micro probe image to highlight the subhedral to euhedral pyrite growth and small (5µm) galena within siderite veining. d) CPL image showing areas of chlorite growth proximal to few larger grains left within sample. e) CPL image displaying amalgamated dolomite/calcite and chlorite growth proximal to sulphides. f) Reflected light image of same area in (e)) which details different areas of sulphide growth . g) CPL – with reflected light image of larger pyrite and amalgamated dolomite/calcite and chorite growth within brecciated cracks within the matrix. h) CPL – with reflected light image displaying chalcopyrite and pyrite (py within cpy) within a single sulphide and sharing a border with chlorite growth. i) CPL image of oxide veining within larger quartz vein within k-feldspar-quartz matrix. j) Reflected light image of same area in (i)) detailing Hem/mag oxide vein and smaller disseminated oxides within k-feldspar-quartz matrix. k) Electron back scatter image highlighting the presence of LREE mineral bastnäsite and its spatial relationship to ilminite and apatite. l) Electron back scatter image of Ce to show evidence of high LREEs residing within bastnäsite. m) Electron back scatter image of La to show evidence of high LREEs residing within bastnäsite. Symbols – Apa – apatite, Bas – bastnäsite, Chl – chlorite,CPL – Cross polarised light, Cpy – chalcopyrite, Dol – dolomite, Gal – galena, Hem – hematite, Ilm – ilmenite, Mag – magnetite, Py – pyrite, Sid – siderite, Qtz – quartz. Mineralogical symbols will be used throughout paper..... Figure 6 - Selected qualitative element maps for sample 1949789 and 1949023 showing back scattered electron image (BSE) Ca, Ce, Cu, Fe, La, Mg, S and Si content. a) Annotated BSE image detailing minerals in sample. b) Qualitative element map for Ca. c) Ce qualitative element map showing small LREE mineral within quartz-k-feldspar matrix. d) Cu qualitative element map. e) Fe qualitative element map highlight Fe content of siderite vein and pyrites within vein. f) La qualitative element map highlighting small LREE mineral within quartz-k-feldspar matrix. g) Mg qualitative element map. h) S qualitative element map highlighting sulphides present in sample. i)	8 9 23 25 28 28
--------------------------------------------------------------------------------------------------------------------------------------------------------------------------------------------------------------------------------------------------------------------------------------------------------------------------------------------------------------------------------------------------------------------------------------------------------------------------------------------------------------------------------------------------------------------------------------------------------------------------------------------------------------------------------------------------------------------------------------------------------------------------------------------------------------------------------------------------------------------------------------------------------------------------------------------------------------------------------------------------------------------------------------------------------------------------------------------------------------------------------------------------------------------------------------------------------------------------------------------------------------------------------------------------------------------------------------------------------------------------------------------------------------------------------------------------------------------------------------------------------------------------------------------------------------------------------------------------------------------------------------------------------------------------------------------------------------------------------------------------------------------------------------------------------------------------------------------------------------------------------------------------------------------------------------------------------------------------------------------------------------------------------------------------------------------------------------------------------------------------------------------------------------------------------------------------------------------------------------------------------------------------------------------------------------------------------------------------------------------------------------------------------------------------------------------------------------------------------------------------------------------------------------------------------------------------------------------------------------------------------------------------------------------------------------------------------------------------------------------------------------------------------------------------------------------------------------------------------------------------------------------------------------------------------------------------------------------------------------------------------------------------------------------------------------------------------------------------------------------------------------------------------------------------------------------------------------------------------------------------------------------------------------------------------------------------------------------------------------------------------------------------------------------------------------------------------------------------------------------------------------------------------------------------------------------------------------------------------------------------------------------------------------------------------------------------------------------------------------------------------------------------------------------------------------------------------------------------------------------------------------------------------------------------------------------------------------------------------------------------------------------------------	--------------------------------

Si qualitative element map showing Si content in background matrix. j) Annotated BSE image detailing minerals in sample. K) Qualitative element map for Ca showing Ca content in dolomite/calcite. l) Ce qualitative element map showing LREE mineral within quartz matrix. m) Cu qualitative element map showing Cu content in chalcopyrite. n) Fe qualitative element map highlighting varying Fe content in sulphides (light and dark blue). o) La qualitative element map highlighting small LREE mineral within quartz matrix. p) Mg qualitative element map shows Mg content in dolomite. q) S qualitative element map highlighting two different sulphides present (Pyrite lighter blue/chalcopyrite dull blue). r) Si qualitative element map showing Si content in background matrix..... 31

Figure 7 - - Selected qualitative element maps for sample 1949023 showing back scattered electron image (BSE) Ca, Ce, Cu, Fe, La, Mg, S and Si content. a) Annotated BSE image detailing minerals in sample. b) Qualitative element map for Ca showing Ca content in dolomite/calcite. c) Ce qualitative element map showing small LREE within quartz matrix. d) Cu qualitative element map showing possible Cu rich area in pyrite inclusion zonation. e) Fe qualitative element map highlighting Fe content in pyrite and chlorite. f) La qualitative element map highlighting possible small monazite within quartz matrix. g) Mg qualitative element map shows Mg content in dolomite. h) S qualitative element map highlighting sulphides present. i) Si qualitative element map showing Si content in background matrix. j) Annotated BSE image detailing minerals in sample. k) Qualitative element map for Ca showing Ca content in dolomite. l) Ce qualitative element map showing small LREE mineral within quartz matrix. m) Cu qualitative element map showing Cu rich area in chalcopyrite. e) Fe qualitative element map highlighting varying Fe content sulphides and chlorite. f) La qualitative element map highlighting small LREE mineral within quartz matrix. g) Mg qualitative element map shows Mg content in dolomite/chlorite. h) S qualitative element map highlighting two sulphides present. i) Si qualitative element map showing Si content in background matrix..... 32

Figure 8 - Selected qualitative element maps for sample 1960847 showing back scattered electron image (BSE) Ca, Ce, Cu, Fe, La, Mg, S and Si content. a) Annotated BSE image detailing minerals in sample. b) Qualitative element map showing Ca content in apatite. c) Ce qualitative element map showing Ce residing within bastnäsite . d) Cu qualitative element map. e) Fe qualitative element map highlighting varying Fe content in Ti/Fe oxide and ilmenite. f) La qualitative element map showing La residing within bastnäsite. g) Mg qualitative element map shows Mg content in variation of Ti/Fe oxide. h) S qualitative element map displaying no sulphides present. i) Si qualitative element map showing Si content in background matrix. j) Annotated BSE image detailing minerals in sample. k) Qualitative element map for Ca showing Ca content in apatite. l) Ce qualitative element map showing Ce residing within bastnäsite . m) Cu qualitative element map. n) Fe qualitative element map highlighting varying Fe content in Ti/Fe oxide and ilmenite. o) La qualitative element map showing La residing within bastnäsite. p) Mg qualitative element map shows Mg content in variation of Ti/Fe oxide. q) S qualitative element map displaying no sulphides present. r) Si qualitative element map showing Si content in background matrix. Symbols – Apa – Apatite, Bas – bastnäsite, ilm – ilmenite 33

Figure 9 – BSE images highlighting where individual spots were analysed within sample 1949023. a) Analysis was undertaken on a larger pyrite with apparent inclusion. 10 spots were analysed; locations numbered recorded in image. b) Analysis undertaken

on area that preserved large primary growth and smaller remobilized growth. 11 spots were analysed (7 chalcopyrite, 4 pyrite); locations numbered recorded in image. c) Analysis was undertaken on chalcopyrite as complete chalcopyrite and area of intergrown chalcopyrite growth. 15 spots were analysed (11 chalcopyrite, 4 pyrite);); locations numbered recorded in image.....	38
Figure 10 - Details how the element values of sulphide grains measured against stoichiometric values for each sulphide. Stoichiometric values for chalcopyrite ($S= 1.08$ mol – $Cu=0.54$ mol) and pyrite ($S= 1.66$ mol – $Fe= 0.83$ mol). Purple dot in plots represents stoichiometric values for each sulphide	38
Figure 11 - Trace element v's Fe plots to determine trace element concentrations within selected sulphide phases. Pyrite data displayed in green; chalcopyrite data displayed in red. a) Ag showing slight elevations in chalcopyrite but mainly hosted in pyrite. b) As showing most samples low in Ag except for two high in pyrite data. c) Au showing the majority of sulphides sampled show no elevations except for one chalcopyrite and 4 pyrite. d) Bi showing majority of Bi readings are hosted in pyrite. e) Cu showing highest concentrations attributed to chalcopyrite and much smaller amounts in pyrite. f) Mo showing readings are hosted within pyrite. g) S showing content hosted within both sulphides. h) W showing concentrations are low from selected samples.....	39
Figure 12 - Geochemical plots of major and trace elements displaying separation of lithological groups. a) MgO v's SiO_2 displaying a negative linear trend showing clear separation of lithological groups. b) TiO_2 v's SiO_2 showing separation of lithological groups, yet displays overlap through TiO_2 concentrations. c) V v's Zr showing separation of lithological groups as ratios of element concentrations.....	42
Figure 13 – Assigned pathfinders elements within Yorke Peninsula basement rocks and their passed criteria a) Ag . b) As. c) Au. d) Bi	45
Figure 14 - Assigned pathfinders elements within Yorke Peninsula basement rocks and their passed criteria a) Ce. b) Cu. c) La. d) Mo	46
Figure 15 - Assigned pathfinders elements within Yorke Peninsula basement rocks and their passed criteria a) S. b) W	47
Figure 16 - – Gridded maps displaying the prospectivity index concentrations across central northern Yorke Peninsula highlighting the Alford Ridge as a potential area for further exploration. Prospectivity index scores: >0.8 is highly significant, 0.6-0.8 is very significant, 0.4-0.6 is significant. Note representative highs along the Alford Ridge achieved a prospectivity score of 0.7.....	56
Table 1 - Representative data of major elements from Wallaroo basement lithologies	14
Table 2 – Representative trace element concentrations for lithological groups.....	15
Table 3 - Stratigraphy of the northern Yorke Peninsula region from (Forbes 2012a) modified after Cowley et al. (2003) with additional information from (Schwarz 2003), (Reid et al. 2008) and Conor et al. (2010).	20
Table 4 - Summary of LA-ICP-MS trace element data for sulphide phases (ppm)	37

INTRODUCTION

Anomalous concentrations of elements that are linked to hydrothermal alteration can be recognised in whole rock geochemical data (eg. Mark et al. (2006); Belperio et al. (2007); Fabris et al. (2013a). Iron oxide-copper-gold (IOCG) mineralisation is demonstrably associated with specific pathfinder elements such as Ag, As, Au, Ba, Bi, Ca, Cd, Ce, Co, Cr, Cs, Cu, F, Fe, K, La, Mn, Mo, Ni, S, Sb, Se, Sn, Te, U and W (Mark et al. 2006; Fabris et al. 2013a; Wang et al. 2013; Hill et al. 2014; Fabris et al. 2013b) and are often preserved within hydrothermal alteration halos that can be linked to mineralisation, and can be used as geochemical vectors towards mineralisation (e.g. Mark et al. 2006; Large and McGoldrick 1998; Wang et al. 2013; Fabris et al. 2013b). Anomalous pathfinder element concentrations may be recognisable within one or more lithologies, and may be host within different mineral species that are linked to processes of hydrothermal alteration (Ismail et al. 2014; Belperio et al. 2007)

The Olympic Copper-Gold Province within the Gawler Craton is host to IOCG mineralisation including the Olympic Dam, Prominent Hill, Carapateena, and Hillside deposits and the historic Moonta/Wallaroo District (Fig. 1). IOCG mineralisation throughout the Gawler Craton has been temporally (Reid et al. 2011) and genetically (Conor et al. (2010) linked to the shallow-intrusives of the ca. 1600-1580 Ma Hiltaba Suite Granites (e.g. Reid et al. 2011; Fanning et al. 2007; Morales-Ruano et al. 2002; Ferris et al. 2002; Skirrow et al. 2002). The geochemical signature of mineralisation associated with the IOCGs in the Gawler Craton Olympic Province and other known IOCGs from around the world have been described in detail, and are attributed to hydrothermal alteration during the mineralising event (Groves et al. 2010; Skirrow et al. 2002; Hitzman 2000; Belperio et al. 2007). The alteration halos are generally

characterised into a number of discrete alteration shells corresponding to elemental distributions. As an example, the alteration signature may progress from regional Na-enriched, K-depleted alteration (Porter 2010) to camp-scale Mn, K, and Ba enriched and Na-depleted alteration to deposit scale alteration enriched in Ag, Au, Bi, Cu, Fe, K, Mo, Sb and U (Ernest Henry:(Mark et al. 2006). Mineralisation within the Moonta Wallaroo District on Yorke Peninsula in the southern Gawler Craton (Figs. 1 & 2) is host within the Palaeoproterozoic Wallaroo Group (e.g. Conor et al. 2010; Zang 2002; Conor 2002), and is considered part of the major IOCG mineralisation event throughout the Gawler Craton (Conor et al. 2010; Both et al. 1993; Reid et al. 2011). However, the pathfinder elements associated with mineralisation in this region and the processes and/or lithological controls affecting the distribution of potential pathfinder elements within mineral phases are poorly understood. The links between whole rock geochemical analysis, element deployment, hydrothermal alteration and mineralisation processes is then discussed and criteria for mineral exploration given.

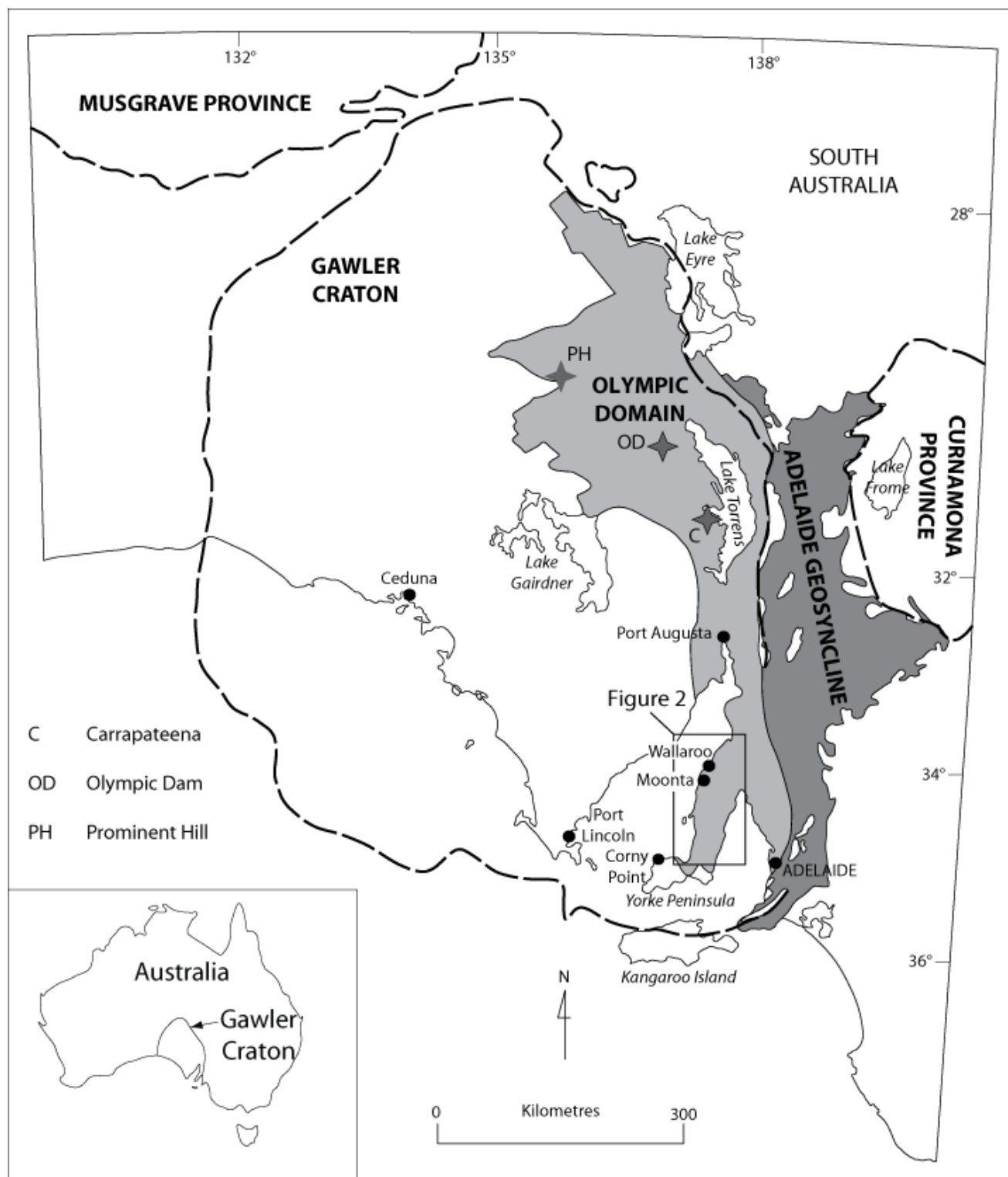


Figure 1 - Geological map showing the Olympic Domain within the Galwer Craton and location of major IOCG mineralisation in the area. The location of the Yorke Peninsula area is also shown in boxed area. Modified after Conor et al. (2010)

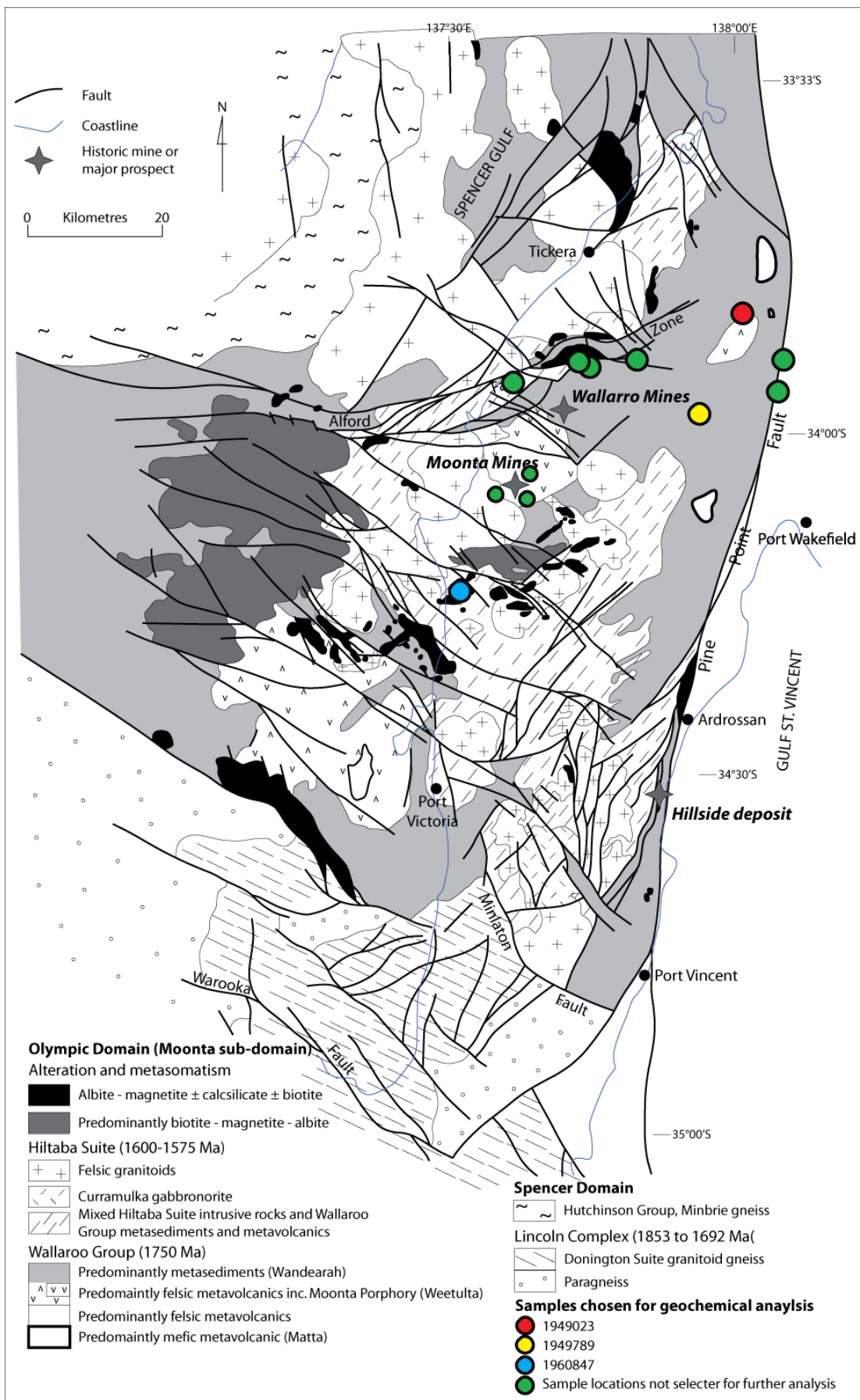


Figure 2 - Interpreted solid geology map of Northern Yorke Peninsula highlighting the Moonta-Wallaroo and Hillside mineralised areas and associated alteration within and around these deposits. Locality of samples chosen for analysis highlighted by coloured circles. Location shown on figure 1. Modified after Conor et al. (2010)

GEOLOGICAL SETTING/BACKGROUND

The central Yorke Peninsula in the southern Gawler Craton, South Australia (Fig. 1) comprises the ~1.75 Ga Wallaroo Group. The Wallaroo Group is dominated by metasedimentary rocks comprising siltstones, calcsilicates, psammites, quartzites and iron-rich sediments of the Wandearah Formation (Conor 1995; Cowley et al. 2003; Zang 2002). Felsic volcanics of the Weetulta Formation and mafic volcanics and amphibolites of the Matta Formation were contemporaneously emplaced with deposition of the metasediments (Cowley et al. 2003).

The Wallaroo Group has undergone metamorphism and multiple stages of deformation. Metamorphic grades range from upper greenschist in the northern Yorke Peninsula to mid amphibolite facies in the central Yorke Peninsula (Conor et al. 2010; Conor 2002; Ferris et al. 2002). The timing of metamorphism of the Wallaroo Group is currently unconstrained. Deformation involved initial generation of isoclinal folds that are suggested to have developed either during the ca. 1730-1690 Ma Kimban Orogeny (Hoek and Schaefer 1988; Ferris et al. 2002; Hand et al. 2007) or during the ca. 1600-1580 Ma Olarian Orogeny (Conor et al. 2010; Conor 1995; Conor 2002). The isoclinal folds are overprinted by a second generation of upright folds that are suggested to have developed at ca. 1600-1580 Ma (Conor et al. 2010; Zang 2002; Carthew 1993)

The Wallaroo Group has been intruded by the Tickera and Arthurton Granites (Fig. 2), which are equivalents to the ca. 1600-1580 Ma Hiltaba Suite Granites (e.g. Creaser and Cooper 1993; Conor 1995; Conor et al. 2010; Cowley et al. 2003). The granites vary across the A-, I- and S-type range and exhibit a considerably diverse grain size and texture (Conor et al. 2010). The granites also show evidence of variation in depth of emplacement from foliated and lineated granites emplaced at depth and non-foliated

granites that contain miarolitic cavities and that are suggested to have been emplaced at shallow crustal levels (Conor et al. 2010). The granites are located proximal to known mineralisation and alteration in the central Yorke Peninsula (Fig. 2) (Reid et al. 2011; Morales-Ruano et al. 2002; Ferris et al. 2002). Magmatically-derived hydrothermal fluid has been suggested as a possible mechanism for intense alteration of rocks in the region, and is used as evidence for the intrusive Hiltaba Suite being linked with mineralisation and alteration of the Wallaroo Group (Conor 1995; Both et al. 1993; Jack 1917).

Mineralisation within the Wallaroo Group on Yorke Peninsula is generally copper dominated and can be separated into two main mineralisation styles. In the Moonta-Wallaroo district (Fig. 2), mineralisation is dominantly vein-style and associated with earlier developed ductile shear zones and intense regional magnetite-bearing alteration (Conor et al. 2010; Zang 2002). Mineralisation in the Moonta-Wallaroo region is hosted within the Moonta Porphyry (Weetulta Formation) and the Doora Schist (Wanderarah Formation). Mineralisation associated with the Hillside Cu Prospect in the eastern Yorke Peninsula (Fig. 2) is hosted within the Wallaroo Group metasediments (Wandearah Formation), and is controlled by north-trending steeply-dipping structures that are associated with the Pine Point Fault Zone (Conor et al. 2010). Mineralisation in the Hillside area appears be skarn-like and have developed higher in the crust as evidenced by hematite replacing magnetite (Conor et al. 2010; Ismail et al. 2014). Alteration in the Moonta-Wallaroo district has been constrained to ca. 1585 Ma from dating of hematite-chlorite-carbonate-sericite mineralisation associated with Moonta-style veins (Skirrow et al. 2007), which supports the interpreted association with emplacement of the 1600-1580 Ma Hiltaba Granite Suite.

METHODS

Logging and sampling

This project utilises the same sample set as used by Forbes et al. (2012), collected in April-July 2012. Samples were taken from open file drill holes across the central Yorke Peninsula, and stored at the Department of State Development Glenside and Moonta Core Library Facilities. Drill holes were selected based on them preserving the intersection of basement and cover, and to give maximum spread and representation of basement lithologies of the region.

Samples taken are composite 1m intervals from the top of basement and from 10-11m beneath the basement-cover interface where possible. In total, 96 samples were taken from the top of basement, and 68 samples were taken from 10-11m below the basement-cover interface.

Geochemistry

All 164 samples were crushed, milled and analysed by Genalysis Laboratories Pty Ltd in Adelaide, South Australia. Samples were analysed using standard XRF ICP-MS, ICP-OES and fire assay techniques. Representative data is shown in (Table. 1,2). Raw data and detail of individual element analysis are given in Appendix A. Data was used to determine background chemistry of various lithologies, to identify potential pathfinder elements that may be used as geochemical vectors towards IOCG mineralisation, and to determine how pathfinder elements partition into particular lithologies and/or minerals.

Petrological analysis and elemental mapping

Petrological analysis and qualitative element maps were used to identify mineral phases that host potential pathfinder elements. Twelve drill core samples were chosen for thin section preparation. Samples were chosen to cover a range of lithologies, preserving the greatest amount of alteration, and being located proximal to known IOCG mineralisation in the area. Samples were prepared to a thickness of 30µm and polished at Adelaide Petrographic Labs, South Australia. Petrographic analysis was undertaken using standard transmitted and reflected light microscopy at the University of Adelaide. Selected areas were used for qualitative element mapping using a XL40 SEM with EDAX Genesis energy dispersive X-ray analyser at Adelaide Microscopy, University of Adelaide. Mapped areas were chosen based on preservation of possible IOCG alteration and mineral phase(s) that would best show deployment of potential pathfinder elements. Maps were produced under conditions of 20.0kV and 95µA using spot size of 6.000nm, dwell time of 250ns at a resolution of 512 x 400 pixels.

Mineral chemistry

Laser-Ablation Inductively-Coupled Mass Spectroscopy (LA-ICP-MS) analysis was undertaken to quantify the concentration of potential pathfinder elements within sulphide minerals. Analysis was undertaken using an Agilent 7500cx with attached New Wave UP-213 laser ablation (LA-ICPMS) system at Adelaide Microscopy. A fluence of 4.5J/cm², laser energy of 45%, repetition rate of 5Hz and spot size of 30µm were used. Concentrations of Fe were set using known stoichiometric concentrations within the sulphides (59.8860 wt.% for pyrite).

Table 1 - Representative data of major elements from Wallaroo basement lithologies

Samp #	Lith type	Samp type	Al2O3%	CaO %	Fe2O3%	MgO %	MnO%	SiO2%	TiO2%
1946904	Amphibolite	Core	14.97	3.65	16.24	5.81	0.17	47.79	1.58
1946905	Amphibolite	Core	15.18	2.8	12.1	5.48	0.1	51.45	1.33
1937386	Carbonate	Cuttings	4.63	20	4.96	14.55	0.31	19.59	0.24
1949043	Carbonate	Drill core	7.48	29.22	2.15	4.35	0.6	24.65	0.21
1949782	Carbonate	Drill core	4.87	18.18	5.01	10.79	1.08	29.12	0.25
1949038	Felsic volcanic	Drill core	11.09	0.13	10.03	5.75	0.01	62.65	0.51
1949054	Felsic volcanic	Drill core	15.65	0.65	12.78	3.85	0.06	56.17	0.63
1960847	Felsic volcanic	Drill core	11.06	0.45	12.67	1.02	0.03	65.57	0.78
1937190	Gneiss	Drill core	14.36	3.49	6.4	2.27	0.09	64.49	0.63
1937617	Gneiss	Cuttings	15.41	2.58	10.32	1.81	0.03	56.78	2.44
1946898	Gneiss	Cuttings	13.25	1.11	3.48	0.24	0.01	70.02	0.63
1937612	Granite	Drill core	12.54	0.92	7.94	1.08	0.03	67.47	0.8
1937615	Granite	Cuttings	12.69	0.88	2.4	0.47	0.01	73.27	0.47
1946900	Granite	Cuttings	14.16	0.12	1.13	0.23	0.01	72.73	0.21
1949011	Mafic extrusive	Drill core	1.02	26.43	4.12	17.73	0.98	5.26	0.08
1949020	Mafic extrusive	Drill core	15.3	1.53	10.58	4.97	0.18	53.59	1.58
1949802	Mafic intrusive	Drill core	12.72	7.98	9	6.83	0.41	44.98	1.14
1937185	Mafic intrusive	Drill core	14.74	8.36	11.2	5.63	0.19	44.05	1.28
1949819	Mafic intrusive	Drill core	13.34	6.89	15.04	5.92	0.21	47.83	1.29
1949812	Metasomatite	Drill core	16.95	0.58	6.84	5.06	0.01	56.3	0.69
1949780	Metasomatite	Drill core	11.43	4.54	12.59	3.2	0.15	58.88	0.51
1949813	Metasomatite	Drill core	9.08	13.35	3.53	3.7	0.17	53.45	0.39
1960886	Sediment	Drill core	16.11	0.28	5.74	3.23	0.03	63.85	0.65
1949023	Sediment	Drill core	14.26	2.87	5.43	2.71	0.15	60.16	0.59
1949789	Sediment	Drill core	15.74	0.29	5.37	3.25	0.01	63.69	0.6

Table 2 – Representative trace element concentrations for lithological groups

Samp #	Lith type	Samp type	Au ppb	Ag ppm	As ppm	Ba ppm	Bi ppm	Ce ppm	Co ppm	Cr ppm	Cs ppm	Cu ppm	Hf ppm	La ppm	Mo ppm	Ni ppm	S ppm	Sb ppm	Ta ppm	Te ppm	Th ppm	U ppm	V ppm	W ppm	Zr ppm	
1946904	Amphibolite	Core	13	0.35	52.4	183.8	0.04	25	79.8	69	11.6	74	2.8	13.7	2.1	68	128	0.16	0.5	0.05	2.9	6.08	381	0.05	97	
1946905	Amphibolite	Core	2	0.24	9.7	245.7	0.08	23.9	44.6	154	4.95	216	3.1	12.2	1.1	65	171	0.17	0.4	0.05	2.83	7.14	349	2	110	
1937386	Carbonate	Cuttings	0.5	0.51	197.2	153.6	0.59	33.9	23.9	21	1.64	481	1.5	21.8	5.6	12	99	1.45	0.4	0.2	6.6	2.36	54	0.05	73	
1949043	Carbonate	Drill core	1	0.025	3	465.6	0.005	36.8	3.7	38	3.33	180	2	18.7	0.4	20	25	0.15	0.7	0.05	10.4	1.61	18	1	66	
1949782	Carbonate	Drill core	0.5	1.11	85.8	218.1	0.32	44.6	58.1	39	1.56	216	2.5	22.9	2.1	31	8616	1.1	0.5	0.07	7.83	5.38	44	1	94	
1949038	Felsic volcanic	Drill core	0.5	0.26	19.9	97.3	0.13	41.1	29.2	10	0.92	173	14	20.3	3.8	26	25	0.16	3.6	0.18	36.12	8.96	14	1	519	
1949054	Felsic volcanic	Drill core	6	0.28	35.9	442	0.76	59.5	24.3	83	6.97	201	3.7	28.3	0.7	26	894	0.29	1.3	0.09	14.05	2.88	116	4	134	
1960847	Felsic volcanic	Drill core	2	0.025	9	767.1	0.005	540.3	47.9	10	0.82	117	17.3	280.	7	6.1	100	57	0.52	3.8	0.2	27.12	21.0	52	1	633
1937190	Gneiss	Drill core	0.5	0.025	0.5	751.7	0.03	95.6	15.4	53	2.25	16	7.4	48.3	1.3	25	86	0.02	1.6	0.1	10.24	2.25	77	0.05	283	
1937617	Gneiss	Cuttings	0.5	0.06	0.5	102.2	0.07	296.6	25	35	1.59	76	5.4	150	0.7	14	324	0.24	1.4	0.05	13.95	8.13	432	2	206	
1946898	Gneiss	Cuttings	0.5	0.18	1.9	822.3	0.14	231.3	4.3	172	3.01	17	13.4	136.	5	0.9	5	168	0.07	2.8	0.07	22.5	7.29	32	3	510
1937612	Granite	Drill core	0.5	0.11	0.5	509.9	0.005	69.8	16.6	10	1.24	25	13	34.4	0.6	9	25	0.02	2.1	0.05	14.44	2.4	45	0.05	489	
1937615	Granite	Cuttings	0.5	0.11	4.1	449.9	0.08	19.2	2.3	88	1.08	7	8.8	10.1	1.9	3	200	0.49	1.8	0.06	13.27	2.07	56	2	322	
1946900	Granite	Cuttings	0.5	0.025	5.8	618.1	0.07	1345.8	1.6	97	2.78	15	6.2	742.	4	0.5	3	257	0.27	3.5	0.05	196.29	25.0	32	3	200
1949011	Mafic extrusive	Drill core	0.5	0.69	33.7	87	0.17	15.1	19	38	0.26	602	0.5	7.8	2	7	6551	0.94	0.1	0.05	2	2.35	16	0.05	19	
1949020	Mafic extrusive	Drill core	1	0.31	15.9	151.3	0.81	39.1	21.8	101	0.42	554	2.8	16.7	1.4	33	1285	0.75	0.7	0.05	4.05	4.7	361	13	99	
1949802	Mafic intrusive	Drill core	12	0.025	63	140.1	0.39	73.9	47.6	219	3.83	331	3	40.6	0.4	108	2064	1.18	0.6	0.05	2.28	1.65	251	11	106	
1937185	Mafic intrusive	Drill core	0.5	0.025	6	104	0.07	14.7	32.6	265	1.02	68	2.5	7.1	0.8	61	565	0.22	0.5	0.1	1.85	0.83	318	3	91	
1949819	Mafic intrusive	Drill core	32	3.1	44	186.3	1.49	20.9	64.1	158	4.33	1099	5	2.6	9	0.7	90	1174	1	0.5	0.1	2.56	1.67	314	3	88
1949812	Metasomatite	Drill core	0.5	0.025	8	555.1	0.13	121.3	19.1	71	3.2	25	10.4	88.3	0.05	39	176	0.23	1.7	0.1	26.06	6.7	84	2	368	
1949780	Metasomatite	Drill core	0.5	0.06	16.7	14.6	0.05	37.8	10.9	58	0.44	34	5.8	12.3	0.2	24	25	0.18	1.3	0.08	35.83	7.94	123	1	212	
1949813	Metasomatite	Drill core	2	0.025	8	233.1	0.005	112.6	35.5	54	1.88	33	6.6	60.9	0.8	10	954	0.34	1.2	0.05	16.06	5.1	40	0.05	245	
1960886	Sediment	Drill core	6	0.025	6	602	0.19	69.5	18.3	72	9.79	32	4.5	35.9	0.5	56	156	0.58	1.4	0.05	17.83	3.33	153	15	166	
1949023	Sediment	Drill core	0.5	0.55	30.7	694.1	12.55	115.7	34.1	69	3.77	545	4.6	56.4	4.4	15	1044	9	1.63	1.5	0.19	16.59	3.45	155	10	170
1949789	Sediment	Drill core	1	0.06	17.8	613.6	0.25	88.5	17.5	71	7.28	10	4.1	46.8	0.2	32	124	0.34	1.5	0.15	18.17	2.69	124	5	143	

OBSERVATIONS AND RESULTS

Logging and sampling

One hundred and sixty four drill holes were logged by (Forbes 2012b) to characterise the broad lithologies across Yorke Peninsula. Lithologies logged included granites, felsic volcanics, mafic volcanics, metasediments, gneiss and metasomatite (Table. 3). General lithological characteristics such as mineralogy, grain size, alteration and the degree of weathering were documented. Logging was undertaken to cover an area that incorporated the cover/basement relationship and to a depth of 10-12m into basement lithologies if core samples were available. Samples for geochemical analysis were taken from 1m of composite core taken from either 1m into basement or 10-12m into basement lithologies. 135 samples came from $\frac{1}{4}$ or $\frac{1}{2}$ core depending on availability from the core library and 29 samples were from rock chips. Further detailed analysis of each identified lithology was undertaken in this study to characterise the separate rock types and geochemical relationships.

GRANITES

Granites generally consist of medium to coarse grained quartz, k-feldspar, and plagioclase with varying small amounts of (<15%) biotite, (<5%) amphibole and minor mafics (<10%). Samples come from the Tickera and Arthurton Granites (Table. 3). The Tickera Granite is coarser grained (~30% quartz up to 30mm; ~50% K-feldspar/Plagioclase up to 50mm) with an overall pinkish granitic appearance. The Tickera Granite displays small amounts weathering. The Arthurton Granite has a finer grained (~40% quartz 5-20mm, ~45% K-feldspar/Plagioclase 5-20mm) ademellite/monzonitic composition, more whiteish pink in colour and is highly

weathered. Both granites preserve a diverse range of alteration including hematite/magnetite and epidote-chlorite alteration. Minor sulphides (<2%) as pyrite and chalcopyrite were occasionally observed throughout the granites.

METASEDIMENTS

Metasediments cover a large array of rock types from the Wandearah Formation (Table. 3) including sandstones, siltstones, mudstones, clays, psammites, dolomites and limestones. The metasediments can broadly be separated into a sediment and carbonate component. The dominant sedimentary rock type is siltstone with many samples appearing brecciated. The siltstone is generally laminated, light or dark grey in colour and shows variation of pigment within the greys (red/blue/green). Grainsize is fine grained ranging from (0.25mm – 1mm). The dominant carbonate rock type is dolomite which can be siliceous or preserve fine laminations. The main alteration observed within the dominant sedimentary rock units is Fe and carbonate with lesser chlorite and epidote. Oxides are commonly hematite or magnetite and small amounts of malachite. Sulphides are very fine grained within carbonate veins therefore difficult to determine composition.

FELSIC VOLCANICS

Felsic volcanics form part of the Weetulta Formation and include the Moonta Porphyry (Table. 3). Samples are generally porphyritic or metaporphyritic, fine to medium grained (0.25-2 mm) and pink/grey in colour. Most felsic volcanics preserve strong hematite/magnetite alteration with lesser of chlorite/potassium and sericite alteration. Fe (hematite) alteration appears to be more prominent in samples proximal to the Moonta Porphyry member.

MAFIC VOLCANICS

Mafic volcanics from the Matta Formation (Table. 3) are comprised of amphibolites, basalts, dolerites or diorites with minor gabbro. Dolerite is the dominant rock type within the rock unit. Mineralogy is generally (~50% plagioclase, ~40% pyroxene/amphibole ± biotite). Samples are very fine to medium grained (0.25-3mm), show euhedral to subhedral grain shape and dark green in colour. Carbonate veining is seen throughout samples with minor chlorite/epidote alteration. Fe staining and alteration is consistently seen throughout samples. Pyrite and chalcopyrite are present as disseminated sulphides and within carbonate and quartz veins.

GNIESS

Gneisses are dominantly comprised of (~15%) potassium-feldspar, (~20%) quartz and (~15%) plagioclase. Samples contain variable amounts of hornblende (20-70%) or biotite (20-50%) and depending on which mineral is most dominant the gneisses is categorised as either a hornblende or biotite bearing gneiss. Samples are generally fine to coarse grained, pinkish coloured and with varying amounts of weathering seen across samples. Pegmatite veining up to ~10mm is common through samples. Alteration is restricted to Fe alteration. No sulphides were observed in the samples.

METASOMATITE

The metasomatite samples are from the Oorlano Metasomatite (Table. 3). Mineralogy is generally (~25%) quartz; ~1mm, (~50%) k-feldspar; 1-2mm and (~25%) mafics which are comprised of biotite-magnetite-amphibole. Most samples show a striking green/red

banded appearance. The red/pink altered layer shows feldspar/ potassic/albitic alteration and green layer is dominated by quartz and feldspar and green appearance possibly due to epidote/chorite/amphibolite alteration. Carbonate veining up to 10mm is common throughout samples. Fe alteration is seen as hematite and magnetite and minor sulphides (<2%) as pyrite and chalcopyrite. Logging data determined that samples generally altered siltstones or calcsilicates from the metasediments but determining the true protolith of the metasomatite is difficult to determine as the formation has been so heavily altered.

Table 3 - Stratigraphy of the northern Yorke Peninsula region from (Forbes 2012a) modified after Cowley et al. (2003) with additional information from (Schwarz 2003), (Reid et al. 2008) and Conor et al. (2010).

Group/Suite	Formation	Member	Lithological description
Alteration	Magnetite alteration?		Albite-magnetite ± calcsilicate ± biotite
	Oorlano Metasomatite		Skarn-like metasomatic rock. Calcsilicate (feldspar, scapolite, actinolite, diopside, carbonate, phlogopite, epidote, magnetite, pyrite), feldspathic (albite>>microcline, lesser opaques and calcsilicate minerals) and iron-rich (magnetite>>hematite, feldspar, biotite, pyrite) metasomatite; precursor lithology usually obliterated or uncertain. Local kaolin alteration (± siderite ± alunite ± pyrite ± chalcocite) [late phase of metasomatism??]
Hiltaba Suite (ca. 1600-1580 Ma)	Tickera Granite		Variable I- and S-type granitoids; monzogranite, quartz monzonite, leucotonalite, commonly intensely deformed
	Arthurton Granite		A-type granite, monzogranite, quartz monzonite, generally undeformed
	Curramulka Gabbronorite		Gabbronorite comprising plagioclase, clinopyroxene (augite), orthopyroxene, hornblende, biotite ± quartz or orthoclase.
Hiltaba Suite?	Bute Metadolerite		Metadolerite comprising albited and sericitised plagioclase laths, amphibole, biotite and/or chlorite replacing interstitial pyroxene, accessory epidote, opaques, carbonate, seromite and sphene, ophitic texture. Mostly massive, locally sheared. Locally metagabbro with feldspar glomerophenocrysts.
Wallaroo Group (ca. 1750 Ma) Metasediments, felsic and mafic metavolcanics and minor associated subvolcanic intrusives	Wandearah Formation		Clastic and chemical metasediments.
		Wokurna Member	Dominantly laminated muscovite-bearing argillite interlayered with quartz siltstone, occasionally graded, minor iron-oxide, carbonate, albite and calcsilicate, pale green and buff reduction spotting common. Locally becomes more siltstone- to sandstone-rich with disseminated magnetite and hematite as accessory phases; or chloritic metasediments, carbonaceous or calcareous. Includes thin calcsilicate, carbonate and albitic units.
		Delken Member	Cherty, finely laminated, layer parallel albite-quartz metasediment, trace amphibole, magnetite and calcite.
		New Cornwall Member	Metasiltstone and chemical sediments, often layered. Variable proportions of calcsilicate, minor limestone and dolomite, laminated albite, layered albite-magnetite ironstone, graphitic and calcareous metasiltstone, argillite and metasandstone.
		Doora Member	Schistose, medium-grained, thinly planar layered to laminated metasediments of variable composition including quartz-plagioclase rich, iron-rich and calcsilicate metasediments (e.g. quartz-amphibole (actinolite and cummingtonite)-biotite ± magnetite calcsilicate; biotite-quartz-albite pelite; quartz-albite-magnetite-biotite iron formation). Minor marble and quartz-albitite.
		Aagot Member	Planar to bedded micaceous metasandstone or psammite, sandy or tuffaceous argillite with minor interlayered calcsilicate and albitic rocks. Locally includes volcanoclastic conglomerate.
	Weetulta Formation		Felsic volcanics - porphyritic rhyodacite, dacite, latite with bedded tuff and tuffaceous siltstone.
		Mona Volcanics Member	Acid porphyry (dacite to rhyodacite) with plagioclase phenocrysts (altering to K-feldspar or sercite) with lesser quartz and altered ferromagnesian minerals in quartz + plagioclase or flow banded K-feldspar ± chlorite ± quartz ± Fe-oxides, locally amygdaloidal and spherulitic; and thinly bedding tuffaceous siltstone to tuff with local microphenocrysts, minor crystal tuff and lapilli tuff.
		Moonta Porphyry Member	Plagioclase-phyric rhyodacite locally showing volcanic or ignimbritic characteristics. Plagioclase phenocrysts altered to K-feldspar.
		Wardang Volcanics Member	Plagioclase-phyric rhyodacite, dacite and latite, locally rhyolite; locally preserves flow banding, flow folding, columnar cooling structures and hyaloclastics.
	Matta Formation		Mafic volcanics - amphibolite intrusives and gneisses
		Willamulka Metabasalt Member	Fine- to medium-grained, massive to amygdaloidal basalt, replaced by albite, chlorite, biotite, amphibole, calcite, quartz and accessory minerals. Amygdales filled with quartz, chlorite and/or carbonate.
		Renowden Metabasalt Member	Basalt with crystals (phenocrysts?) of hornblende and plagioclase. Locally contains quartz-rich vesicles that may be scoriascous texture.
		Wandilla Amphibolite Member	Amphibolite and layered plagioclase-hornblende-biotite rock.
Donington Suite (ca. 1850 Ma)		Intrusives of variable composition including gabbro, gabbronorite, charnockite, and granodiorite to alkali granite.	

Whole Rock Geochemistry

Major element geochemical analyses was undertaken to determine lithogeochemical relationships within the data. Relationships were assessed to determine geochemical signatures that can be used to distinguish the lithologies from one another, and to determine background geochemistry. Trace element analyses was used to determine which elements preferentially partition into certain lithological groups.

MAJOR ELEMENT CHEMISTRY

Granites characteristically show high SiO₂ (>65 wt.%) and low MgO (<2wt.%), Al₂O₃ concentrations between (11-15 wt.%) and TiO₂ (<0.8 wt.%) (Fig. 3a,b,c). The geochemical data for granites is consistently clustered (Fig. 3a,b,c). Felsic volcanics show similar characteristics to the granites with respect to SiO₂ between (65-77 wt.%) and Mg (< 2.wt%) (Fig. 3a), but show broader Ti and Al composition (Fig. 3b,c).

Mafics lithologies are distinguished by their typically high TiO₂ contents (>0.9 wt.%) and low SiO₂ concentrations between (55-45 wt.%) (Fig. 3a,c).

Metasediments show a very broad range of SiO₂ (20-70 wt.%), Al₂O₃ (0.10-1.25 wt.%) and TiO₂ (2-22 wt.%), likely due to them being a mixture of sandstones, clays and carbonates. The formation was separated out into a sediment and carbonate component (Fig. 3a,b,c). The sediments are best distinguished by SiO₂ (50-67 wt.%), TiO₂ (0.4 – 0.7 wt.%) and MgO (2-5 wt.%) concentrations that plot between the felsic and mafic data (Fig. 3a,b,c). Carbonate component displays the least overlap between lithologies and was best discriminated by SiO₂ (<40 wt.%) (Fig. 3a) and Al₂O₃ (<9 wt.%) (Fig. 3b).

As the protolith of the metasomatite is relatively unknown and could be derived from either the metasediments or possibly the Moonta porphyry member within the Yorke Peninsula basement rocks (Cowley et al. 2003; Conor et al. 2010), the data shows variable chemistry as it is highly altered. The alteration seen will depend on fluids involved within the alteration processes and the protolith chemistry, and will in turn dictate the chemistry of individual samples. The metasomatite data overlaps with data from most other basement lithologies apart from the carbonate component of the sedimentary unit (Fig. 3a,b,c). Broad element concentrations for the metasomatite as follows; SiO_2 (35-80 wt.%), MgO (1-12 wt.%) and Al_2O_3 (2-21 wt.%) (Fig.4-a,b). The only preferential grouping of data is displayed in (Fig. 3c) with TiO_2 concentrations between (0.25-0.75 wt.%).

The gneissic samples show a broad range in data which overlaps with other lithologies but preferentially towards high SiO_2 (50-77 wt.%) and low MgO (1-5 wt.%) concentrations (Fig. 3a). Al_2O_3 data displayed a range between (11-20 wt.%) which is similar for felsic, sediment and mafic derived lithologies but data strays away from the carbonate component of the metasediments (Fig. 3b). Gneissic TiO_2 content displays the largest variation over all lithologies. Data ranges from (0 – 2.5 wt. %) which incorporates all lithological groups within this range (Fig. 3c).

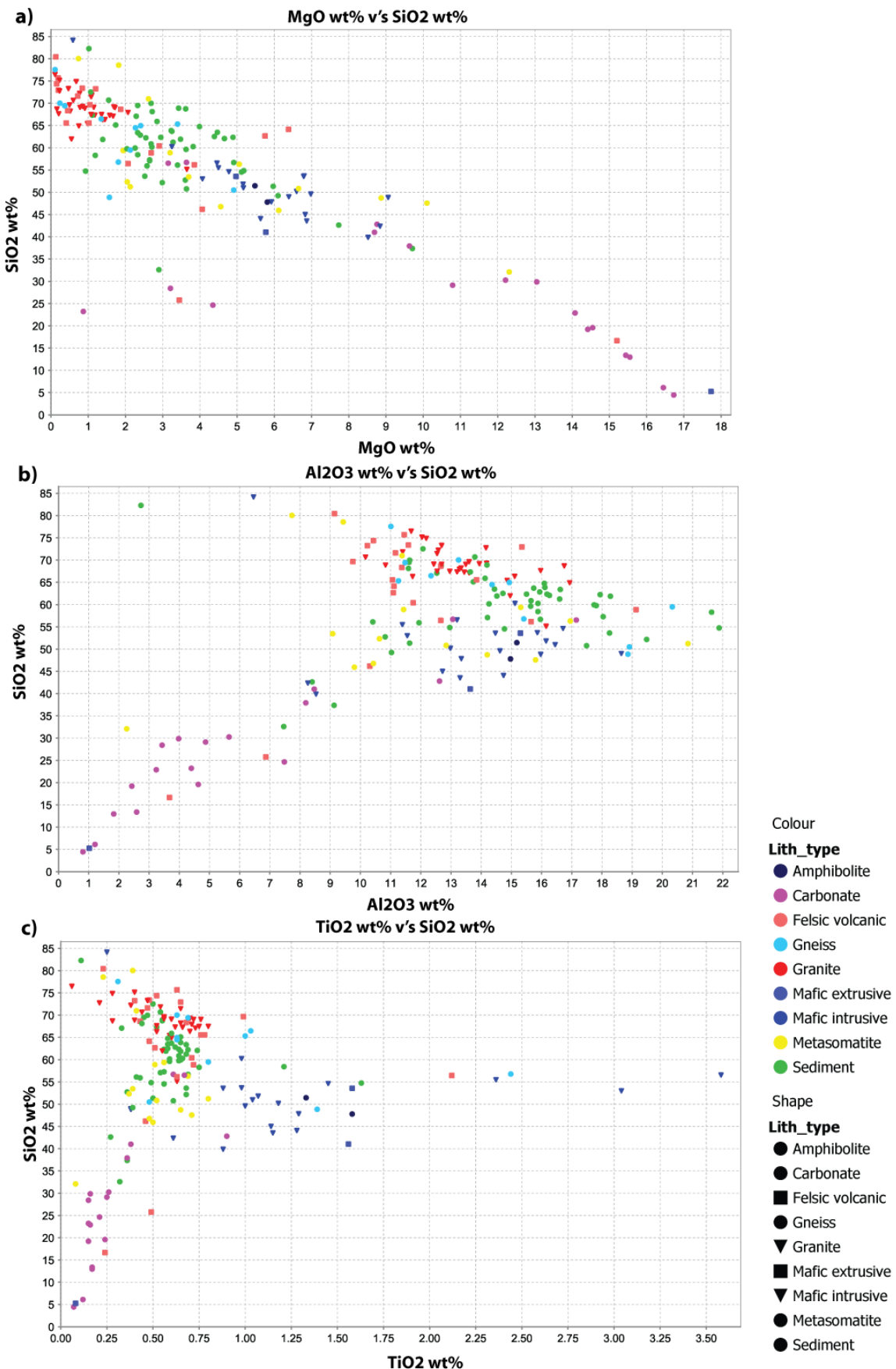


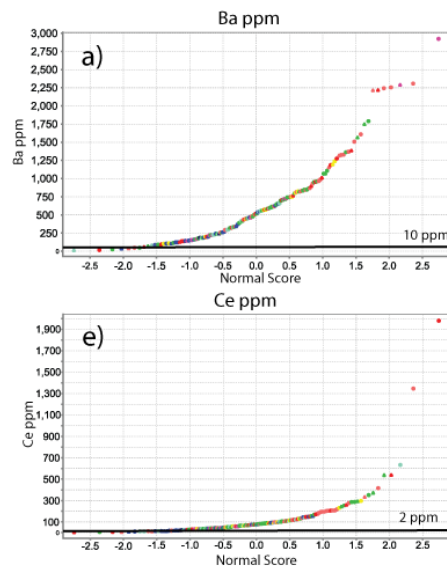
Figure 3 - Major element geochemical analysis of Wallaroo basement rocks within Central Northern Yorke Peninsula displaying elements that best distinguished lithological groups from one another. a) Wt. % plot SiO₂ v's MgO. b) Wt. % plot SiO₂ v's Al₂O₃. c) Wt. plot SiO₂ v's TiO₂

TRACE ELEMENT CHEMISTRY

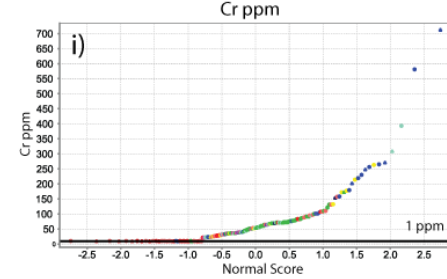
Elements associated with IOCG mineralisation can preferentially be hosted within certain lithological units, therefore display high concentrations of that element when compared to other lithologies. Potential pathfinder elements Ba, Ce, La and U are preferentially hosted within felsic dominated lithologies (felsic volcanics and granites) (Fig. 4a,e,f,h). Mafic dominated lithologies (amphibolite, mafic intrusive, mafic extrusive) host high concentrations of Cr, Co and Ni compared to other lithological groups (Fig. 4i,j,k) and the metasedimentary unit preferentially host high concentrations of Sb, W, Te and Cs (Fig. 4m-p). Other elements not directly associated with IOCGs can also be preferentially hosted within certain lithological units. Hf, Nb, Th and Zr shows high concentrations within felsic dominated units (Fig. 4b,c,d,g) and mafic units hosts high concentrations of V (Fig. 4k).

The metasomatite and gneiss show minimal preferential partitioning of any one trace element. This is possibly attributed to the unknown protoliths, the varying levels of alteration seen throughout the lithologies and how the alteration will manifest in different lithological groups.

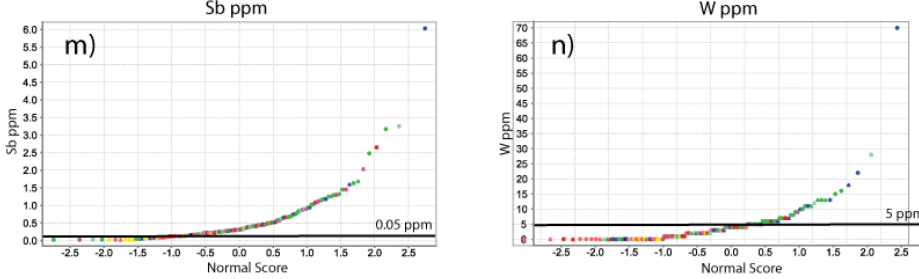
Felsic volcanics and Granites



Mafics



Metasediment



- Colour**
- | Lith_type |
|-----------------|
| Amphibolite |
| Carbonate |
| Felsic volcanic |
| Gneiss |
| Granite |
| Mafic extrusive |
| Mafic intrusive |
| Metasomatite |
| Sediment |

Figure 4 - Probability plots for trace elements within Wallaroo basement rocks on the Central Northern Yorke Peninsula showing concentration of elements in individual lithologies. Black line shows element detection limit. a) Ba ppm. b) Hf ppm. c) Zr ppm. d) Ta ppm. e) Ce ppm. f) U ppm. g) Th ppm. h) La ppm. i) Cr ppm. j) Co ppm. k) V ppm. l) Ni ppm. m) Sb ppm. n) W ppm. o) Te ppm. p) Cs ppm.

Petrology

Twelve core samples were chosen for petrological analyses. Samples were chosen based on preservation of sulphide/oxide phase and if samples originated from close proximity to known mineralisation. Of these twelve samples, three samples (1949023, 1949789, 1960847) were chosen for further petrological analyses as they best preserved alteration phases and show elevated concentrations potential IOCG pathfinder elements. Sample localities given in (Fig. 2)

SAMPLE 1949789 -

Sample 1949789 is a metasediment (psammite) from the Wandearah Formation. The sample is dominated by a quartz and k-feldspar rich matrix (up to 90% of the whole rock). Thin siderite veins (~0.5mm) are preserved throughout sample which appears to be late staged and cross cutting the laminations within the quartz/k-feldspar matrix. Angular inclusions of small (~50µm) pyrite grains are preserved within the thicker portions of the veining (Fig. 5b,c). Small (<5 µm) galena and disseminated barite were also seen to be growing within the thicker zones of siderite veining (Fig. 5c). Minor chlorite and carbonate (dolomite or calcite) grains were observed proximal to siderite veining, hematite staining and an unidentified and highly weathered mineral (Fig. 5d)

SAMPLE 1949023 -

Sample 1949023 is a metasediment (siltstone) from the Wandearah Formation. The sample contains large up to 3mm angular sulphides within a brecciated quartz rich matrix (Fig. 5e-h). Sulphides are dominated by chalcopyrite and pyrite. Chalcopyrite and pyrite are present as large (~3mm) grains (Fig. 5e-g), smaller growths along the

edges of carbonates (Fig. 5e,f) and areas of pyrite growth within a larger chalcopyrite grain (Fig. 5h). Dolomite and chlorite are observed as infill within brecciated zones, and are commonly in contact with sulphides (Fig. 5e,g,h). Dolomite grains are subhedral to euhedral (~1mm). Chlorite grains vary from large (5mm x 2mm) clustered growths to small thin strips (<0.5mm) growing within the brecciated matrix (Fig. 5e-h). Most larger sulphide grains are in contact with chlorite (Fig. 5e-h). Thin (<0.5mm) carbonate veins are also observed in areas to be occupying the brecciated cracks (Fig. 5g).

SAMPLE 1960847 –

Sample 1960847 is a felsic volcanic from the Weetulta Formation. The sample comprises (~70% quartz/k-feldspar matrix). Veins up to 5mm thickness comprising of quartz (~1mm) with Fe-oxides cross cut the sample (Fig. 5i,j). Oxides are predominately hematite with lesser magnetite. Oxides occur within the quartz veins as thin (~1mm) veins (Fig. 5i,j). Smaller disseminated oxide grains (~10µm) are seen throughout the quartz/k-feldspar matrix (Fig. 5i,j). Ilminite and apatite were observed as small (~200µm) grains growing within the quartz-oxide vein but not directly proximal to the oxide alteration (Fig. 5k). Light rare earth minerals are occasionally preserved through the sample (Fig. 5k,l,m). The LREEs are host within bastnäsite and was found to be occupying areas proximal to ilminite and apatite (Fig. 5k,l,m).

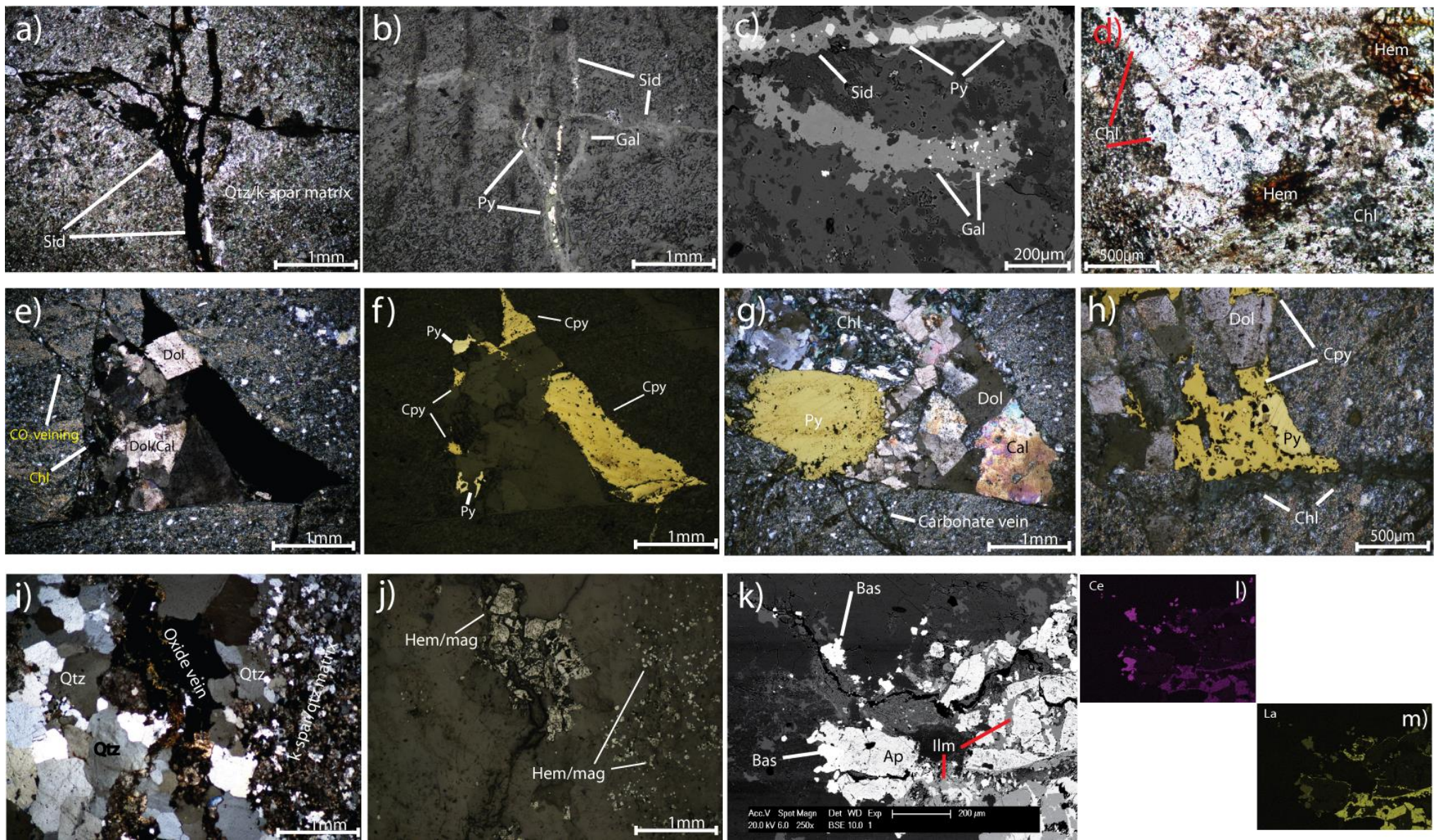


Figure 5 - Petrological images from selected samples; 1949789 (a,b,c,d), 1949023 (e,f,g,h), 1960847 (i,j,k,l,m). a) CPL image of siderite vein within a quartz/k-feldspar matrix. b) Reflected light image of same area in (a) displaying small pyrite and galena growth within siderite veining. c) Micro probe image to highlight the subhedral to euhedral pyrite growth and small ($5\mu\text{m}$) galena within siderite veining. d) CPL image showing areas of chlorite growth proximal to few larger grains left within sample. e) CPL image displaying amalgamated dolomite/calcite and chlorite growth proximal to sulphides. f) Reflected light image of same area in (e) which details different areas of sulphide growth . g) CPL – with reflected light image of larger pyrite and amalgamated dolomite/calcite and chorite growth within brecciated cracks within the matrix. h) CPL – with reflected light image displaying chalcopyrite and pyrite (Py within Cpy) within a single sulphide and sharing a border with chlorite growth. i) CPL image of oxide veining within larger quartz vein within k-feldspar-quartz matrix. j) Reflected light image of same area in (i)) detailing Hem/mag oxide vein and smaller disseminated oxides within k-feldspar-quartz matrix. k) Electron back scatter image highlighting the presence of LREE mineral bastnäsite and its spatial relationship to ilminite and apatite. l) Electron back scatter image of Ce to show evidence of high LREEs residing within bastnäsite. m) Electron back scatter image of La to show evidence of high LREEs residing within bastnäsite. Symbols – Apa – apatite, Bas – bastnäsite, Chl – chlorite, CPL – Cross polarised light, Cpy – chalcopyrite, Dol – dolomite, Gal – galena, Hem – hematite, Ilm – ilmenite, Mag – magnetite, Py – pyrite, Sid – siderite, Qtz – quartz. Mineralogical symbols will be used throughout paper

Element Mapping

Qualitative elemental maps were collected from three samples (1949023, 1949789/1960847) that were identified to preserve elevated concentrations of trace elements that may be potential pathfinders towards IOCG mineralisation (Ag, Al, As, Au, Bi, Ca, Ce, La, Mg, Mo, Na, Si, S, W and Zn). Six areas within samples were mapped to target oxide veining and sulphides to characterise potential zoning and identify potential LREE hosts. Representative maps are given in (Fig. 6,7,8). All maps given in Appendix B.

SAMPLE 1949789

Sample was used to map an area preserving Fe alteration within a k-feldspar/quartz matrix. Siderite veining is highlighted by elevations of Fe (Fig. 6e). Fine grained sulphides within the oxide veining are highlighted on the S map (Fig 6h), and are coincident with elevated Fe (Fig. 6e) and no Cu (Fig. 6d), indicating they are pyrite. Elevated regions of La and Ce indicate fine-grained LREE bearing mineral(s) occur throughout the sample.

SAMPLE 1949023

Sample preserves pyrite and chalcopyrite as both primary and secondary growth. Element maps show the pyrite is highlighted by elevated Fe and no Cu and the chalcopyrite by coincident lower Fe and higher Cu (Fig. 6m,q)(Fig. 7d,h,m,q). Ce and La maps show small LREE highs within the chlorite/dolomite/quartz matrix surrounding the sulphides (Fig. 6l,o)(Fig. 7c,f,l,o). Map (Fig. 7a) displays inclusion-rich areas within the pyrite structure. Inclusions appear to be zoned with areas of barren

clean pyrite and areas of inclusion rich growth. Zoned areas are (~100µm) and alternate across the pyrite. Inclusions within the inclusion rich areas range from very small (~1µm) to larger (~20µm) elongated cracks that have a brecciated appearance (Fig. 7a).

SAMPLE 1960847

Sample preserves sporadic oxide alteration within a quartz rich alteration vein. High Fe content is hosted within an Fe-Ti oxide with variable Fe and Ti content (Fig. 8e,n). Mapping identified LREE-rich areas are host within the LREE mineral bastnäsite (Fig. 8a,c,f,j,l,o). Bastnäsite is hosted within the oxide/quartz veining and has a close spatial relationship to the Fe-Ti oxide and apatite growth. (Fig. 8a,b,c,e,f,j,k,l,n,o)

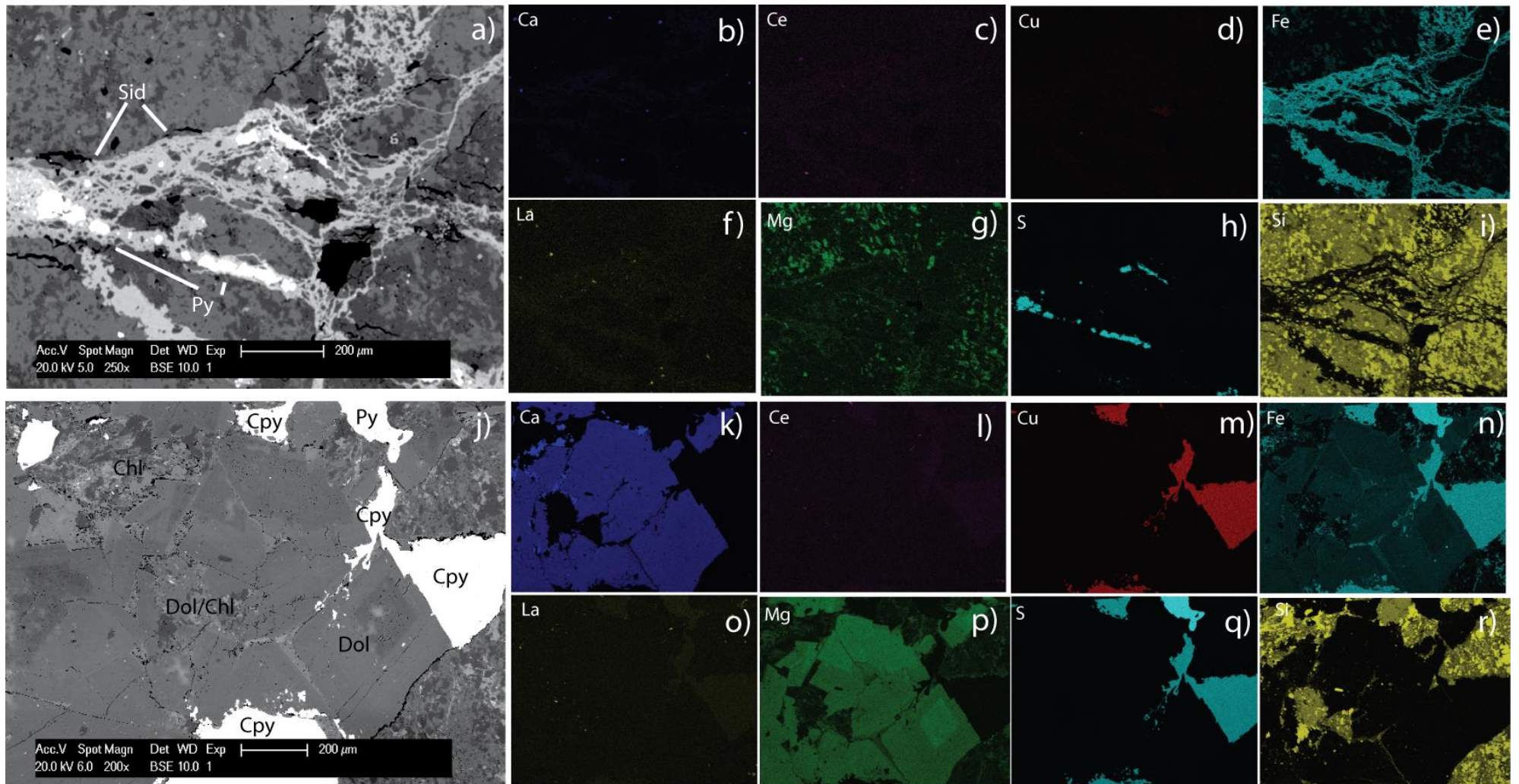


Figure 6 - Selected qualitative element maps for sample 1949789 and 1949023 showing back scattered electron image (BSE) Ca, Ce, Cu, Fe, La, Mg, S and Si content. a) Annotated BSE image detailing minerals in sample. b) Qualitative element map for Ca. c) Ce qualitative element map showing small LREE mineral within quartz-k-feldspar matrix. d) Cu qualitative element map. e) Fe qualitative element map highlight Fe content of siderite vein and pyrites within vein. f) La qualitative element map highlighting small LREE mineral within quartz-k-feldspar matrix. g) Mg qualitative element map. h) S qualitative element map highlighting sulphides present in sample. i) Si qualitative element map showing Si content in background matrix. j) Annotated BSE image detailing minerals in sample. k) Qualitative element map for Ca showing Ca content in dolomite/calcite. l) Ce qualitative element map showing LREE mineral within quartz matrix. m) Cu qualitative element map showing Cu content in chalcopyrite. n) Fe qualitative element map highlighting varying Fe content in sulphides (light and dark blue). o) La qualitative element map highlighting small LREE mineral within quartz matrix. p) Mg qualitative element map shows Mg content in dolomite. q) S qualitative element map highlighting two different sulphides present (Pyrite lighter blue/chalcopyrite dull blue). r) Si qualitative element map showing Si content in background matrix.

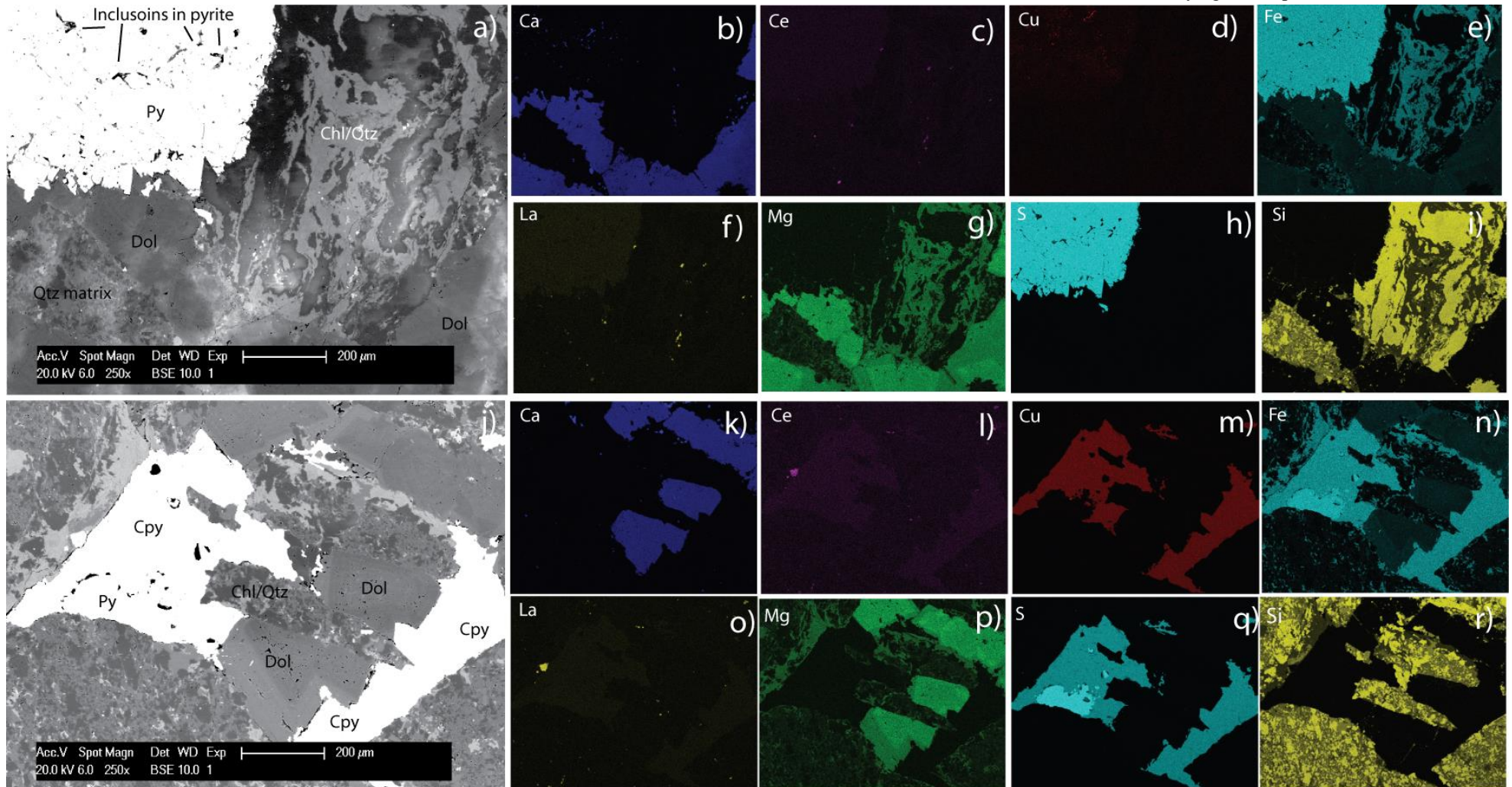


Figure 7 - - Selected qualitative element maps for sample 1949023 showing back scattered electron image (BSE) Ca, Ce, Cu, Fe, La, Mg, S and Si content. a) Annotated BSE image detailing minerals in sample. b) Qualitative element map for Ca showing Ca content in dolomite/calcite. c) Ce qualitative element map showing small LREE within quartz matrix. d) Cu qualitative element map showing possible Cu rich area in pyrite inclusion zonation. e) Fe qualitative element map highlighting Fe content in pyrite and chlorite. f) La qualitative element map highlighting possible small monazite within quartz matrix. g) Mg qualitative element map shows Mg content in dolomite. h) S qualitative element map highlighting sulphides present. i) Si qualitative element map showing Si content in background matrix. j) Annotated BSE image detailing minerals in sample. k) Qualitative element map for Ca showing Ca content in dolomite. l) Ce qualitative element map showing small LREE mineral within quartz matrix. m) Cu qualitative element map showing Cu rich area in chalcopyrite. e) Fe qualitative element map highlighting varying Fe content sulphides and chlorite. f) La qualitative element map highlighting small LREE mineral within quartz matrix. g) Mg qualitative element map shows Mg content in dolomite/chlorite. h) S qualitative element map highlighting two sulphides present. i) Si qualitative element map showing Si content in background matrix.

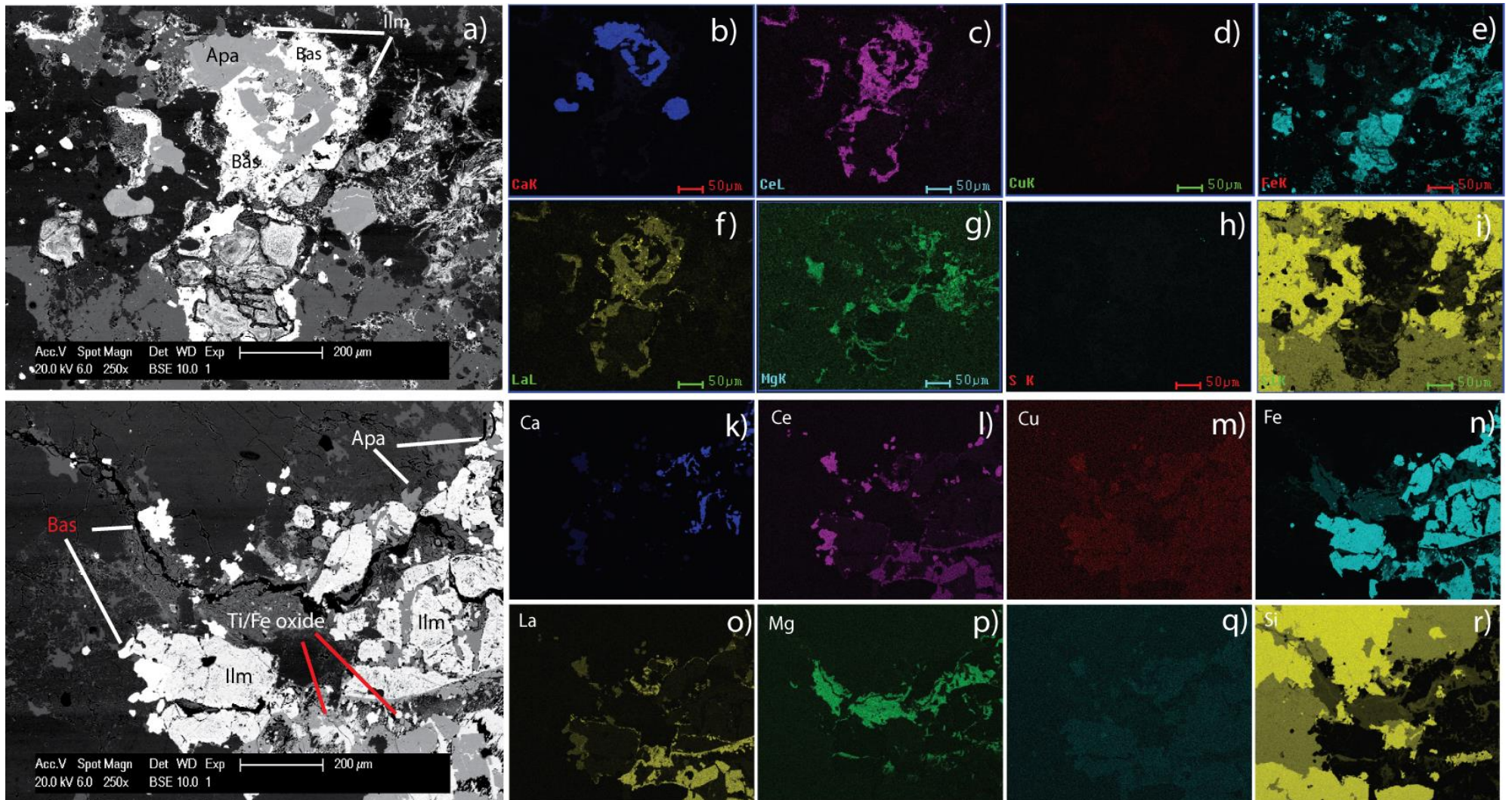


Figure 8 - Selected qualitative element maps for sample 1960847 showing back scattered electron image (BSE) Ca, Ce, Cu, Fe, La, Mg, S and Si content. a) Annotated BSE image detailing minerals in sample. b) Qualitative element map showing Ca content in apatite. c) Ce qualitative element map showing Ce residing within bastnäsite . d) Cu qualitative element map. e) Fe qualitative element map highlighting varying Fe content in Ti/Fe oxide and ilmenite. f) La qualitative element map showing La residing within bastnäsite. g) Mg qualitative element map shows Mg content in variation of Ti/Fe oxide. h) S qualitative element map displaying no sulphides present. i) Si qualitative element map showing Si content in background matrix. j) Annotated BSE image detailing minerals in sample. k) Qualitative element map for Ca showing Ca content in apatite. l) Ce qualitative element map showing Ce residing within bastnäsite . m) Cu qualitative element map. n) Fe qualitative element map highlighting varying Fe content in Ti/Fe oxide and ilmenite. o) La qualitative element map showing La residing within bastnäsite. p) Mg qualitative element map shows Mg content in variation of Ti/Fe oxide. q) S qualitative element map displaying no sulphides present. r) Si qualitative element map showing Si content in background matrix. Symbols – Apa – Apatite, Bas – bastnäsite, ilm – ilmenite

Mineral chemistry

Laser-Ablation Inductively-Coupled Mass Spectroscopy (LA-ICP-MS) analysis was undertaken on sample 1949023 as it preserved multiple stages of sulphide growth. Chalcopyrite and pyrite are preserved as large primary sulphides with inclusions, possible remobilized secondary phases and areas where chalcopyrite is replacing pyrite. Analysis was undertaken on three areas within sample to determine if potential pathfinder trace element signatures were apparent within these sulphide phases. Representative data in (Table. 4). Raw data in Appendix C.

PYRITE

Stoichiometric values for pyrite displayed a bimodal distribution of data (Fig. 9a). A general linear trend is apparent yet displays less clustering than chalcopyrite data (Fig. 9b). The negative linear trend begins at Fe rich/S poor values of (Fe: 0.90 – S:1.55 mol) and progress to Fe poor/S rich values of (Fe:0.88 – S:1.70 mol) (Fig. 9a). When compared to stoichiometric values for pyrite, data derived from Yorke Peninsula generally plots lower than stoichiometric values (Fig. 9a). Two high Fe outliers are from the inclusion-rich areas of a larger pyrite (Fig. 10a, spot 6,10).

Trace Element Analysis

Ag and Bi showed the majority of the pyrite data host some elevated concentrations of these elements. Ag data shows concentrations range between 5-25 ppm (Fig. 11a). Three high values correspond to zoned inclusion rich areas within a larger pyrite (Fig. 10a,spot 7,9,10). Bi data displays concentrations between 10-330 ppm (Fig. 11d). Three highest readings also correspond to the zoned inclusion-rich areas within a large pyrite

(Fig. 10a, spots 8,9,10). As and Mo data display a bimodal distribution of data. As concentrations range from 50-4400 ppm (Fig. 11c) and Mo concentrations range from 10-615 ppm (Fig. 11d). High As readings correspond to the edge of a pyrite within a larger chalcopyrite (Fig. 10c, spot 1,2). High Mo readings correspond to inclusion poor areas within a larger pyrite (Fig. 10a, spot-5,7,8). Much of the data for Au is low except for four points. These four points data ranges from 37-74 ppb (Fig. 11e). The four points are attributed to a larger pyrite with zoned inclusions (Fig. 10a, spot-2,6,7,9). Cu content in pyrite is low when compared to chalcopyrite data with all readings falling <15000ppm (Fig. 11f). W data shows concentrations within pyrite are low except for one reading that corresponds to the edge of a pyrite growing within larger chalcopyrite (Fig. 10c, spot 11); high reading 1.32 ppm.

Chalcopyrite

Stoichiometric values for chalcopyrite displays a negative relationship between Cu and S content. Cu rich/S poor values begin at Cu: 0.52 – S:1.150 mol and progress to Cu poor/S rich values of Cu:0.47 – S:1.340 (Fig. 9b). Data shows a general grouping of concentrations between S: 1.2 -1.35 mol and Cu: 0.47 – 0.51 mol, which when compared to true stoichiometric value for chalcopyrite shows that the overall S content for chalcopyrite high and Cu content is low (Fig. 9b). Data displays three clear outliers away from average concentrations. The S rich/Cu poor data was taken from a small pyrite inclusion within a larger chalcopyrite grain (Fig. 10c, spot 8). The high Cu/S poor data is from near the centre of a larger chalcopyrite (Fig. 10c, spots 4, 9).

Trace element analysis

Ag displayed a clustering of data (~4ppm) but is low when compared to pyrite data (Fig. 11a). Bi, As and Mo displayed low concentrations <20ppm (Fig. 11 b,c,d). Au and W is predominantly at low concentrations within chalcopyrite except for one data point for each element; Au: 200ppb, W: 0.58ppm (Fig. 11e,h) and corresponds to an area of possible secondary immobilized chalcopyrite growth next to larger chalcopyrite (Fig. 10b,spot 4). Cu concentrations are host within chalcopyrite as expected (Fig. 11f).

Table 4 - Summary of LA-ICP-MS trace element data for sulphide phases (ppm)

Element	Sulphide	S33	Fe57	Cu65	Zn66	As75	Mo95	Ag107	W184	Au197	Bi209
923-1-01	Pyrite	496005.09	465500.44	9703.67	13.36	126.49	11.74	15.48	0	0	149.79
923-1-02	Pyrite	508062.5	465500.44	3735.23	41.36	149.2	15.86	14.97	0	0.054	184.73
923-1-03	Pyrite	549157.63	465500.44	5742.8	13.89	83.53	48.7	10.76	0	0	170.28
923-1-04	Pyrite	532321.88	465500.47	8651.27	6.73	55.76	41.29	6.15	0	0	133.05
923-1-05	Pyrite	523433.97	465500.41	2146.25	29.83	122.84	391.48	7.01	0	0	136.1
923-1-06	Pyrite	466953.88	465500.44	530.53	12.72	144.2	59.58	17.94	0	0.074	130.89
923-1-07	Pyrite	551877.38	465500.47	5522.88	39641.85	125.46	613.54	20.96	0	0.058	153.49
923-1-08	Pyrite	538131.5	465500.47	15978.45	2125.47	140.11	423.97	16.26	0	0	313.01
923-1-09	Pyrite	526380.94	465500.47	1325.13	66.18	157.37	15.95	23.3	0	0	237.6
923-1-10	Pyrite	466541.44	465500.44	1767.13	89.97	715.04	34.73	20.8	0	0	247.7
923-2-01	Chalcopyrite	498030.81	304300.13	349077.47	16.17	0	0	4.71	0	0	0.176
923-2-02	Chalcopyrite	435278.31	304300.16	347644.94	14.56	0	0	5.35	0	0	0.209
923-2-03	Chalcopyrite	447556.25	304300.16	349083.69	20.83	0	0	4.43	0	0	0.59
923-2-04	Chalcopyrite	456490.94	304300.16	330785.66	39.55	5.08	0	6.23	0.58	0.2	16.88
923-2-05	Pyrite	496724.66	465500.47	153.42	76.57	181.18	0.19	0.79	0.163	0	23.92
923-2-06	Pyrite	567154.69	465500.44	932.67	10.75	360.32	0	3.89	0	0	29.99
923-2-07	Pyrite	490172.84	465500.44	260.98	2.95	50.22	0	0.69	0	0	14.97
923-2-08	Pyrite	551442.56	465500.47	281.01	7.72	671.21	1.67	0.97	0.095	0	35.39
923-2-09	Chalcopyrite	497333.53	304300.16	344485.16	9.31	3.78	0	3.8	0	0	0.275
923-2-10	Chalcopyrite	467420.94	304300.16	343024.19	35.2	0	0	4.46	0	0	0.261
923-2-11	Chalcopyrite	455710	304300.16	349644.81	12.19	0	0	4.41	0	0	0.301
923-3-01	Pyrite	532536.94	465500.47	4168.51	47.71	3103.26	0.193	3.49	0.098	0	35.77
923-3-02	Pyrite	538525	465500.44	24643.83	117.21	4490.07	0.61	11.97	1.32	0	111.67
923-3-03	Pyrite	527272.19	465500.44	1374.7	4.81	61.6	0	1.74	0	0	22.08
923-3-04	Chalcopyrite	406647.19	304300.16	347278.25	16.56	0	0	2.55	0	0	1.12
923-3-05	Chalcopyrite	433320.97	304300.16	340959.06	16.39	0	0	2.66	0	0	0.99
923-3-06	Chalcopyrite	459539.94	304300.19	341721.81	13.66	0	0	3.28	0	0	0.9
923-3-07	Chalcopyrite	452564.66	304300.16	342046.19	74.6	150.49	0	3.38	0	0	2.4
923-3-08	Chalcopyrite	479619.31	304300.13	261745.2	20.66	0	0	3.22	0	0	2.62
923-3-09	Chalcopyrite	384433.78	304300.16	344156.38	25.1	0	0	3.04	0	0	1.56
923-3-10	Chalcopyrite	445795.31	304300.19	349102.78	14.63	0	0	2.26	0	0	0.461
923-3-11	Pyrite	529581.88	465500.5	19019.35	7747.34	165.1	0.37	4.57	0	0.037	30.27
923-3-12	Chalcopyrite	450336.16	304300.19	351986.91	13.67	0	0	2.33	0	0	0.286
923-3-13	Chalcopyrite	435062.5	304300.19	349860.75	9.55	0	0	2.59	0	0	0.424
923-3-14	Chalcopyrite	438268.72	304300.19	347481.78	118.63	9.34	0.66	3.82	0	0	1.17
923-3-15	Chalcopyrite	493631.53	304300.19	341048.56	13.51	0	0	2.53	0	0	0.78

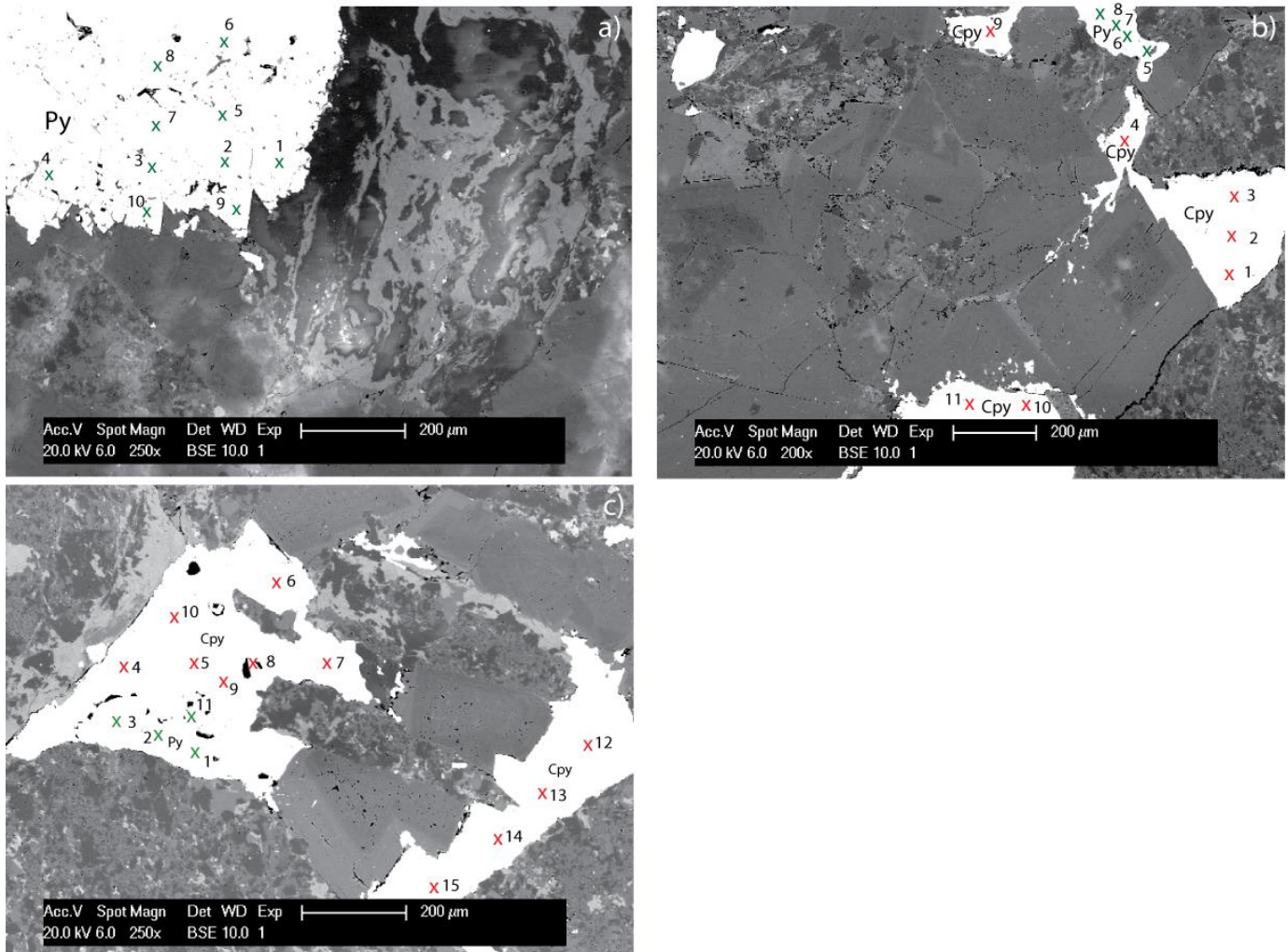


Figure 9 – BSE images highlighting where individual spots were analysed within sample 1949023. a) Analysis was undertaken on a larger pyrite with apparent inclusion. 10 spots were analysed; locations numbered recorded in image. b) Analysis undertaken on area that preserved large primary growth and smaller remobilized growth. 11 spots were analysed (7 chalcopyrite, 4 pyrite); locations numbered recorded in image. c) Analysis was undertaken on chalcopyrite as complete chalcopyrite and area of intergrown chalcopyrite growth. 15 spots were analysed (11 chalcopyrite, 4 pyrite); locations numbered recorded in image

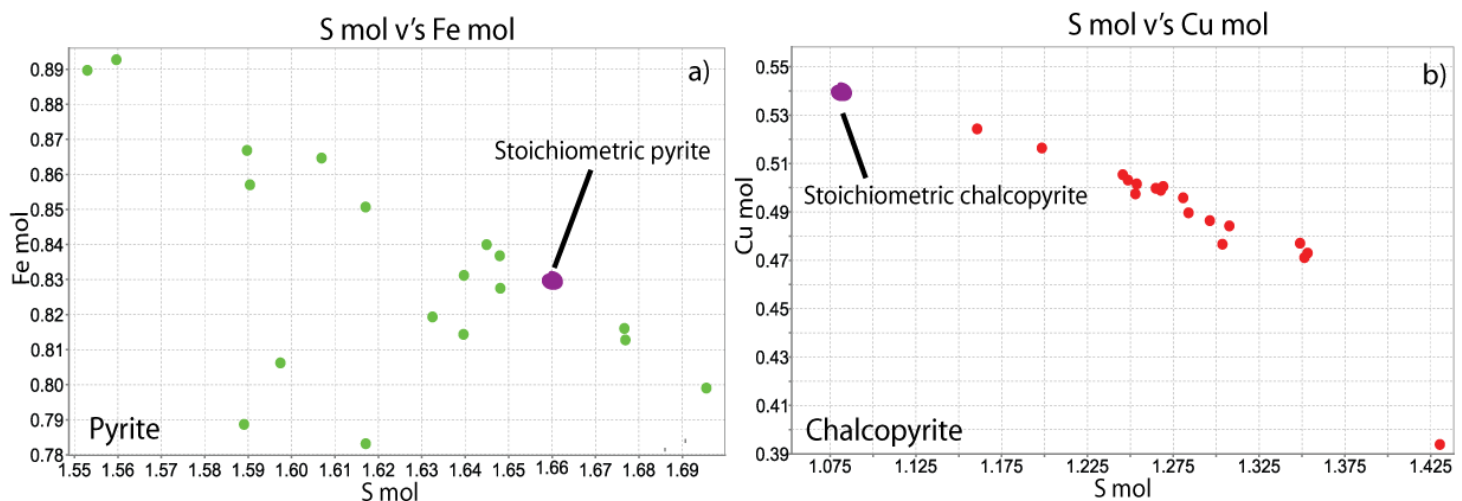


Figure 10 - Details how the element values of sulphide grains measured against stoichiometric values for each sulphide. Stoichiometric values for chalcopyrite ($S = 1.08 \text{ mol}$ – $\text{Cu} = 0.54 \text{ mol}$) and pyrite ($S = 1.66 \text{ mol}$ – $\text{Fe} = 0.83 \text{ mol}$). Purple dot in plots represents stoichiometric values for each sulphide

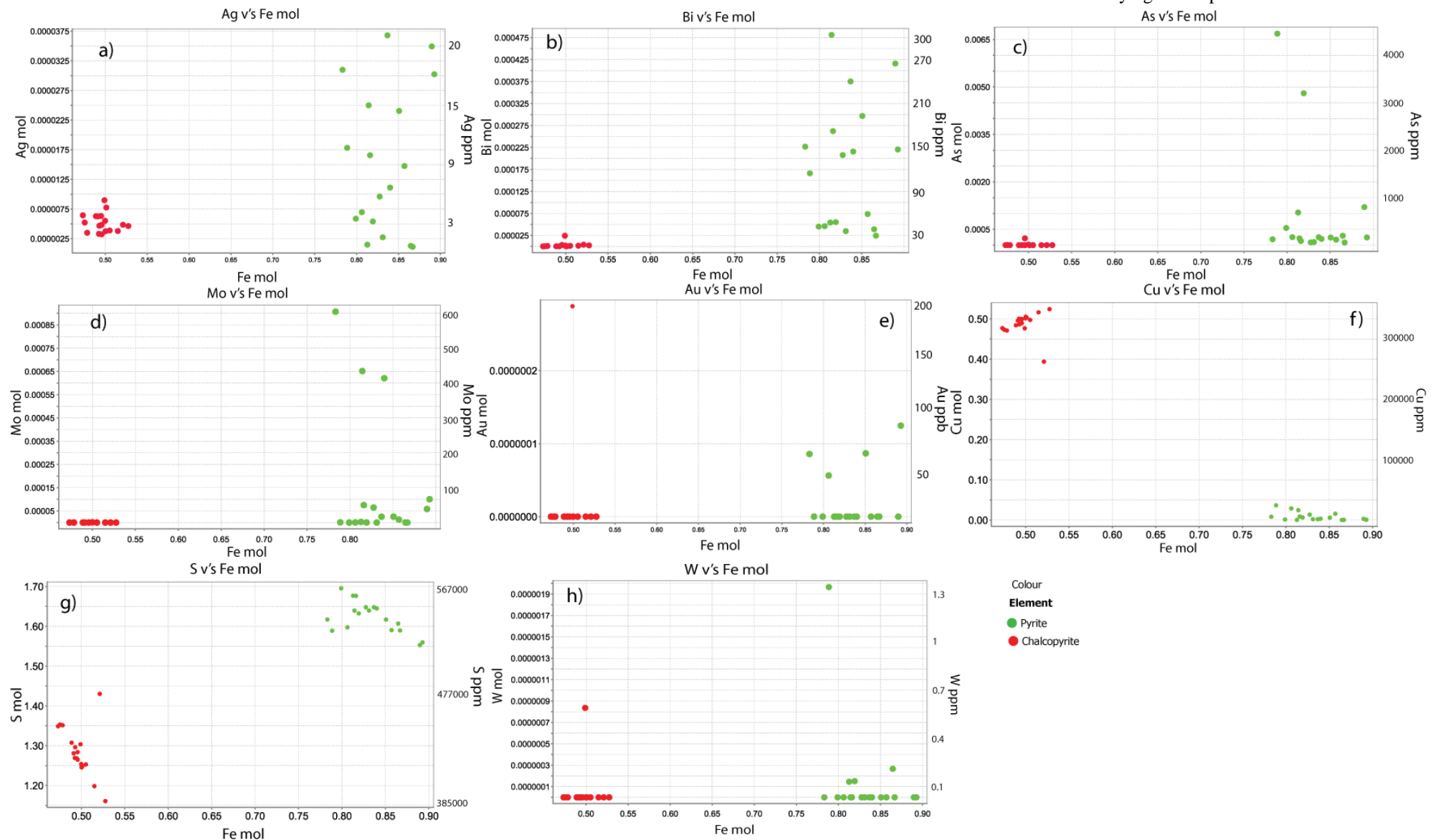


Figure 11 - Trace element v's Fe plots to determine trace element concentrations within selected sulphide phases. Pyrite data displayed in green; chalcopyrite data displayed in red. a) Ag showing slight elevations in chalcopyrite but mainly hosted in pyrite. b) As showing most samples low in Ag except for two high in pyrite data. c) Au showing the majority of sulphides sampled show no elevations except for one chalcopyrite and 4 pyrite. d) Bi showing majority of Bi readings are hosted in pyrite. e) Cu showing highest concentrations attributed to chalcopyrite and much smaller amounts in pyrite. f) Mo showing readings are hosted within pyrite. g) S showing content hosted within both sulphides. h) W showing concentrations are low from selected samples.

DISSCUSSION

Whole rock geochemistry

Whole rock geochemical analysis was undertaken to determine background element concentrations and lithogeochemistry of each defined lithological group within the Wallaroo basement lithologies. Determining basic lithological characteristics of the lithological groups is crucial in determining a background chemistry of the formation units (e.g. Reimann et al. 2005; Kyser et al. 2015), determining an element standard for further normalising data (e.g. Warren et al. 2015; Sakan et al. 2015) and to be able to measure potentially anomalous data against (e.g. McQueen 2006; Kyser et al. 2015). Samples were separated out into six generic groups based on logging data; felsic volcanics, granites, metasediments, mafics, gneiss and metasomatite.

MAJOR ELEMENTS

The lithological groups were best discriminated using SiO_2 and MgO concentrations (Fig. 12a). For the purpose of this analysis the metasediments were separated into clastic and carbonaceous sediment (Fig. 12a). The MgO vs SiO_2 diagram displays a negative linear trend that separates out lithologies. Felsic derived lithologies (felsic volcanics and granites) occupy the high SiO_2 /low MgO section of the diagram (65-80 wt.% SiO_2 ; 0-2 wt.% MgO). The carbonate component of the metasediments occupies the high MgO / low SiO_2 area and plots between (9-14 wt. % MgO ; 30-40 wt. % SiO_2) (Fig. 12a). Mafic derived lithologies (mafic intrusive, mafic extrusive, amphibolite) and the purely sediment component of the metasediments plots between these two lithologies (Sediment; (1-4 wt. % MgO)/50-70 wt. % SiO_2), Mafic; (4.5-10 wt.% MgO)/45-55 wt.% SiO_2).

MgO) (Fig. 12a). This separation of lithological groups along this negative linear trend gives each lithology a clear distinctive area. SiO₂ vs TiO₂ diagram (Fig. 12b) also displays a separation of lithologies; felsic component (0.25-0.75 wt. % TiO₂)/(60-80 wt. % SiO₂), sediment; (0.45-0.75 wt. % TiO₂)/(50-70 wt. % SiO₂), mafic; (1-3 wt. % TiO₂/45-55 wt. % SiO₂) and carbonate; (0.10-0.35 TiO₂)/(15-40 wt. % SiO₂) (Fig. 12b). Yet displays much more overlap within element concentrations eg. TiO₂ concentrations through felsic, sediment and carbonate lithologies.

Distinguishing the metasomatite and the gneiss is difficult to determine as of an unknown photolith of the metasomatite and varying levels of metamorphic mineral growth in the gneiss, yet as the two lithological units still generally plot along this negative linear trend it suggests the lithologies are still controlled by mineral partitioning of SiO₂ and MgO content (Fig. 12a).

TRACE ELEMENTS

Lithological groups discriminated nicely using Zr ppm and V ppm (Fig. 12c). Zr vs V shows that felsic derived data (felsic volcanics and granites) plots below a V:Zr ratio of 0.35:1, sediment and carbonate of the metasediments plots between ratios of V:Zr 0.35:1 and 3:2 and mafic data (mafic intrusive, mafic extrusive, amphibolite) plots above a V:Zr ratio of 3:2. Showing clearly that felsic lithologies have high Zr/low V and mafic lithologies have high V/low Zr. Sediment and carbonates plot clearly between the two (Fig. 12c)

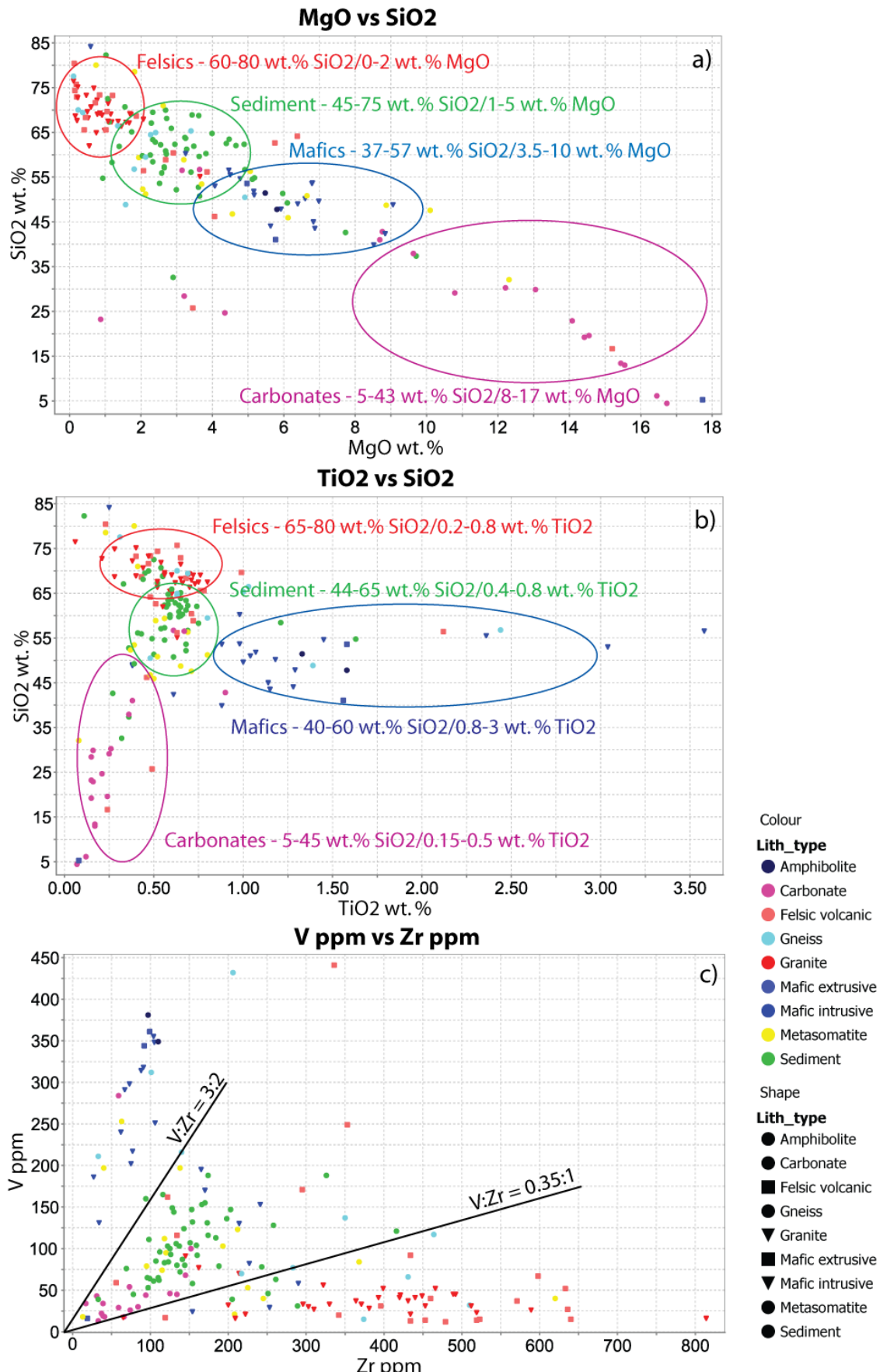


Figure 12 - Geochemical plots of major and trace elements displaying separation of lithological groups. a) MgO v's SiO₂ displaying a negative linear trend showing clear separation of lithological groups. b) TiO₂ v's SiO₂ showing separation of lithological groups, yet displays overlap through TiO₂ concentrations. c) V v's Zr showing separation of lithological groups as ratios of element concentrations.

Pathfinder elements to potential IOCG mineralisation

The whole rock element suite (appendix D) was assessed for potential pathfinder elements, with emphasis placed on known elements associated with IOCG mineralisation Ag, As, Au, Ba, Bi, Ca, Cd, Ce, Co, Cr, Cs, Cu, F, Fe, K, La, Mn, Mo, Ni, S, Sb, Se, Sn, Te, U and W (Mark et al. 2006; Fabris et al. 2013a; Wang et al. 2013; Hill et al. 2014). Individual lithologies can show elevations of potential pathfinders (e.g. La and Ce in felsic lithologies, Co in mafics) (Fig. 4). However, the overall raw data of the broad lithological groups cannot be compared without normalisation (Warren et al. 2007; Sakan et al. 2015). Lithological groups across Yorke Peninsula can be discriminated using a number of elements – Mg, Si, Ti V, and Zr (Fig. 12). To compare data between the lithological groups so potential pathfinder elements can be recognised, data needs to normalise against an element that clearly displays unique element concentrations within the lithological unit. MgO vs SiO₂ diagram displays a clear linear trend that separates out lithologies (Fig. 12a) and either element (SiO₂/ MgO) could potentially be used for normalisation. Each element was assessed and tested for normalisation but ultimately MgO was selected as it best accommodated the data.

A criteria was set for identifying and determining the validity of potential pathfinder elements.

1. Elements histogram and probability plots must be relatively uniform, show three potential populations of data (background-interesting-anomalous) and display potential high anomalous element concentration outliers.
2. High concentrations observed from histogram and probability plots must be anomalous (10x) average crustal abundance (e.g. Fabris et al. 2013). Average crustal abundance table in appendix **xx**.
3. Elements with high concentrations must be above detections limits and preference given to elements associated with IOCGs.
4. Element concentrations must vector to known mineralisation or possible exploration prospects within the area.

From these analyses ten elements (Ag, As, Au, Bi, Ce, Cu, Mo, La, S, W) were selected and assigned as pathfinder elements for the central Yorke peninsula. These elements were assigned based on the geochemical pathfinder criteria and association with IOCGs (Fabris et al. 2013a; Fabris et al. 2013b; Corriveau 2006; Foster et al. 2007; Darwish and Poellmann 2010; Cook 2015; Marschik and Fontboté 2001; Haynes et al. 1995; Wood and Samson 2000; Heinrich 1990). All elements in (Fig. 13-15). Example of pathfinder criteria in Appendix:D.

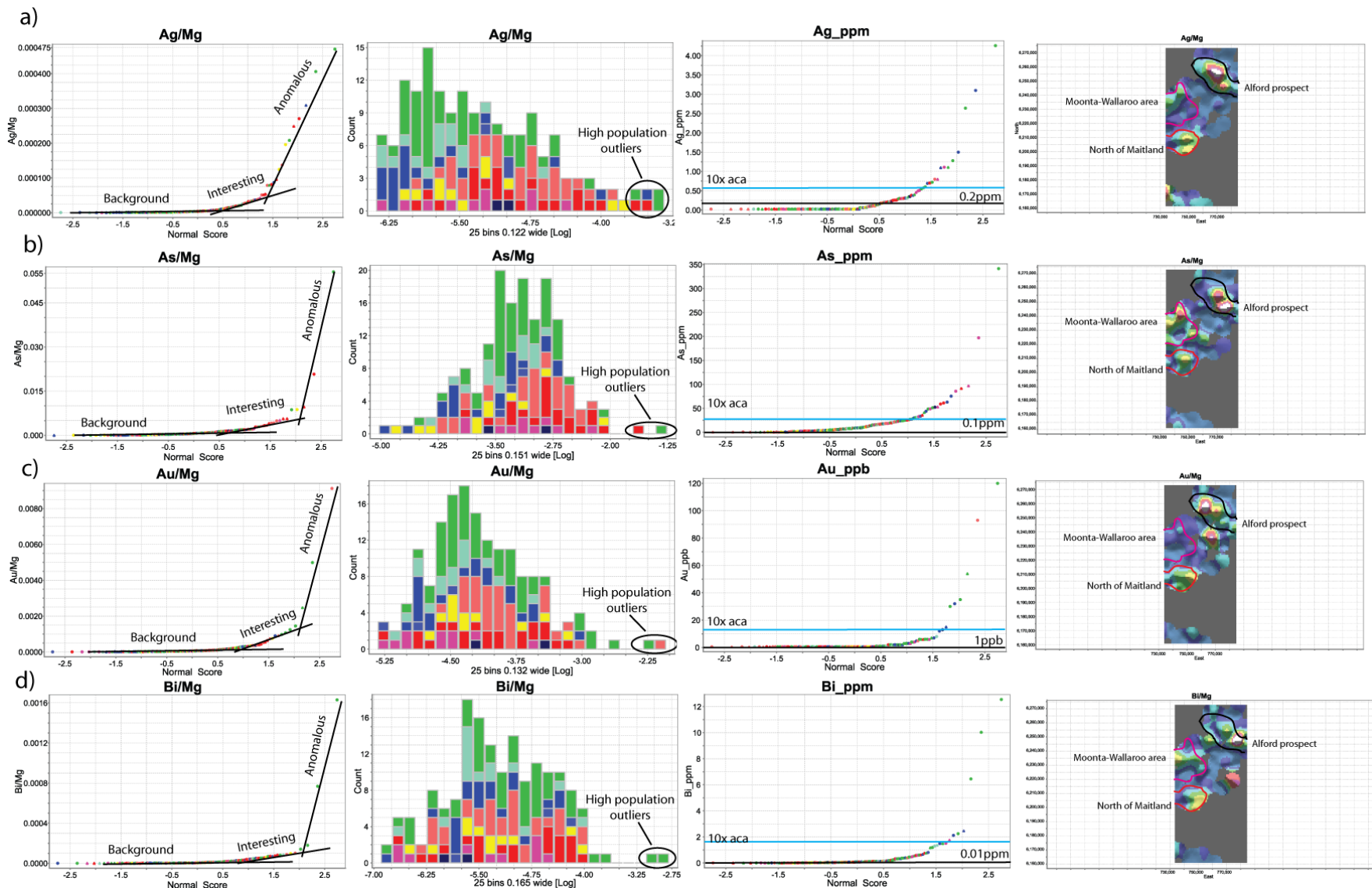


Figure 13 – Assigned pathfinders elements within Yorke Peninsula basement rocks and their passed criteria a) Ag . b) As. c) Au. d) Bi

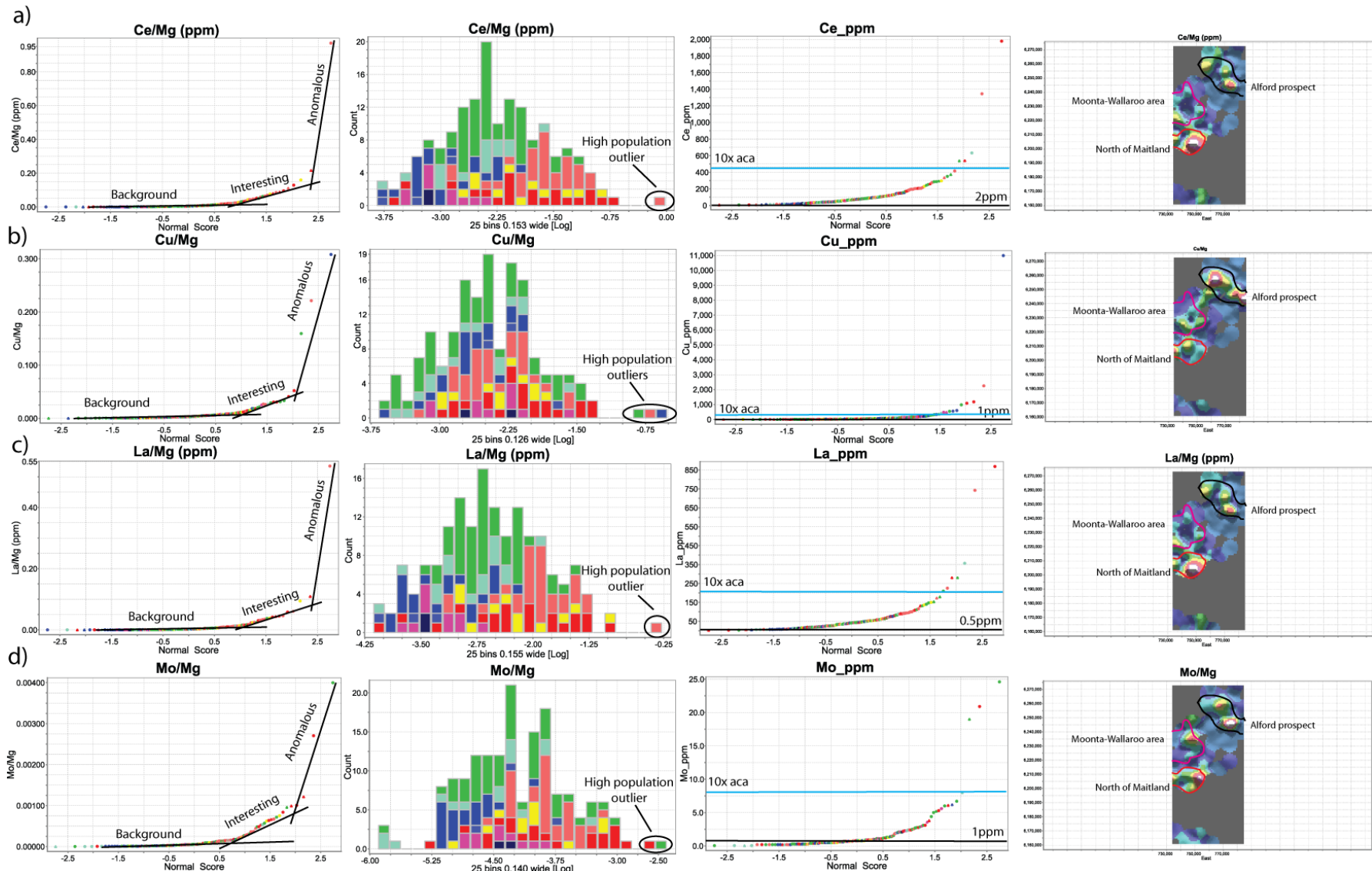


Figure 14 - Assigned pathfinders elements within Yorke Peninsula basement rocks and their passed criteria a) Ce. b) Cu. c) La. d) Mo

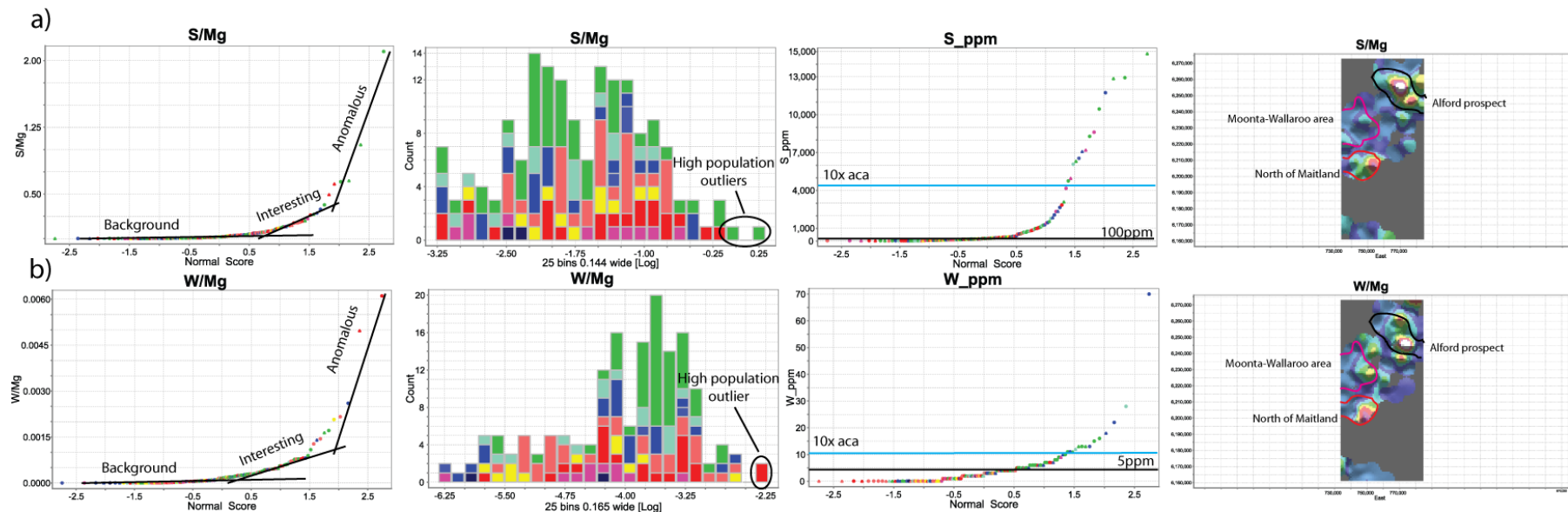


Figure 15 - Assigned pathfinders elements within Yorke Peninsula basement rocks and their passed criteria a) S. b) W

Element deployment

The following elements have been determined as pathfinder elements towards potential IOCG mineralisation in the northern Yorke Peninsula: Ag, As, Au, Bi, Cu, Ce, La, Mo, S and W. SEM and (LA-ICP-MS) analysis was undertaken on sulphide and oxide phases to constrain which minerals these elements may reside within.

Ag

Silver is a common trace element within sulphides, especially pyrite (Large et al. 2009; Deditius et al. 2014; Abraitis et al. 2004; Foster et al. 2007). Silver concentrations within pyrite from sample 1949023 ranged from 5-25 ppm and showed elevations within majority of the pyrite data, and is particularly elevated within the inclusion-rich rim of the pyrite (Fig. 11a) (Fig. 9a, spot9,10). Silver is often coincident with elevated As and Bi within pyrite data (Fig. 11b,c), which is commonly observed in inclusion-rich pyrite growth (Foster et al. 2007; Huston et al. 1995; Reich et al. 2013). Silver is a trace element associated with mineralisation on Yorke Peninsula and has been documented as trace element concentrations within ore zones at the Moonta and Poonta deposits in the Moonta-Wallaroo mining district (Fig. 2) by Both et al. (1993); Keeling et al. (2003) and Drexel et al. (1993), yet a mineral host was not stated. However there are a number of possible mineral hosts on Yorke Peninsula including; electrum AuAg, hessite Ag₂Te, petzite Ag₃AuTe₂ and have been observed within ore zones at the Hillside deposit (Fig. 2) (Twining et al. 2013; Ismail et al. 2014). SEM analyses determined small 5µm galena growing within siderite veining in sample 1989789. Galena PbS is a mineral that commonly holds trace element concentrations of silver (George et al. 2015; Simanenko 2007; Qian 1987) and has been reported across Yorke Peninsula in the Hillside and the

Moonta-Wallaroo area (Conor et al. 2010; Zang 2002; Ismail et al. 2014). The presence of galena may be attributing to the silver geochemical signature.

As

Arsenic is an element commonly associated with pyrite and is often with occurrences of other trace elements via coupled substitutions (Abraitis et al. 2004; Foster et al. 2007; Huston et al. 1995; Large et al. 2009). Element concentrations were observed to be residing within pyrite in sample 1949023. Concentrations proximal to the boundaries of the inclusion-rich pyrite growth were high ~3500ppm relative to other pyrite grains analysed <1000ppm (Fig. 11b). Other possible mineral hosts on Yorke Peninsula include; Arsenopyrite (FeAsS) which is the most common arsenic bearing mineral (King 2002), tennantite $\text{Cu}_6[\text{Cu}_4(\text{Fe},\text{Zn})_2]\text{As}_4\text{S}_{13}$, cobaltite CoAsS and smaltite ($\text{Co},\text{Fe},\text{Ni}\text{As}_2$ and have been documented as minor/trace minerals at Hillside and Moonta- Wallaroo (Fig. 2) (Ismail et al. 2014; Twining et al. 2013; Jones 1940). Hematite and magnetite also have an association with arsenic (Giménez et al. 2007) and as the two are the dominant oxide phases on Yorke Peninsula (Conor et al. 2010; Zang 2002; Kontonikas-Charos et al. 2014) the oxides may also be attributing to the arsenic anomaly.

Au

Gold is an element found within sulphide phases and is commonly present as inclusions within sulphide growth eg. (Foster et al. 2007; Large et al. 2009). Four data points within pyrite from sample 1949023 showed elevated Au concentrations within inclusion-rich growth and ranged between 37-74 ppb (Fig. 11c). One high reading of

200ppb was attributed to a smaller secondary chalcopyrite (Fig. 11c). Trace element concentrations of gold within chalcopyrite has been documented by Both et al. (1993); Conor et al. (2010) and Skirrow et al. (2007) who observed Au mainly occurring as inclusions within chalcopyrite in the Moonta-Wallaroo area. As sulphide analysis determined Au concentrations to be hosted within chalcopyrite and previous studies documented a similar Au occurrence it is possible the sulphide may host a significant portion of the gold geochemical anomaly. Other possible mineral hosts on Yorke Peninsula include; electrum (AuAg) and petzie (Ag_3AuTe_2) as seen at nearby Hillside (Twining et al. 2013)

Bi

Bismuth is an element commonly accommodated within pyrite (Large et al. 2009; Deditius et al. 2014; Reich et al. 2013; Huston et al. 1995; Foster et al. 2007). High concentrations ranged from 300-330ppm and corresponded to the inclusion-rich edge of pyrite growth from sample 1949023 (Fig. 9a). High Bi concentrations were coupled with elevations of Ag and As (Fig. 9a,spot 9,10)(Fig. 11a,c). Trace element concentrations of Bi have been observed within ore rich areas in the Moonta-Wallaroo area by Both et al. (1993); Drexel et al. (1993) and Keeling et al. (2003) but a mineral host was not documented. However there are a number of possible mineral hosts on Yorke Peninsula including; bismuthinite Bi_2S_3 which Conor et al. (2010) recorded seeing rare cases of across Yorke Peninsula and aikinite PbCuBiS_3 seen at nearby Hillside (Fig. 2) by (Twining et al. 2013). Galena PbS is a mineral that commonly holds trace element concentrations of bismuth (George et al. 2015; Simanenko 2007; Qian

1987) and has been reported across Yorke Peninsula (Conor 1995; Zang 2002; Twining et al. 2013). This occurrence of galena may also be attributing to the Bi anomaly.

Ce/La –

Light rare earth trace element signature was observed within sample 1960847 which contained the LREE mineral bastnäsite $(Ce,La,Y)CO_3F$ (Fig. 8a,c,f,j,l,o). Bastnäsite was observed to have a spatial relationship with apatite and Ti-Fe oxides (Fig. 8a,j). Kontonikas-Charos et al. (2014) observed bastnäsite growing with a similar spatial relationship to Ca rich minerals and Fe-Ti oxides and documented widespread emplacement within igneous rich rocks throughout the Moonta-Wallaroo area. Bastnäsite is also documented at Hillside (Fig. 2) (Twining et al. 2013). As SEM analysis uncovered the LREE mineral host and Kontonikas-Charos et al. (2014) documented seeing the same bastnäsite relationship within Moonta-Wallaroo studies, it is likely that bastnasite is attributing to the Ce/La geochemical anomaly. Other rare earth minerals; synchysite $Ca(Ce,La)(CO_3)_2F$, allanite $(Ce,Ca,Y,La)_2(Al,Fe^{+3})_3(SiO_4)_3(OH)$ and monazite $(Ce,La)PO_4$ have been documented across Yorke Peninsula (Kontonikas-Charos et al. 2014; Ismail et al. 2014; Conor et al. 2010; Twining et al. 2013) which may also be attributing to the geochemical anomaly.

Cu –

Copper trace element signature was observed within the chalcopyrite sampled as is expected (Fig. 11e). Analysis determined pyrite was also holding some trace element concentrations of Cu. High concentrations ranged from 8,000-15000ppm within a larger pyrite with inclusion-rich growth (Fig. 9a) and up to 25,000ppm from a pyrite within a

larger chalcopyrite (Fig 9c) but may be picking up residual Cu from the surrounding chalcopyrite (Fig. 11e). Cu concentrations attained from pyrites analysed may be attributing to the Cu geochemical signature, yet chalcopyrite Cu concentrations ~ 340,000ppm would be much more dominant. Common Cu minerals chalcocite Cu_2S , bornite Cu_5FeS_4 and covellite CuS and minor Cu minerals carrollite CuCo_2S and digenite Cu_9S_5 have been observed within ore zones in the Moonta-Wallaroo area and Hillside and could be contributing to the Cu geochemical anomaly (Both et al. 1993; Zang 2002; Twining et al. 2013; Ismail et al. 2014; Hafer 1991; Morales Ruano et al. 2002).

Mo –

Molybdenum is a common trace element within pyrite (Abraitis et al. 2004; Large et al. 2009; Deditius et al. 2014; Huston et al. 1995). Molybdenum concentrations within pyrite from sample 1949023 displayed a bimodal distribution of data with concentrations within inclusion-poor areas displaying high values 450-610ppm compared to other pyrite areas which displayed values <100ppm (Fig. 8f). Studies of Moonta Wallaroo and Hillside have commonly recorded molybdenite MoS_2 to be associated within the ore rich areas which is a likely mineral host for the molybdenum geochemical signature. (Conor 1995; Both et al. 1993; Conor et al. 2010; Skirrow et al. 2007; Twining et al. 2013; Zang 2002)

S –

Sulphur trace element concentrations were hosted within sulphide phases as to be expected. SEM and (LA-ICP-MS) analysis determined high S concentrations coming from pyrite with lesser amounts attributed to chalcopyrite (Fig. 11g). Pyrite is a mineral commonly found in association with ore deposits across Yorke Peninsula (Conor et al. 2010; Twining et al. 2013; Zang 2002; Jones 1940) and is likely to be attributing to some of the S geochemical anomaly. High S stoichiometric values attained from chalcopyrite may indicate chalcopyrite is also possibly attributing to the high S anomaly. Other common S minerals seen across Yorke Peninsula; Pyrrhotite Fe_7S_8 , galena PbS and chalcocite Cu_2S (Conor et al. 2010; Zang 2002; Twining et al. 2013) may also be attributing to the geochemical anomaly.

W –

Tungsten signature was difficult to determine where it may be residing. Sulphide analysis yielded no anomalous tungsten concentrations coming out of pyrite or chalcopyrite (Fig. 11h). Yet tungsten is an element with associations with IOCGs and has been reported as trace element concentrations within ore zones in other IOCG style deposits (Ootes et al. 2010; Montreuil et al. 2015). The most common tungsten bearing mineral is wolframite ($\text{Fe},\text{Mn}\text{WO}_4$) (Wood and Samson 2000), which has not yet been documented on Yorke Peninsula. Rare occurrences of scheelite (CaWO_4) were documented by Jones (1940) petrological study of the Wallaroo and Moonta mining district could be accounting for the some of the tungsten geochemical anomaly.

In an exploration context if elements (Ag, As, Au, Bi, Ce, Cu, La, Mo, S and W) were to be used as IOCG exploration vectors and sampling for mineral exploration was carried out in the field you would look for samples containing these elements. This study shows that interesting elements can be persevered in sulphide phases and LREE hosts within bastnasite, therefore analysis of samples containing these mineral phases will potentially increase the ability to recognise and map out these geochemical signatures. However, it is likely that not all interesting samples will contain pyrite/chalcopyrite or bastnasite, and other mineral phases may host significant concentrations of the pathfinder elements, therefore samples without these mineral phases should not be disregarded.

IOCG prospectivity index

A prospectivity index was created for central Yorke Peninsula in much the same way as Fabris et al. (2013a) constructed an prospectivity index for the eastern Gawler Craton . The index is determined by combining assigned IOCG elements (Ag, As, Au, Bi, Ce, Cu, La, Mo, S and W). Each element is assigned a value of one when above 10 times average crustal abundance and zero when below. The prospectivity index is the average of these assigned values, where a prospectivity index of 1 indicates a highly prospective area that contains high concentration of pathfinder elements, and a prospectivity index of 0 is a low prospectivity area. Each samples prospectivity index and locality are plotted in vectoring maps to highlight hot and not so hot areas for possible exploration/mineralisation across central Yorke Peninsula (Fig. 16).

The prospectivity index highlighted an area proximal to the township of Alford and Bute as a high prospectivity area, yet the index did not highlight areas of known mineralisation around the Moonto-Wallaroo district (Fig. 2). This could potentially be attributed to open file drill holes within the area not being representative of ore related zones. Also may be attributed to employing a 10x average crustal abundance as anomalous element indicator for samples. Potentially this could be lowered to highlight other known mineralised areas in the area.

Central-Northern Yorke Peninsula Prospectivity Index Vecoring Map

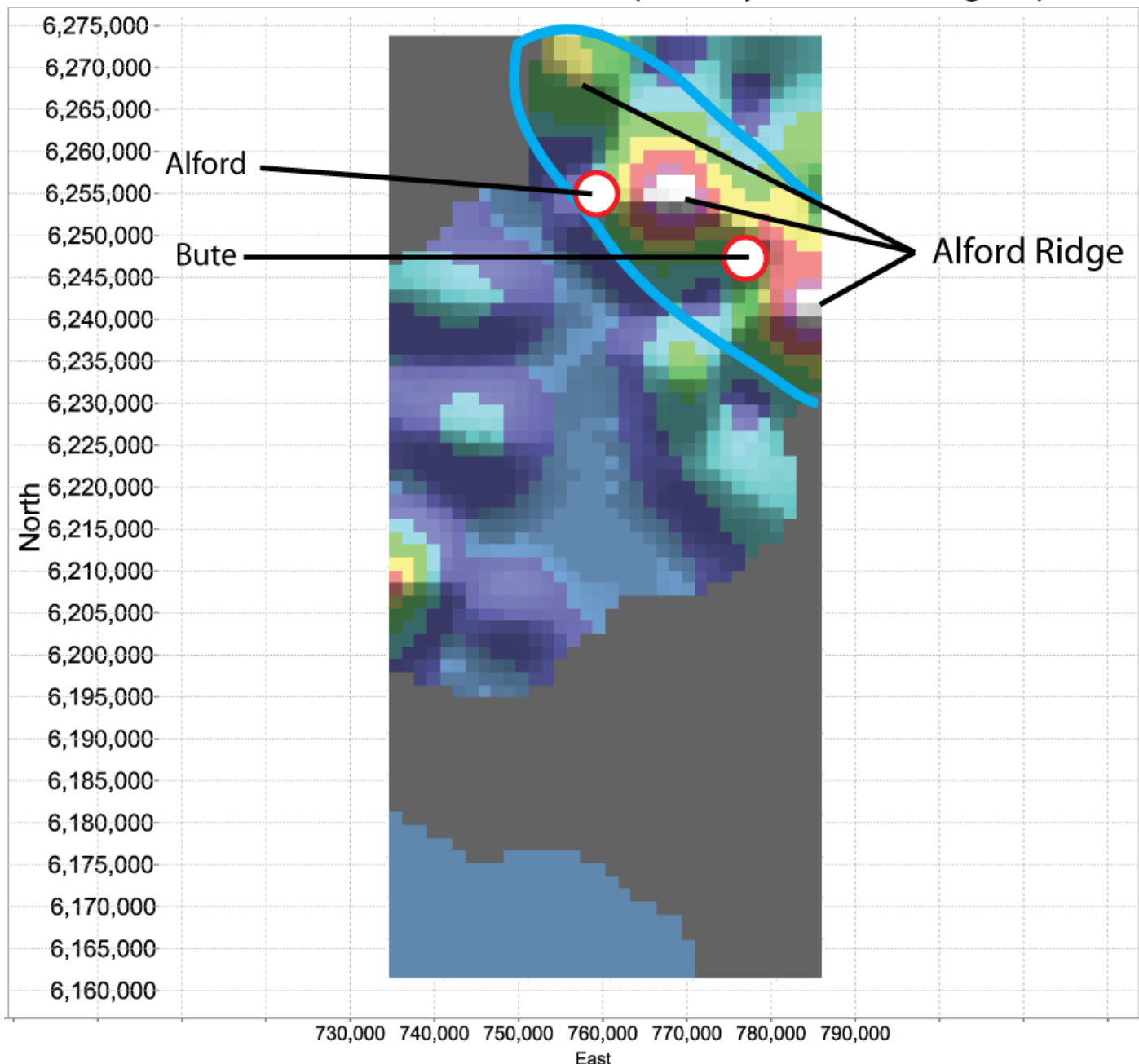


Figure 16 - Gridded maps displaying the prospectivity index concentrations across central northern Yorke Peninsula highlighting the Alford Ridge as a potential area for further exploration. Prospectivity index scores: >0.8 is highly significant, 0.6-0.8 is very significant, 0.4-0.6 is significant. Note representative highs along the Alford Ridge achieved a prospectivity score of 0.7.

Alford Ridge -

The Alford Ridge is a SE-NW trending structure that begins approximately 20kms above the township of Alford and extends down through Bute (Fig. 16). The area achieved ‘very significant’ prospectivity index numbers of 0.7 for respective highs along the Alford Ridge (Fig. 13). The Alford Ridge is considered a potential prospect for exploration and mineral exploration tenement is currently held by Sandfire Resources and Goyder Resources. Drill hole data from surrounding areas displays evidence for mineralisation in the area and was documented by Adelaide Resources Limited and AMALG Resources NL. Adelaide resources reported significant drill hole Cu intercepts of 10m @ 2.3% Cu from 59m (Washbourne 2014). AMALG returned significant Cu or Cu+Au values (e.g. Drillhole AL 9: 10 m @ 1.69% Cu, containing 5 m @ 2.78% Cu and 3.17 g/t Au) and documented a shallow, oxide copper resource comprising 60 000 t @ 2% Cu with potential for extraction by open cut. Data more proximal to the Alford Ridge was documented by Argonaut Resources whom have a joint venture with Sandfire Resources. Argonaut Resources recorded multiple significant drill hole intercepts of Cu and Ag (eg. Drillhole ALDDH01: 76m @ 0.95% Cu from 138m including 12 @ 2.18% Cu from 146m and ALDDH027: 10.04m @ 0.32% Cu and 6.69 g/t Ag from 180m including 5m @ 0.5% and 11.76 g/t from 180m) (Argonaut 2015). The presence of known mineralisation in the area highlights the prospectivity index being a useful exploration tool and could potentially be used in less explored areas to highlight areas of mineralisation/exploration prospects.

Implications for exploration

If exploration was carried out on central Yorke Peninsula 1m composite core samples would be adequate to generate geochemical data to determine geochemical anomalies. An understanding of background geochemical characteristics of lithological units is crucial for assigning pathfinder elements. Interesting pathfinder elements Ag, As, Au, Bi, Ce, Cu, La, Mo, S and W can be present within pyrite, chalcopyrite and bastnasite and should be targeted when sampling. However, samples that do not contain these minerals should not be disregarded as interesting element concentrations may be present in other mineral phases. A prospectivity index can be created unique to central Yorke Peninsula to highlight prospective areas for mineralisation by assigning a threshold of 10 times average crustal abundance as an anomalous indicator.

Future work

Sulphide analysis from samples derived from areas directly proximal to ore zones to camp scale area to categorise trace element concentrations within sulphides to determine if concentrations increase toward ore zones.

Further analysis on different sulphide/oxide phases and mineral species to further constrain where interesting pathfinder elements may be residing.

Create an alteration index for central Yorke Peninsula independent of Au and Cu concentrations and compare to prospectivity index created in this study.

CONCLUSIONS

Whole rock geochemical analysis can distinguish the six defined lithological groups from one another by major and trace element concentrations that are unique to each lithology.

Elements Ag, As, Au, Bi, Ce, La, Mo, S, and W can be recognised from whole rock geochemical analysis and assigned as pathfinder elements toward potential IOCG mineralisation on central Yorke Peninsula

Element deployment uncovered inclusion-rich zonation growth seen from pyrite holds concentrations of Ag, As, Bi and Mo. Chalcopyrite holds concentrations of Au. LREE trace element concentrations are host within bastnäsite.

A prospectivity index unique to central Yorke Peninsula can be created by combining assigned pathfinder elements to highlight prospective areas. An area proximal to the township of Alford and Bute is highlighted as a prospective area. As area is already known for significant mineralisation it strengthens the usefulness of the prospectivity index as an exploration tool.

ACKNOWLEDGEMENTS

I wish to sincerely express my gratitude to my supervisor, Dr. Caroline Forbes for her advice, support and valuable guidance in the preparation of this thesis. Her generosity was considerable in investing so much time and effort. I would like to acknowledge the Deep Exploration Technologies Cooperative Research Centre for their project opportunities and financial contribution. I would also like to acknowledge Prof. David Giles for his support as my secondary supervisor, Colin Conor for his valuable insights into geology across the Yorke Peninsula, Ben Wade for his patience and guidance in my time over at Adelaide Microscopy and Katie Howard for her training and assistance throughout the year. Finally, I would especially like to thank my fellow honours students for their continued support through this testing and trying year.

REFERENCES

- ABRAITIS P. K., PATTRICK R. A. D. & VAUGHAN D. J. 2004 Variations in the compositional, textural and electrical properties of natural pyrite: a review, *International Journal of Mineral Processing*, vol. 74, no. 1–4, pp. 41-59.
- ARGONAUT 2015 Exploration update - Alford, South Australia. In RESOURCES A. ed. ASX Announcement.
- BELPERIO A., FLINT R. & FREEMAN H. 2007 Prominent Hill: A Hematite-Dominated, Iron Oxide Copper-Gold System, *Economic Geology*, vol. 102, no. 8, pp. 1499-1510.
- BOTH R., et al. 1993 Moonta copper deposits, South Australia: Geology and ore genesis of the Poona and Wheal Hughes ore bodies. In FENOLL HACH-ALF T.-R. A. G. E. ed. Current research in geology applied to ore deposits. pp. 49-52. Brazil.
- CARTHEW S. 1993 The geological setting for copper and gold mineralisation at Wheal Hughes (Moonta). Adelaide: Moonta Mining Joint Venture.
- CONOR C. 1995 Moonta-Wallaroo region – an interpretation of the geology of the Maitland and Wallaroo 1:100 000 sheet areas. In CONOR C. ed.: Mines and Energy South Australia.
- 2002 The Palaeo-Mesoproterozoic geology of northern Yorke Peninsula, South Australia: Hiltaba Suite-related alteration and mineralisation of the Moonta–Wallaroo Cu–Au district. South Australia: Department for Primary Industries and Resources
- CONOR C., et al. 2010 ALTERATION AND MINERALISATION IN THE MOONTA-WALLAROO COPPER-GOLD MINING FIELD REGION, OLYMPIC DOMAIN, SOUTH AUSTRALIA. In PORTER T. M. ed. Hydrothermal Iron Oxide Copper-Gold and Related Deposits: A Global Perspective. pp. 147-170. Adelaide: PGC.
- COOK N. J. 2015 Pathfnder suggestion. In CUSTANCE K. ed. Email ed.
- CORRIVEAU L. 2006 Iron oxide copper-gold (\pm Ag \pm Nb \pm P \pm REE \pm U) deposits: A Canadian perspective, *Mineral resources of Canada: a synthesis of major deposit-types, district metallogeny, the evolution of geological provinces, and exploration methods*.
- COWLEY W., CONOR C. & ZANG W. 2003 New and revised Proterozoic stratigraphic units on northern Yorke Peninsula, *MESA Journal*, vol. 29, pp. 46-58.
- CREASER R. & COOPER J. 1993 U-Pb geochronology of Middle Proterozoic felsic magmatism surrounding the Olympic Dam Cu-U-Au-Ag and Moonta Cu-Au-Ag deposits, *South Australia. Economic Geology*, vol. 88, pp. 186-197.
- DARWISH M. A. G. & POELLMANN H. 2010 Geochemical exploration for gold in the Nile Valley Block (A) area, Wadi Allaqi, South Egypt, *Chemie der Erde - Geochemistry*, vol. 70, no. 4, pp. 353-362.
- DEDITIUS A. P., et al. 2014 The coupled geochemistry of Au and As in pyrite from hydrothermal ore deposits, *Geochimica et Cosmochimica Acta*, vol. 140, pp. 644-670.
- DREXEL J. F., PREISS W. V. & PARKER A. 1993 The Geology of South Australia: The Precambrian. Mines and Energy, South Australia, Geological Survey of South Australia.

- FABRIS A., et al. 2013a Characterising alteration in the eastern Gawler Craton: regional geochemical trends within an IOCG province. PACE 2020 exploration mining energy global. Adelaide: Department for Manufacturing, Innovation, Trade, Resources and Energy.
- FABRIS A. J., et al. 2013b IOCG-style mineralisation in the central eastern Gawler Craton, SA; characterisation of alteration, geochemical associations and exploration vectors. Deep Exploration Technologies Cooperative research Centre Department of Innovation, Manufacturing, Trade, Resources and Energy.
- FANNING C., REID A. & TEALE G. 2007 A geochronological framework for the Gawler Craton, *Geological Survey of South Australia*, vol. Bulletin 55, p. 258.
- FERRIS G., SCHWARZ M. & HEITHERSAY P. 2002 The geological framework, distribution and controls of Fe-oxide and related alteration, and Cu-Au mineralisation in the Gawler Craton, South Australia. In PORTER T. M. E. ed. Hydrothermal iron oxide copper-gold and related deposits: A global perspective. pp. 1-23. Adelaide: PGC.
- FORBES C. 2012a Top of basement solid geology map. In CENTRE D. E. T. C. R. ed. Interim Technical Report Adelaide: University of Adelaide.
- 2012b Yorke Peninsula Project - Sampling strategy and background geochemistry. Interim Technical Report. University of Adelaide: Deep Exploration Technologies Cooperative Research Centre.
- FOSTER A. R., WILLIAMS P. J. & RYAN C. G. 2007 Distribution of Gold in Hypogene Ore at the Ernest Henry Iron Oxide Copper-Gold Deposit, Cloncurry District, NW Queensland, *Exploration and Mining Geology*, vol. 16, no. 3-4, pp. 125-143.
- GEORGE L., et al. 2015 Trace and minor elements in galena: A reconnaissance LA-ICP-MS study, *American Mineralogist*, vol. 100, no. 2-3, pp. 548-569.
- GIMÉNEZ J., et al. 2007 Arsenic sorption onto natural hematite, magnetite, and goethite, *Journal of Hazardous Materials*, vol. 141, no. 3, pp. 575-580.
- GROVES D. I., et al. 2010 Iron Oxide Copper-Gold (IOCG) Deposits through Earth History: Implications for Origin, Lithospheric Setting, and Distinction from Other Epigenetic Iron Oxide Deposits, *Economic Geology*, vol. 105, no. 3, pp. 641-654.
- HAFER M. R. 1991 Origin and controls of deposition of the Wheal Hughes and Poona copper deposits, Moonta, South Australia. *Geology and Geophysics*. pp. 124. Adelaide: University of Adelaide
- HAND M., REID A. & JAGODZINSKI L. 2007 Tectonic framework and evolution of the Gawler Craton, South Australia, *Economic Geology* vol. 102, pp. 1377-1395.
- HAYNES D. W., et al. 1995 Olympic Dam ore genesis; a fluid-mixing model, *Economic Geology*, vol. 90, no. 2, pp. 281-307.
- HEINRICH C. A. 1990 The chemistry of hydrothermal tin(-tungsten) ore deposition, *Economic Geology*, vol. 85, no. 3, pp. 457-481.
- HILL E. J., et al. 2014 Using geochemical proxies to model nuggety gold deposits: An example from Sunrise Dam, Western Australia, *Journal of Geochemical Exploration*, vol. 145, pp. 12-24.
- HITZMAN M. W. 2000 Iron Oxide-Cu-Au deposits: What, Where, When and Why. In PORTER T. M. E. ed. Hydrothermal Iron Oxide Copper-Gold & Related Deposits: A Global Perspective. pp. 9-25. Adelaide: PGC Publishing.
- HOEK J. & SCHAEFER B. 1988 Palaeoproterozoic Kimban mobile belt, Eyre Peninsula: timing and significance of felsic and mafic magmatism and deformation, *Australian Journal of Earth Sciences*, vol. 45, pp. 305-313.
- HUSTON D. L., et al. 1995 Trace elements in sulfide minerals from eastern Australian volcanic-hosted massive sulfide deposits; Part I, Proton microprobe analyses of pyrite, chalcopyrite, and sphalerite, and Part II, Selenium levels in pyrite; comparison with delta 34 S values and implications for the source of sulfur in volcanogenic hydrothermal systems, *Economic Geology*, vol. 90, no. 5, pp. 1167-1196.
- ISMAIL R., et al. 2014 Rare earths and other trace elements in minerals from skarn assemblages, Hillside iron oxide-copper-gold deposit, Yorke Peninsula, South Australia, *Lithos*, vol. 184-187, no. 0, pp. 456-477.
- JACK R. 1917 The geology of the Moonta and Wallaroo mining district, *Geological Survey of South Australia*, vol. Bulletin 6, p. 135.
- JONES R. 1940 A petrological study of the Wallaroo and Moonta mining districts. pp. 24. Adelaide: University of Adelaide.
- KEELING J., et al. 2003 Alteration mineralogy and acid-sulphate weathering at Moonta copper mines, South Australia, *Advances in Regolith*, pp. 230-233.
- KING R. J. 2002 Arsenopyrite, *Geology Today*, vol. 18, no. 2, pp. 72-75.

- KONTONIKAS-CHAROS A., CIOBANU C. L. & COOK N. J. 2014 Albitization and redistribution of REE and Y in IOCG systems: Insights from Moonta-Wallaroo, Yorke Peninsula, South Australia, *Lithos*, vol. 208, pp. 178-201.
- KYSER K., BARR J. & IHLENFELD C. 2015 Applied Geochemistry in Mineral Exploration and Mining, *Elements*, vol. 11, no. 4, pp. 241-246.
- LARGE R. R., et al. 2009 Gold and Trace Element Zonation in Pyrite Using a Laser Imaging Technique: Implications for the Timing of Gold in Orogenic and Carlin-Style Sediment-Hosted Deposits, *Economic Geology*, vol. 104, no. 5, pp. 635-668.
- LARGE R. R. & MCGOLDRICK P. J. 1998 Lithogeochemical halos and geochemical vectors to stratiform sediment hosted Zn-Pb-Ag deposits, 1. Lady Loretta Deposit, Queensland, *Journal of Geochemical Exploration*, vol. 63, no. 1, pp. 37-56.
- MARK G., OLIVER N. S. & WILLIAMS P. 2006 Mineralogical and chemical evolution of the Ernest Henry Fe oxide-Cu-Au ore system, Cloncurry district, northwest Queensland, Australia, *Mineralium Deposita*, vol. 40, no. 8, pp. 769-801.
- MARSCHIK R. & FONTBOTÉ L. 2001 The Candelaria-Punta del Cobre Iron Oxide Cu-Au(-Zn-Ag) Deposits, Chile, *Economic Geology*, vol. 96, no. 8, pp. 1799-1826.
- MCQUEEN K. 2006 Identifying geochemical anomalies, *Department of Earth and Marine Sciences, Australian National University, ACT*, vol. 200.
- MONTREUIL J.-F., CORRIVEAU L. & POTTER E. 2015 Formation of albitite-hosted uranium within IOCG systems: the Southern Breccia, Great Bear magmatic zone, Northwest Territories, Canada, *Mineralium Deposita*, vol. 50, no. 3, pp. 293-325.
- MORALES-RUANO S., BOTH R. & GOLDING S. 2002 A fluid inclusion and stable isotope study of the Moonta copper-gold deposits, South Australia: evidence for fluid immiscibility in a magmatic hydrothermal system, *Chemical Geology*, vol. 192, pp. 211-226.
- MORALES RUANO S., BOTH R. A. & GOLDING S. D. 2002 A fluid inclusion and stable isotope study of the Moonta copper-gold deposits, South Australia: evidence for fluid immiscibility in a magmatic hydrothermal system, *Chemical Geology*, vol. 192, no. 3-4, pp. 211-226.
- OOTES L., et al. 2010 Timing and thermochemical constraints on multi-element mineralisation at the Nori/RA Cu-Mo-U prospect, Great Bear magmatic zone, Northwest Territories, Canada, *Mineralium Deposita*, vol. 45, no. 6, pp. 549-566.
- PORTER T. M. 2010 Current understanding of iron oxide associated-alkali altered mineralised systems: Part 1- An overview. In PORTER T. M. E. ed. *Hydrothermal Iron Oxide Copper-Gold and related Deposits: A Global Perspective* pp. 5-32. Adelaide: PGC Publishing
- QIAN Z. 1987 Trace elements in galena and sphalerite and their geochemical significance in distinguishing the genetic types of Pb-Zn ore deposits, *Chinese Journal of Geochemistry*, vol. 6, no. 2, pp. 177-190.
- REICH M., et al. 2013 Pyrite as a record of hydrothermal fluid evolution in a porphyry copper system: A SIMS/EMPA trace element study, *Geochimica et Cosmochimica Acta*, vol. 104, pp. 42-62.
- REID A., et al. 2008 Paleoproterozoic orogenesis in the southeastern Gawler Craton, South Australia*, *Australian Journal of Earth Sciences*, vol. 55, no. 4, pp. 449-471.
- REID A., et al. 2011 Nature and timing of Cu-Au-Zn-Pb mineralisation at Punt Hill, eastern Gawler Craton, *MESA Journal*, vol. 60, pp. 7-17.
- REIMANN C., FILZMOSER P. & GARRETT R. G. 2005 Background and threshold: critical comparison of methods of determination, *Science of the Total Environment*, vol. 346, no. 1, pp. 1-16.
- RUDNICK R. & GAO S. 2003 Composition of the continental crust, *Treatise on geochemistry*, vol. 3, pp. 1-64.
- SAKAN S. M., et al. 2015 Environmental Assessment of Heavy Metal Pollution in Freshwater Sediment, Serbia, *CLEAN – Soil, Air, Water*, vol. 43, no. 6, pp. 838-845.
- SCHWARZ M. 2003 Lincoln, South Australia: Sheet SI53-11 International Index. 1: 250 000 Geological Series Explanatory Notes (Geological Survey of South Australia), *Primary Industries and Resources South Australia, Adelaide*.
- SIMANENKO L. F. 2007 Modes of trace element occurrence in galena from the Partizansky base metal-skarn deposit, Primorye, *Russian Journal of Pacific Geology*, vol. 1, no. 2, pp. 144-152.
- SKIRROW R., et al. 2002 The Geological Framework, Distribution and Controls of Fe-Oxide Cu-Au Mineralisation in the Gawler Craton, South Australia: Part II: Alteration and Mineralisation. In PORTER T. M. ed. *Hydrothermal Iron Oxide Copper-Gold & Related Deposits: A Global Perspective*. pp. 33-47. Adelaide: PGC.

- SKIRROW R. G., *et al.* 2007 Timing of Iron Oxide Cu-Au-(U) Hydrothermal Activity and Nd Isotope Constraints on Metal Sources in the Gawler Craton, South Australia, *Economic Geology*, vol. 102, no. 8, pp. 1441-1470.
- TWINING M., BURGESS J. & TEALE G. 2013 Delivering Australias Largest Undeveloped Copper Project. In MEETING A. T. ed.: Rex Minerals.
- WANG C., *et al.* 2013 Characterization of primary geochemical haloes for gold exploration at the Huanxiangwa gold deposit, China, *Journal of Geochemical Exploration*, vol. 124, no. 0, pp. 40-58.
- WARREN I., SIMMONS S. F. & MAUK J. L. 2007 Whole-Rock Geochemical Techniques for Evaluating Hydrothermal Alteration, Mass Changes, and Compositional Gradients Associated with Epithermal Au-Ag Mineralization, *Economic Geology*, vol. 102, no. 5, pp. 923-948.
- WARREN M. R., *et al.* 2015 The Ni-Cr-Cu content of biotite as pathfinder elements for magmatic sulfide exploration associated with mafic units of the Sudbury Igneous Complex, Ontario, Canada, *Journal of Geochemical Exploration*, vol. 153, pp. 11-29.
- WASHBOURNE M. 2014 New copper target emerges at Alford West.
- WOOD S. A. & SAMSON I. M. 2000 The Hydrothermal Geochemistry of Tungsten in Granitoid Environments: I. Relative Solubilities of Ferberite and Scheelite as a Function of T, P, pH, and mNaCl, *Economic Geology*, vol. 95, no. 1, pp. 143-182.
- ZANG W. 2002 Late Palaeoproterozoic Wallaroo Group and early Mesoproterozoic mineralisation in the Moonta Subdomain, eastern Gawler Craton, South Austaralia. South Australia: Geological Society of Australia.

**APPENDIX A: RAW GEOCHEMICAL DATA AND ELEMENT SUITE ANALYSED
AND ANALYTICAL TECHNIQUES**

Element(s)	Analytical technique
Au, Pt, Pd	Lead collection fire assay
Cu, Li, Ni, Pb, S, Zn	4 acid digest (ICP-OES)
Ag, As, Bi, Cd, Co, Cs, Ge, In, Mo, Nb, Re, Sb, Se, Te, Ti	4 acid digest (ICP-MS)
F	Carbonate fusion/SIE
Al, Ca, Cr, Fe, K, Mg, Mn, Na, P, Si, Ti, V	Lithium borate fusion (ICP-OES)
Ba, Be, Ce, Dy, Er, Eu, Ga, Gd, Hf, Ho, La, Lu, Nd, Pr, Rb, Sc, Sm, Sn, Sr, Ta, Tb, Th, Tm, U, W, Y, Yb, Zr	Lithium borate fusion (ICP-MS)

Raw whole rock geochemical data: Central Yorke Peninsula

Kym Michael Custance
Identifying IOCG pathfinder elements

Samp_R#	Ta ppm	Tb ppm	Te ppm	Th ppm	TiO2%	Tl ppm	Tm ppm	U ppm	V ppm	W ppm	Y ppm	Yb ppm	Zn ppm	Zr ppm
1946904	0.5	0.8	0.05	2.9	1.58	1.28	0.43	6.08	381	0.05	29.6	2.38	307	97
1937386	0.4	0.47	0.2	6.6	0.24	0.8	0.33	2.36	54	0.05	18.7	1.36	84	73
1949042	0.2	0.39	0.05	4.78	0.15	0.07	0.19	1.03	13	1	15.3	1.07	62	33
1949782	0.5	1.04	0.07	7.83	0.25	2.33	0.52	5.38	44	1	36.1	3.01	51	94
1960880	0.8	0.57	0.05	8.04	0.26	1.31	0.2	2.2	30	2	19.8	1.54	28	84
1960883	0.8	0.55	0.05	11.85	0.36	0.58	0.26	2.23	46	4	20.7	1.92	27	125
0000005	2.5	2.5	0.05	11.5	2.12	0.76	1.33	3.13	31	1	90.9	8.42	163	396
1933082	15.1	0.31	0.05	17.52	0.23	0.36	0.57	2.26	17	0.05	28.3	4.27	169	119
1937389	4.8	1.59	0.11	39.74	0.63	0.09	1.27	6.86	37	7	68.9	8.43	14	571
1937392	0.4	0.31	0.05	4.64	0.24	0.9	0.2	2.2	59	1	11.9	1	27	56
1937395	1.6	0.36	0.05	12.51	0.99	0.36	0.3	4.97	171	3	16.6	2.08	47	295
1937398	3.6	1.12	0.22	19.83	0.76	0.36	0.74	11.54	92	2	41.4	4.91	32	434
1949037	3.7	2.46	0.16	36.17	0.48	0.28	2.16	11.06	15	2	148.6	13.23	113	523
1949053	3	1.84	0.05	41.95	0.43	0.29	0.97	5.31	20	4	53.5	6.08	37	342
1949786	3.1	1.54	0.06	27.06	0.4	0.8	1.07	6.64	13	4	62.5	7.02	43	434
1949794	3.4	2.68	0.14	27.54	0.71	0.34	1.9	9.54	67	1	141	11.82	24	598
1960846	4.6	30.34	16.1	23.71	0.49	0.04	11.28	148.78	441	5	1003	61.05	249	336
1937187	2.4	1.36	0.05	16.67	0.69	1.08	0.85	3.11	66	0.05	54.5	5.62	30	431
1937189	2.8	2.34	0.05	22.69	1.03	0.36	1.36	4.22	117	1	97.8	8.56	79	464
1937617	1.4	4.41	0.05	13.95	2.44	0.06	2.28	8.13	432	2	155.6	13.73	35	206
1946898	2.8	2.55	0.07	22.5	0.63	1.22	1.38	7.29	32	3	91.8	8.52	60	510
1946909	0.6	2.52	0.05	8.59	1.39	0.12	1.85	1.94	312	0.05	156.4	11.09	97	101
1947179	2.8	0.35	0.05	27.45	0.8	1.03	0.26	5.43	216	1	14.7	1.88	27	140
1947184	0.2	0.47	0.05	1.43	0.48	0.29	0.28	0.72	211	0.05	18.7	1.64	38	33
1947188	2.1	0.98	0.05	16.83	0.31	0.06	0.75	2.37	15	0.05	45.5	5.02	13	374
1933070	1.6	0.26	0.2	16.44	0.56	0.1	0.26	3.55	70	3	13	1.58	197	214
1933088	6.7	1.97	0.05	77.07	0.28	0.72	1.64	8.9	21	0.05	103.7	11.08	23	222
1933091	2.7	3.61	0.05	27.91	0.59	0.72	1.59	9.83	37	2	148.6	9.82	37	364
1937401	2.4	1.64	0.05	12.36	0.54	0.98	0.89	1.62	21	3	59.4	5.41	45	434
1937404	0.8	0.23	0.11	7.84	0.44	0.36	0.23	2.67	77	2	9.5	1.41	13	162
1937611	2.6	5.33	0.05	21.98	0.76	0.31	2.84	3.07	31	0.05	172.4	17.12	32	512
1937615	1.8	0.56	0.06	13.27	0.47	0.14	0.52	2.07	56	2	26.6	3.47	21	322
1946900	3.5	4.1	0.05	196.29	0.21	0.89	1.24	25.02	32	3	94.9	7.25	26	200
1946911	0.9	0.41	0.05	12.41	0.52	0.37	0.22	2.52	28	0.05	10.9	1.46	23	381

Raw whole rock geochemical data: Central Yorke Peninsula

Samp_R#	Ta ppm	Tb ppm	Te ppm	Th ppm	TiO2%	Tl ppm	Tm ppm	U ppm	V ppm	W ppm	Y ppm	Yb ppm	Zn ppm	Zr ppm
1946913	2.9	2.27	0.05	39.63	0.56	0.86	1.29	14.09	52	0.05	86	8.33	31	399
1947182	1.1	0.35	0.05	12.22	0.55	0.42	0.22	2.77	26	0.05	11.1	1.49	31	589
1947186	2	1.33	0.05	16.57	0.4	0.49	0.73	3.32	30	2	45.3	4.63	17	303
1949014	2.9	1.68	0.07	50.2	0.75	0.59	0.91	8.97	43	2	59.3	5.6	21	449
1949028	3.3	1.99	0.06	50.71	0.65	0.2	0.74	7.49	31	1	54.8	4.62	61	453
1949032	8.8	1.88	0.12	71.85	0.6	0.63	1.43	6.07	16	0.05	99	8.63	52	814
1949035	1.2	0.75	0.09	16.99	0.63	0.93	0.45	2.48	91	0.05	30.8	2.71	169	145
1949047	2.2	2.1	0.13	24.03	0.7	0.71	1.57	10.64	37	4	111.6	9.33	197	431
1949048	3.8	1.43	0.12	32.07	0.65	0.8	0.96	4.71	41	4	73.8	5.87	28	393
1949808	1.5	1.29	0.05	26.09	0.72	0.71	0.62	4.92	44	2	40	3.94	127	421
1960843	1.6	0.98	0.05	11.46	0.52	2.26	0.59	4.72	33	0.05	38.3	3.91	14	330
1960889	1.9	1.71	0.05	24.49	0.73	0.44	0.86	4.94	52	0.05	63.8	5.58	48	466
1949010	0.1	0.37	0.05	2	0.08	1.83	0.14	2.35	16	0.05	13	0.84	33	19
1949020	0.7	0.4	0.05	4.05	1.58	0.39	0.24	4.7	361	13	12.4	1.58	143	99
0000002	1.5	0.88	0.05	15.35	0.98	0.82	0.48	4.16	195	1	31.4	3.09	215	165
1937182	0.4	0.29	0.05	1.06	0.38	0.36	0.21	0.47	186	0.05	11.3	1.17	51	27
1937185	0.5	0.51	0.1	1.85	1.28	0.01	0.42	0.83	318	3	21.8	2.28	44	91
1937609	1	1.37	0.05	6.05	1.04	0.3	0.7	0.99	153	0.05	48.3	4.27	81	241
1949013	1.9	2.24	0.07	15.47	2.36	0.67	1.24	4.07	29	22	85.3	7.62	85	253
1949040	0.5	0.63	0.1	3.19	1.18	0.8	0.29	0.91	348	4	20.6	1.86	75	105
1949044	0.4	0.54	0.07	4.3	0.88	1.87	0.33	2.29	202	4	21.4	2.08	1906	75
1949797	0.3	0.57	1.12	1.61	1	0.3	0.33	1.1	291	3	23.2	2.03	45	67
1949802	0.6	0.76	0.05	2.28	1.14	0.34	0.37	1.65	251	11	26.3	2.32	74	106
1949819	0.5	0.71	0.1	2.56	1.29	0.29	0.44	1.67	314	3	27.1	2.78	73	88
1960891	1.8	1.7	0.05	15.02	3.58	0.59	0.78	5.16	130	70	64.2	5.01	83	214
1933075	1.2	0.35	0.05	18.11	0.39	0.27	0.31	7.09	40	3	14.7	1.92	11	620
1933085	22.1	0.31	0.05	14.03	0.37	0.45	0.34	6.39	74	0.05	16.5	1.73	30	115
1946895	0.5	0.49	0.05	2.39	0.71	0.92	0.26	3.12	253	28	16.2	1.69	89	63
1949008	0.2	0.4	0.05	1.71	0.08	0.28	0.17	1.67	18	2	14	0.96	9	13
1949050	0.7	0.28	0.07	9.52	0.23	0.36	0.2	2.18	21	2	11.5	1.3	18	208
1949055	1.2	1.46	0.64	19.4	0.48	0.36	0.62	2.96	197	0.05	58.6	4.09	29	138
1949812	1.7	0.53	0.1	26.06	0.69	0.92	0.4	6.7	84	2	18.8	2.89	156	368
1960849	1.4	1.01	0.05	16.93	0.56	0.8	0.63	3.11	95	4	44.6	3.97	15	120
1933073	1.5	0.78	0.1	17.83	0.56	0.5	0.42	2.58	92	6	28.7	2.35	39	160
1933078	1.2	0.98	0.11	9.88	0.68	0.27	0.35	4.1	80	1	28.8	2.13	25	144

Kym Michael Custance
Identifying IOCG pathfinder elements

Raw whole rock geochemical data: Central Yorke Peninsula

Kym Michael Custance
Identifying IOCG pathfinder elements

Samp R#	Ta ppm	Tb ppm	Te ppm	Th ppm	TiO2%	Tl ppm	Tm ppm	U ppm	V ppm	W ppm	Y ppm	Yb ppm	Zn ppm	Zr ppm
1933080	1.4	0.71	0.05	16.98	0.69	0.8	0.37	6.06	103	1	24.1	2.13	164	122
1937180	1.5	0.51	0.3	11.57	0.54	0.7	0.33	4.32	53	6	18.3	1.71	26	97
1937383	0.8	0.85	0.05	12.78	0.41	0.41	0.46	2.92	61	4	32.6	2.98	11	104
1937613	0.8	0.74	0.05	10.48	0.36	0.26	0.39	3.05	111	9	31.4	2.51	20	98
1946901	1.3	1.38	0.05	22.94	0.54	0.06	0.4	6.51	58	16	37.7	2.68	21	154
1946902	0.9	0.46	0.05	12.8	0.39	0.17	0.29	0.96	65	8	18.8	1.82	16	96
1946906	1.4	0.76	0.51	19.51	0.65	2.23	0.38	22.48	147	3	26.7	2.61	553	203
1947176	5.5	3.66	0.05	81.43	1.63	1.93	1.84	11.31	188	5	118.2	11.86	246	326
1949006	1.5	0.67	0.13	15.84	0.65	1	0.49	1.77	100	5	31.8	3.15	87	125
1949017	0.1	0.21	0.15	4.92	0.11	3.16	0.1	0.46	39	0.05	7.4	0.74	117	33
1949023	1.5	1.45	0.19	16.59	0.59	2.02	0.82	3.45	155	10	60.6	5.05	45	170
1949026	1.3	0.52	0.07	13.63	0.5	0.92	0.31	2.85	65	6	19.3	1.96	21	110
1949034	0.9	0.66	0.16	13.38	0.45	1.36	0.29	9.65	62	6	21.2	1.78	107	111
1949789	1.5	0.59	0.15	18.17	0.6	0.58	0.37	2.69	124	5	23.2	2.25	48	143
1949791	1.5	0.66	0.22	18.66	0.62	0.82	0.42	4.25	131	8	27.5	2.66	349	173
1949799	1.2	1.08	0.06	18.7	0.65	0.59	0.57	3.46	80	4	45.2	3.69	26	134
1949804	1.5	0.46	0.05	16.38	0.5	0.68	0.31	3.42	31	7	17.4	2.07	13	289
1949806	1.5	1.34	0.05	20.88	0.68	0.75	0.76	6.62	107	11	53.5	4.95	212	151
1949809	1.4	0.72	0.2	17.42	0.55	0.56	0.46	2.21	79	5	31.4	3.26	72	188
1949815	1.5	0.49	0.3	13.77	0.58	0.58	0.32	25.74	149	7	22.1	2.14	143	128
1949817	1.6	0.71	0.05	18.04	0.6	2.27	0.41	3.69	147	6	25.1	2.47	36	153
1949822	1.5	0.81	0.05	20.71	0.59	2.57	0.41	1.91	87	4	28.8	2.77	22	141
1949825	1.1	1.35	0.05	24.41	0.61	0.54	0.36	2.74	103	2	34	2.72	25	137
1949827	0.8	0.63	0.6	10.25	0.36	0.69	0.25	11.59	64	4	23.5	1.82	178	99
1960877	2.8	6.4	2.4	26.92	0.74	0.39	5.11	9.26	121	13	373.2	33.36	92	416
1960886	1.4	0.84	0.05	17.83	0.65	0.61	0.42	3.33	153	15	34.5	2.77	149	166
1960894	1.3	0.79	0.05	15.34	0.58	0.74	0.42	3.78	132	6	34.9	2.74	35	154
0000003	0.8	0.43	0.05	7.18	0.25	0.45	0.18	1.33	24	5	14.9	1.41	19	154
0000006	1.7	1.12	0.05	17.22	0.61	0.37	0.6	3.72	58	3	46.3	3.69	33	290
1933071	1.6	0.32	0.11	13.66	0.4	0.01	0.32	6.71	33	4	11.9	1.75	42	296
1933076	2	0.96	0.05	24.22	0.8	0.4	0.59	8.9	103	2	38.1	3.52	30	193
1933079	3.4	2.65	0.05	46.8	0.56	0.2	1.25	32.17	39	1	82.6	8.13	31	205
1933081	1.4	0.87	0.05	15.95	0.64	0.36	0.55	4.12	96	2	43.8	3.29	41	112
1933083	2.8	0.33	0.1	18.05	0.46	0.3	0.41	7.73	249	0.05	16.7	2.4	78	353

Raw whole rock geochemical data: Central Yorke Peninsula

Kym Michael Custance
Identifying IOCG pathfinder elements

Samp R#	Ta ppm	Tb ppm	Te ppm	Th ppm	TiO2%	Tl ppm	Tm ppm	U ppm	V ppm	W ppm	Y ppm	Yb ppm	Zn ppm	Zr ppm
1933086	2.8	0.23	0.05	12.37	0.5	0.27	0.27	4.63	112	2	12.3	1.72	69	118
1933089	8	1.78	0.05	104.02	0.38	0.9	1.44	15.32	27	0.05	80.8	9.82	19	310
1933092	3.3	2.21	0.11	31.9	0.7	0.63	1.11	6.45	41	0.05	73.1	6.65	31	440
1937181	1.2	0.49	0.22	9.73	0.43	0.01	0.3	3.98	160	4	16.6	1.5	34	94
1937183	0.4	0.18	0.05	1.06	0.38	1	0.16	0.57	131	0.05	7.4	0.66	91	34
1937186	0.4	0.57	0.05	1.53	1.15	0.01	0.38	1.12	298	10	22.6	2.18	53	73
1937188	2.1	1.2	0.05	10.35	1	0.71	0.82	2.81	137	0.05	48.7	5.12	96	350
1937190	1.6	1.34	0.1	10.24	0.63	0.5	0.75	2.25	77	0.05	47.3	4.12	76	283
1937384	1.1	0.68	0.05	14.82	0.52	0.63	0.38	2.62	84	11	26.3	2.38	11	123
1937387	1.7	0.85	0.1	28.53	0.67	3.1	0.51	1.68	68	9	34.1	3.06	39	145
1937390	5.8	2.96	0.05	52.66	0.65	0.2	1.73	8.58	15	6	102	11.37	13	640
1937393	0.7	0.24	0.05	3.13	1.45	1.8	0.26	2.04	355	6	9.8	1.69	42	104
1937396	12.1	0.75	0.08	27.81	0.47	0.08	0.74	6.97	14	2	36.3	5.37	14	453
1937399	2.8	0.66	0.11	29.26	0.52	0.63	0.55	4.71	40	0.05	26.7	3.54	14	460
1937402	2.7	1.72	0.11	19.97	0.6	0.99	1.02	2.47	23	2	65.6	6.37	83	519
1937405	1.2	0.19	0.05	4.45	0.06	0.45	0.17	1.72	17	0.05	9.2	0.95	15	65
1937610	1.8	1.26	0.05	17.87	1.07	0.35	0.76	1.65	170	0.05	49.4	4.56	88	170
1937612	2.1	1.25	0.05	14.44	0.8	0.24	0.77	2.4	45	0.05	51.7	4.81	51	489
1946896	0.4	0.42	0.05	2.79	0.65	0.4	0.27	1.12	197	1	16.6	1.68	31	40
1946903	0.6	0.66	0.05	11.71	0.27	0.18	0.35	0.88	76	5	23.4	2.16	19	69
1946905	0.4	0.62	0.05	2.83	1.33	0.86	0.44	7.14	349	2	24.5	2.87	163	110
1946907	1.4	0.72	0.48	19.52	0.68	2.21	0.37	45.26	188	6	25.2	2.32	117	174
1946912	0.5	1.15	0.05	5.42	0.28	0.4	0.44	2.82	16	0.05	30.4	2.55	26	209
1947177	4.2	1.98	0.08	67.07	1.21	1.62	1.15	8.47	128	4	77.1	7.3	265	258
1947180	1.5	2.48	0.05	22.72	0.75	0.87	0.71	13.01	116	2	47.1	4.53	23	174
1949009	1.1	0.54	0.18	19.19	0.52	0.73	0.27	4.11	79	12	17.6	1.72	17	95
1949015	2.4	1.55	0.1	36.51	0.66	0.59	0.82	7.46	41	0.05	54.3	5.1	18	420
1949018	0.9	0.42	0.06	13.15	0.44	0.7	0.22	1.3	106	0.05	15.4	1.34	63	133
1949021	0.7	0.63	0.05	3.58	1.56	0.39	0.39	4.2	344	7	25.1	2.52	239	92
1949024	2.7	1.62	0.16	26.33	0.33	0.53	1.16	4.3	46	3	65.4	7.66	47	251
1949027	1.2	0.69	0.12	15.85	0.49	1.03	0.31	1.76	85	5	22.5	1.84	15	107
1949029	3.6	1.88	0.09	71.91	0.62	0.54	1.11	13.06	33	0.05	72	7.02	97	371
1949038	3.6	1.4	0.18	36.12	0.51	0.23	1.85	8.96	14	1	102.3	12.3	133	519
1949043	0.7	0.36	0.05	10.4	0.21	0.23	0.23	1.61	18	1	15.6	1.5	40	66
1949045	0.5	0.48	0.1	4.18	0.98	1.26	0.32	4.1	217	18	19.9	2	215	77

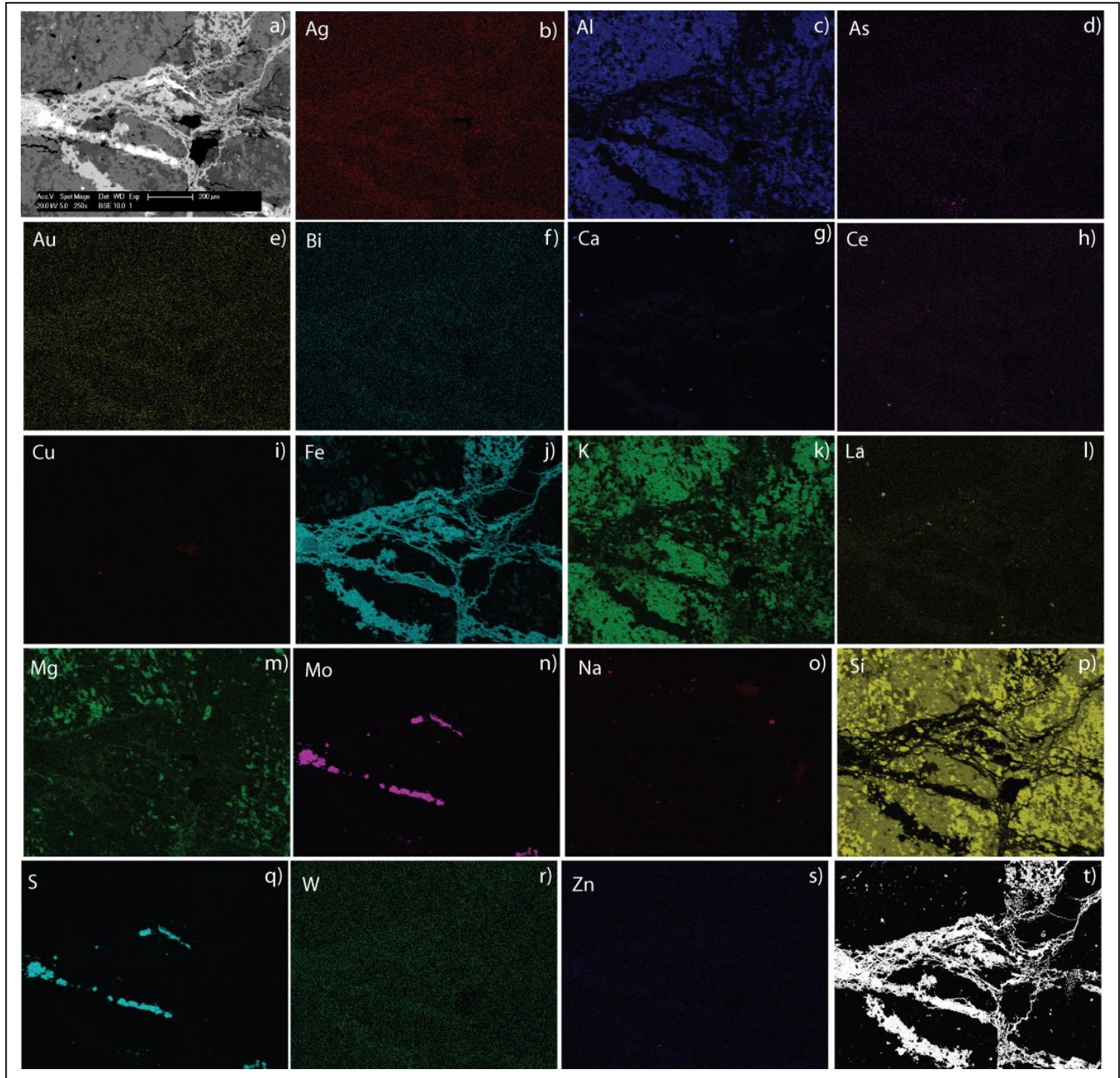
Raw whole rock geochemical data: Central Yorke Peninsula

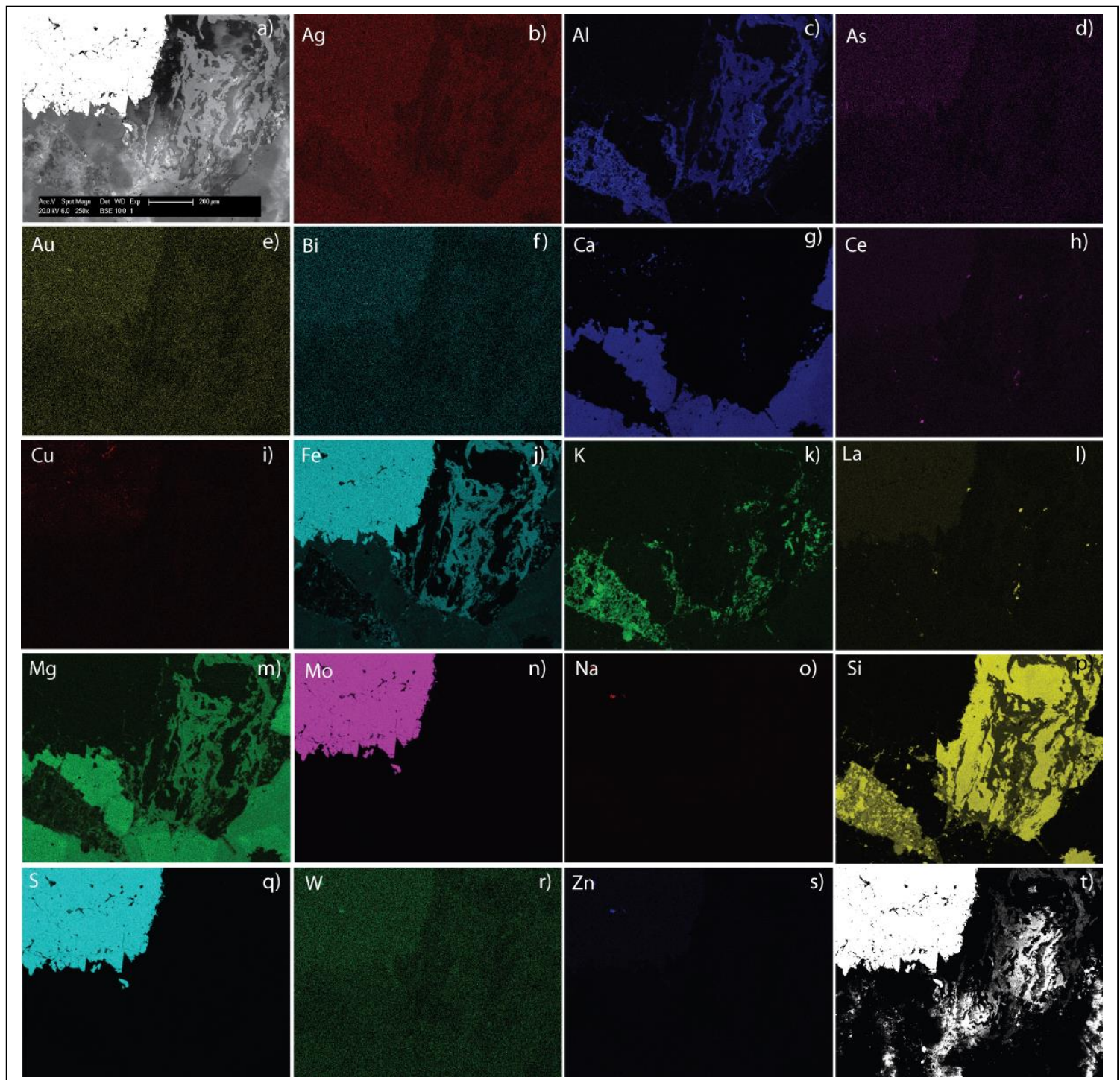
Samp R#	DH_No	East	North	Depth from	Depth to	Strat_Name	Lith_type	Samp_type	Samp_from	Au ppb	Ag ppm	Al2O3%	As ppm	Ba ppm	Be ppm	Bi ppm	CaO%
1949049	23052	752291	6225060	123.7	124.7	Arthurton Granite	Granite	Drill core	B2	0.5	0.025	13.28	18.7	1317.4	3.5	0.03	0.62
1949051	23674	759856	6246503	126.5	127.5	Oorlano Metasomatite	Metasomatite	Drill core	B2	0.5	0.025	11.38	16.4	84.4	1	1.37	0.35
1949054	23730	775944	6248599	50.5	51.25	Mona Volcanics Member	Felsic volcanic	Drill core	B2	6	0.28	15.65	35.9	442	2.4	0.76	0.65
1949780	139488	759504	6267846	167.3	168.3	Oorlano Metasomatite	Metasomatite	Drill core	B2	0.5	0.06	11.43	16.7	14.6	3	0.05	4.54
1949783	23729	776876	6249028	98.2	99.2	New Cornwall Member	Carbonate	Drill core	B2	0.5	0.46	13.06	22.8	730.9	2.2	0.53	5.43
1949787	23723	777295	6249394	80	81	Mona Volcanics Member	Felsic volcanic	Drill core	B2	0.5	0.26	11.59	20.5	898.2	2.8	0.17	0.22
1949792	23048	770327	6233976	51.3	52.3	Unnamed GIS unit	Sediment	Drill core	B2	1	0.35	15.88	23.9	480.3	4.6	0.56	0.57
1949795	23701	741389	6240671	52.8	53.8	Weetulta Formation	Felsic volcanic	Drill core	B2	0.5	0.26	11.37	26.2	2220.1	1.4	0.005	0.25
1949798	30047	784258	6246312	348.9	349.9	Mona Volcanics Member	Felsic volcanic	Drill core	B2	0.5	0.025	19.13	91.7	588	3	0.63	1.99
1949800	23027	745198	6225492	27.4	28.4	Doora Member	Sediment	Drill core	B2	1	0.025	15.65	22.8	404	3.5	0.005	0.67
1949805	23672	752805	6242398	149.9	150.6	Wandearah Formation	Sediment	Drill core	B2	2	0.025	11.63	5	521	2.1	0.34	1.41
1949810	23046	768768	6233533	58.8	59.9	Wandearah Formation	Sediment	Drill core	B2	7	0.025	16.18	9	259.4	4.7	0.22	0.85
1949813	23669	751171	6243568	126.8	127.8	Oorlano Metasomatite	Metasomatite	Drill core	B2	2	0.025	9.08	8	233.1	1.4	0.005	13.35
1949818	23726	777294	6247803	63.7	64.7	Wandearah Formation	Sediment	Drill core	B2	1	0.4	14.52	14	868.3	3.1	1.18	2.77
1949820	30048	784207	6244524	436.3	437.3	Bute Metadolerite	Mafic intrusive	Drill core	B2	15	0.025	8.53	4	36.9	1.3	0.07	13.24
1949823	30050	781823	6257617	302	303	Wandearah Formation	Sediment	Drill core	B2	0.5	0.025	17.94	11	1567.1	4	0.19	1.35
1949826	23700	741294	6240971	60.6	61.6	Doora Member	Sediment	Drill core	B2	0.5	0.025	19.48	8	1071.5	4.9	0.05	0.37
1949828	23691	760919	6243044	57.7	58.7	Unnamed GIS unit	Sediment	Drill core	B2	0.5	0.025	7.46	3	1749.8	2.4	0.005	26.23
1960844	143972	744329	6163730	49.5	50.5	Unnamed GIS unit	Gneiss	Drill core	B2	0.5	0.025	14.93	4	1198.2	1.7	0.005	0.94
1960847	23028	733429	6208620	46.3	47.3	Wandearah Formation	Felsic volcanic	Drill core	B2	2	0.025	11.06	9	767.1	4.2	0.005	0.45
1960878	23047	769461	6233877	111.5	112.5	Unnamed GIS unit	Sediment	Drill core	B2	54	0.3	12.68	7	69.5	2.6	0.005	1.62
1960881	30065	778298	6242989	168.4	169.4	Wandearah Formation	Carbonate	Drill core	B2	3	0.5	2.43	53	225	1.2	1.75	23.05
1960884	30051	778309	6244444	179.8	180.8	Wandearah Formation	Carbonate	Drill core	B2	0.5	0.025	8.47	19	2293.6	2.6	0.13	12.51
1960887	23037	769374	6233729	63	64	Unnamed GIS unit	Sediment	Drill core	B2	3	0.025	14.44	9	566.1	3.7	0.26	0.42
1960892	23697	770244	6235564	235.7	236.7	Unnamed GIS unit	Mafic intrusive	Drill core	B2	5	0.025	11.55	11	202.1	4.6	0.11	3.04
1960895	23698	769811	6234551	281.1	282.1	Unnamed GIS unit	Sediment	Drill core	B2	6	0.025	15.5	8	745	4.3	0.02	1.85

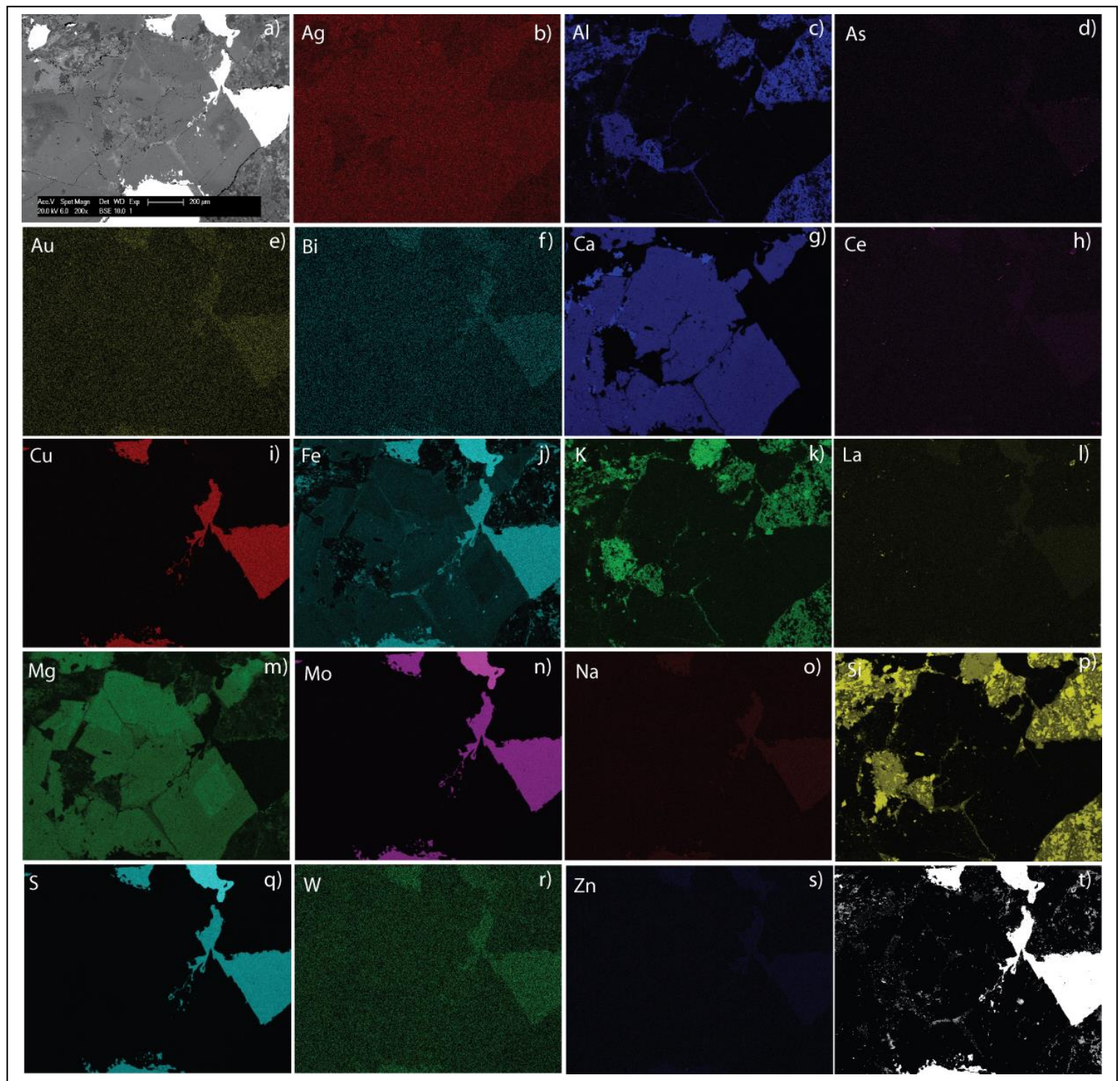
Raw whole rock geochemical data: Central Yorke Peninsula

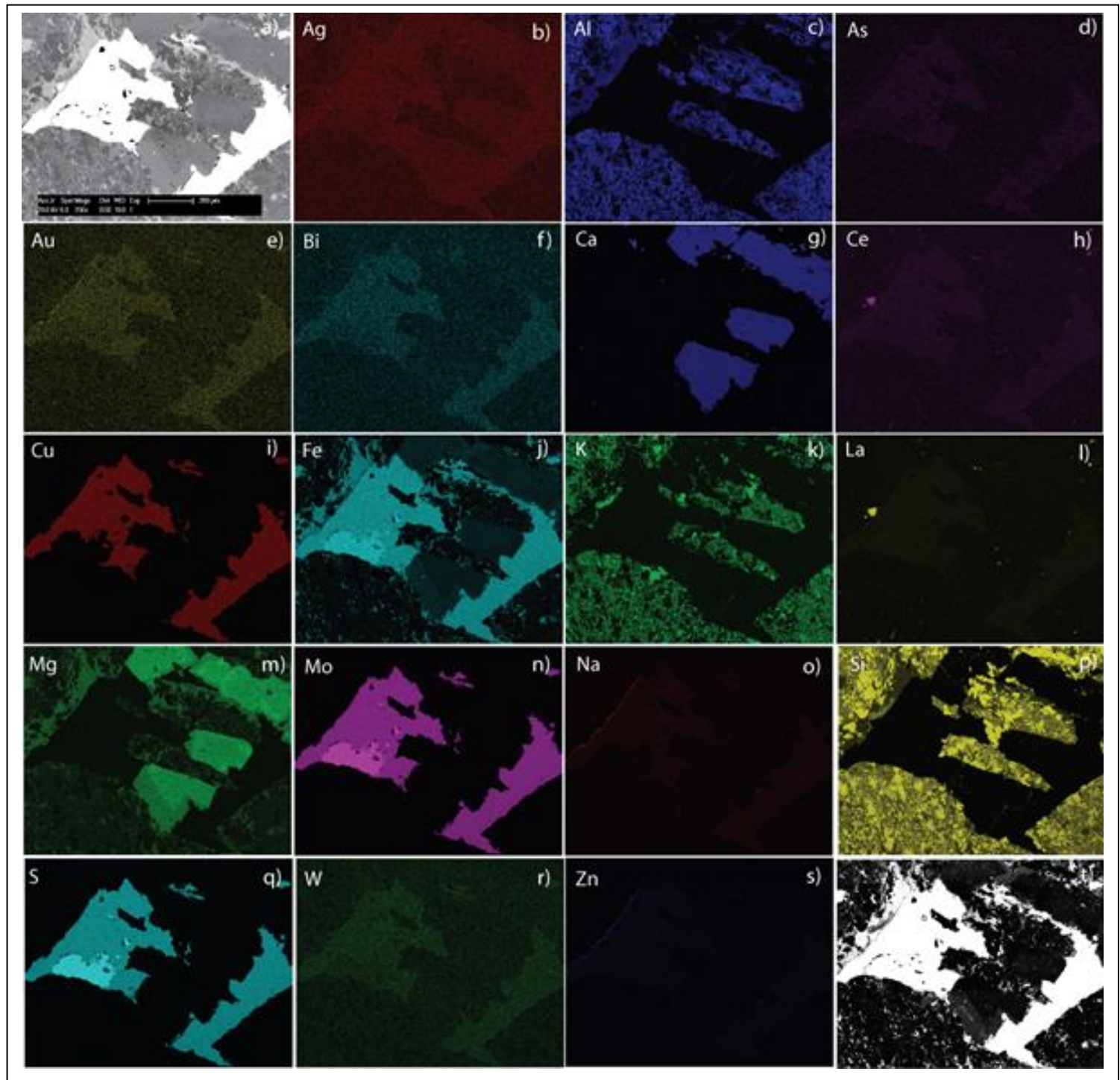
Samp R#	Ta ppm	Tb ppm	Te ppm	Th ppm	TiO2%	Tl ppm	Tm ppm	U ppm	V ppm	W ppm	Y ppm	Yb ppm	Zn ppm	Zr ppm
1949049	2.9	1.8	0.05	28.55	0.71	0.59	1.05	6.23	45	1	66.9	6.7	55	492
1949051	1	0.64	0.06	17.76	0.41	0.6	0.35	4.47	53	5	23.9	2.27	212	225
1949054	1.3	0.63	0.09	14.05	0.63	0.9	0.33	2.88	116	4	21.7	2.06	75	134
1949780	1.3	1.29	0.08	35.83	0.51	0.01	0.85	7.94	123	1	55.3	5.28	17	212
1949783	1.4	0.72	0.12	19.19	0.61	0.49	0.42	6.58	100	2	26.7	2.71	64	152
1949787	3.9	2.13	0.1	33.78	0.48	0.54	1.38	7.09	12	4	83	8.86	21	479
1949792	1.7	0.5	0.23	20.85	0.66	1.5	0.35	4.24	113	2	20.8	2.25	133	184
1949795	4.1	1.04	0.14	28.48	0.68	0.37	0.72	6.46	27	0.05	46.2	4.98	10	636
1949798	1.3	1.08	0.26	19.02	0.72	0.5	0.54	3.12	162	7	39.1	3.19	29	122
1949800	1.2	0.57	0.11	18.3	0.64	0.44	0.39	4.19	72	5	26.1	2.47	36	138
1949805	1.4	0.53	0.05	16.24	0.47	0.53	0.31	2.33	63	5	18.3	1.97	48	261
1949810	1.5	0.73	0.4	15.85	0.64	0.51	0.49	2.36	104	6	32.1	2.94	57	159
1949813	1.2	0.45	0.05	16.06	0.39	0.25	0.31	5.1	40	0.05	17.8	2.3	37	245
1949818	1.4	0.78	0.1	16.1	0.57	0.56	0.38	3.52	144	4	25.7	2.49	32	130
1949820	0.4	1.03	0.05	1.53	0.88	0.06	0.48	1.81	240	6	36.7	2.94	66	62
1949823	1.8	0.67	0.05	20.04	0.69	0.85	0.44	1.98	93	4	29.1	2.73	20	126
1949826	1	1.48	0.05	13.73	0.68	0.49	0.55	2.52	83	0.05	48.4	3.69	61	118
1949828	0.7	0.53	0.05	9.65	0.32	0.36	0.21	5.37	45	4	19.5	1.58	94	78
1960844	1.1	0.65	0.05	17.28	0.63	0.96	0.24	2.21	70	0.05	21.6	1.8	37	217
1960847	3.8	3.45	0.2	27.12	0.78	0.14	1.56	21.09	52	1	102.4	10.26	79	633
1960878	1.3	0.5	1.2	20.17	0.55	0.22	0.28	3.05	78	13	21.6	2.09	54	243
1960881	0.4	0.36	0.05	3.84	0.15	2.16	0.11	2.7	18	3	12.6	0.95	32	41
1960884	0.9	0.76	0.05	12.02	0.38	0.44	0.3	1.74	45	5	25.7	2.13	24	134
1960887	1.4	1.05	0.2	20.33	0.58	0.98	0.47	3.97	136	13	34	3.13	113	198
1960892	1.8	2.03	0.05	15.76	3.04	0.59	0.94	3.14	82	2	69	6.08	69	227
1960895	1.3	0.46	0.05	18.49	0.56	1.01	0.21	2.62	165	7	16.9	1.62	36	116

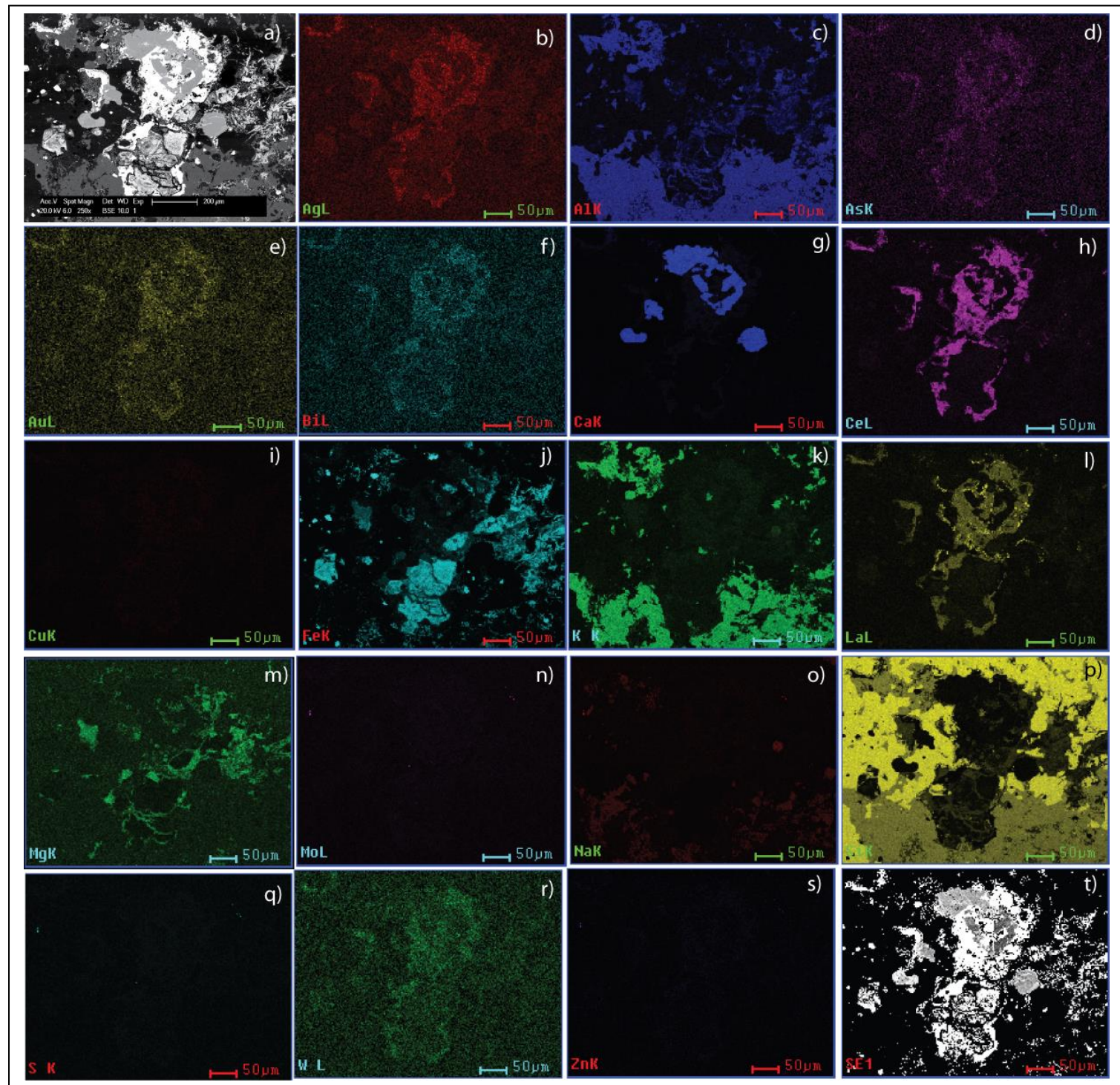
**APPENDIX B: SEM IMAGES ORDER: (MAP 1 - 1949789) – (MAP 2,3,4 1949023)
– (MAP 5,6 – 1960847)**

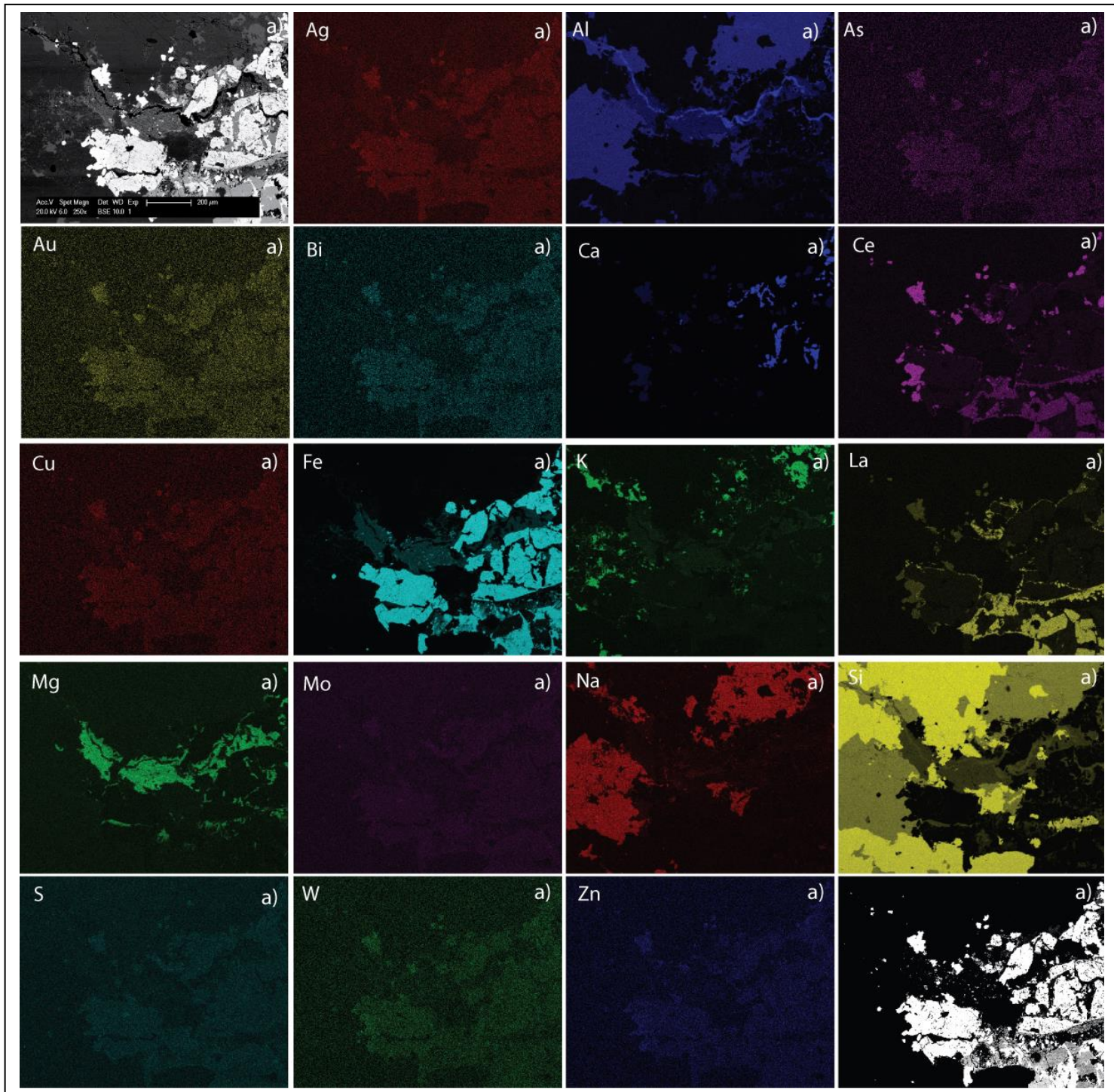












APPENDIX C: RAW LA-CP-MS DATA FROM SULPHIDES ANALYSED

APPENDIX D: PATHFINDER ELEMENT CRITERIA

Pathfinder criteria 1 – histogram and probability plots

Normalised histogram and probability plots were used to assess the distribution of data within each element. Elements needed to show three potential populations of data (background – interesting – potentially anomalous), display a relatively evenly distributed bell curve set of data and show high population outliers. Example given in (Fig.18-a)

Pathfinder criteria 2 – High element populations from histogram need to be anomalous.

Element concentrations needed to be assessed to determine if their high population outliers are in fact anomalous and above background concentrations. Lack of sample points within each selected lithological unit meant that creating a true background for the Wallaroo Basement rocks on central Yorke Peninsula was beyond the scope of this thesis. However, a medium must be used for comparing data as to determine anomalous concentrations. (Fabris et al. 2013b) work on characterising alteration in the Eastern Gawler Craton on identifying an IOCG index also used a 10x average crustal abundance anomalous indicator and utilized an average upper crustal abundance by (Rudnick and Gao 2003) as the datum point for measuring anomalous concentrations against. As both study areas are within the Olympic Copper Gold Province and areas share similar characteristics in alteration styles the same table by (Rudnick and Gao 2003) was used for this project. Table given in (appendix.aa). Example of criteria in (Fig.18-b)

Pathfinder criterion 3 - Elements with high populations must be high enough above detection limits to not impede the data, yet with preference given to elements that are already associated with IOCGS

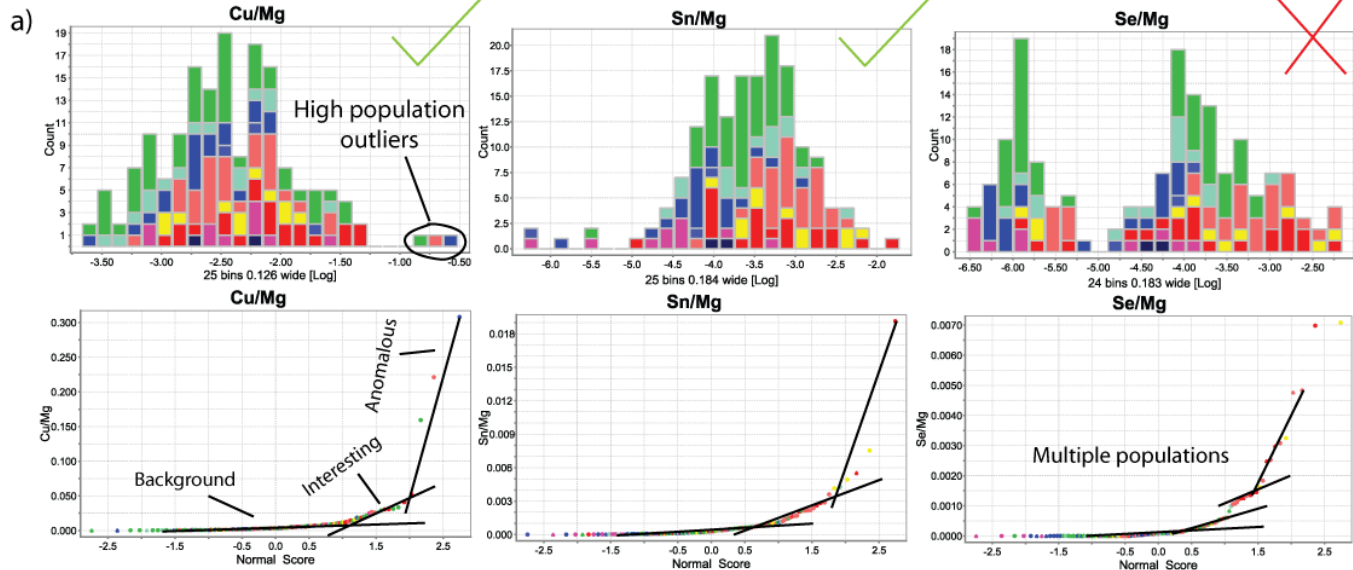
As detection limit issues are a factor for each individual element, elements had to be assessed to determine if the data may be influenced by detections limits for that element. Yet, if an element is considered to be a known interesting pathfinder and vectors towards known mineralisation in the area it may still be further looked at.

Detection limits examples for elements given in (Fig.18-c).

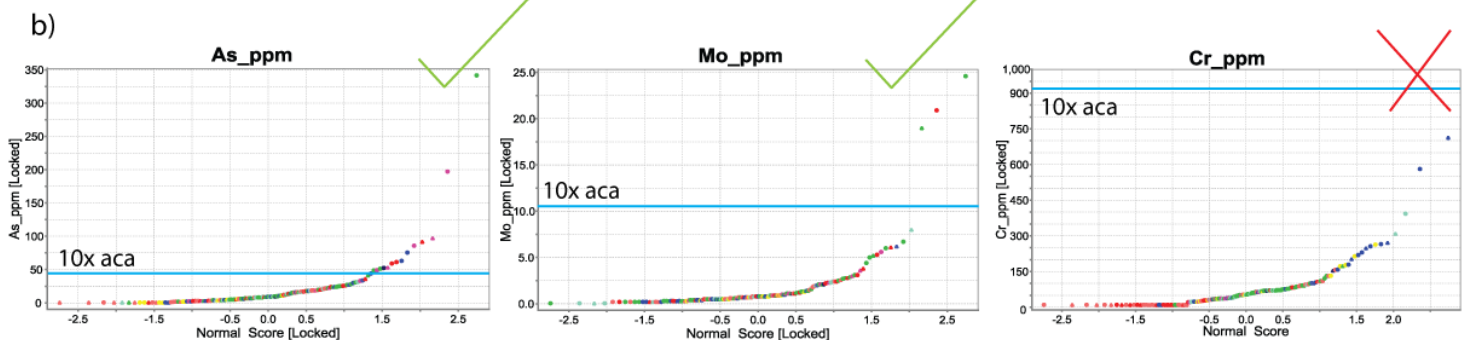
Pathfinder criterion 4 – Elements should show vectoring towards areas of known or potential IOCG mineralisation.

Three areas have been identified as prospective areas for mineralisation. The already known mineralised area of Moota-Wallaroo, the Alford prospect and potential mineralised area north of Maitland (Fig. 19.d). Elements that passed previous criteria had to vector towards these areas and show correlation with other potential pathfinder elements.

Pathfinder criteria 1 example



Pathfinder criteria 2 example



Pathfinder criteria 3 example

